Aspects of Screened Modified Gravity

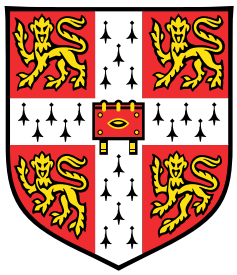

Nathan Procter

Supervisor: Prof. A.C. Davis

Department of Applied Mathematics and Theoretical Physics

University of Cambridge

This dissertation is submitted for the degree of

Doctor of Philosophy

Robinson College March 2020

Declaration

I hereby declare that except where specific reference is made to the work of others, the contents of this dissertation are original and have not been submitted in whole or in part for consideration for any other degree or qualification in this, or any other university. This dissertation is my own work and contains nothing which is the outcome of work done in collaboration with others, except as specified in the text and Acknowledgements. This dissertation contains fewer than 65,000 words including appendices, bibliography, footnotes, tables and equations and has fewer than 150 figures.

Nathan Procter

March 2020

Acknowledgements

First and foremost I would like to thank my supervisor, Anne-Christine Davis, for her guidance and support over the course of my PhD. I am extremely grateful for all your help.

Thank you also to those in the scientific community with whom I have held many useful conversations, and to all those members of Pavilion B that have made my time here enjoyable.

I would also like to thank the Science and Technology Facilities Council for funding my studies, and the Cambridge Philosophical Society and Robinson College who also provided financial support.

Abstract

The currently accepted standard model of cosmology uses general relativity with a ΛCDM matter content to describe the universe on the largest scales. It is an overwhelmingly successful theory, consistent with all observational tests. Despite this, theoretically unsatisfying elements to the theory exist and these have motivated various theories of modified gravity that challenge general relativity. In order to pass the stringent observational tests on a solar system level, the deviation of modified gravities from general relativity must be suppressed. This is known as screening, and different modified gravity theories use different screening mechanisms. We motivate modifying gravity and the need for screening mechanisms. Three explicit models of modified gravity which exhibit screening are presented. These are the Galileon, K-mouflage and Chameleon models. In this thesis we investigate several aspects of these models.

We study astrophysical black holes in Galileon and K-mouflage theories. The no-hair theorem of General Relativity states that, under certain specific assumptions, the scalar field is trivial around a black hole. The assumptions going into the no-hair theorem are the absence of external matter and time independence. An astrophysical black hole typically has an accretion disk, so automatically circumvents the no-hair theorem. We display the scalar field profile around such black holes, compute the fifth force and demonstrate that the work done by the fifth force is small compared to the energy lost due to radiation in General Relativity. Further we drop the assumption of a static black hole and investigate the time-dependent solution of the scalar field in both theories. We find exact time-dependent vacuum

K-mouflage black hole solutions and further consider time-dependent solutions with an accretion disk. For K-mouflage the solution is similar to the time-independent one whereas the Galileon theories solutions resembles closely the time-dependent vacuum solution.

The most general coupling of the scalar field to matter contains both a conformal and disformal term. We investigate the effect of a disformal coupling in K-mouflage theories, calculating the cosmological background evolution of the theory and extending our results on the behaviour of the scalar field around a black hole to include the disformal coupling. We find that large regions of the parameter space provide only percent level deviations from the ΛCDM evolution, despite qualitative differences from the conformal-only case.

Often spherical symmetry is assumed to demonstrate the screening of K-mouflage theories. We present preliminary calculations exploring the effect the shape of a source object has on the scalar field it generates. We find that the shape dependence is similar to that of the D-BIon, another theory that screens when the first derivative of the field is large. In particular we find that screening is strongest for planar objects, in contrast to Galileon theories for which screening is entirely absent.

We move on from K-mouflage theories to consider Chameleon theories. We propose a logarithmic potential, which differs from the standard power law potential usually assumed, and use observational data to constraint the parameter space of the theory.

Table of contents

List of figures

List of tables

Nomenclature

Definitions by Description

c	Speed of Light
$\hbar$	Reduced Planck Constant
G	Gravitational Constant
M_{Pl}	Reduced Planck Mass
Φ_N	Newtonian Gravitational Potential
z	Red Shift
$g_{\mu\nu}$	Einstein Frame Metric
$\tilde{g}_{\mu\nu}$	Jordan Frame Metric
$A^2(\phi)$	Einstein Frame to Jordan Frame Coupling
r_*	Chameleon Screening Radius
r_s	Black Hole Schwarzschild Radius
Q	Scalar charge of an Object

Definitions by Equation

$M_{Pl} = \sqrt{\frac{\hbar c}{8\pi G}}$

$\beta = M_{Pl}\frac{dA(\phi)}{d\phi}$

$M_c = M_{Pl}/\beta$

$X = -g^{\mu\nu}\partial_\mu\phi\partial_\nu\phi/2$

$\chi = -g^{\mu\nu}\partial_\mu\phi\partial_\nu\phi/2\mathscr{M}^4$

$z = 1/a(t) - 1$

$\tilde{g}_{\mu\nu} = A^2(\phi)g_{\mu\nu}$

$r_s = 2GM_{BH}$

Chapter 3 Specific Definitions

$\rho_\phi = -\mathscr{M}^4K(\chi) + 2\chi K'(\chi)$

$p_\phi = \mathscr{M}^4K(\chi)$

$\hat{\rho} = \rho_E/A\sqrt{1-2BX/M^4}$

$\rho_{eff} = \rho_\phi + \hat{\rho}(A\sqrt{1-2BX/M^4} - 1)$

$\omega_\phi = p_\phi/\rho_{eff}$

$\varepsilon = 1 - \sqrt{1-2B\chi(0)}$

Chapter 1

Introduction

At the beginning of the twentieth century conventional wisdom dictated that the universe was static and eternal. Having formulated his theory of General Relativity [46], which still stands as the currently accepted theory of gravitation, Einstein added a "cosmological constant" into his field equations to ensure that this was the case, as otherwise General Relativity only permits an expanding or contracting universe. However in 1929 Hubble discovered that nearby galaxies were receding from us, and in particular that the recession velocities increased linearly with distance [57]. This discovery of an expanding universe led Einstein to abandon the cosmological constant, which he famously described as his "greatest blunder."

In the final decade of the twentieth century our understanding of the universe was again shaken. Observations of type 1A supernovae indicated that, not only was the universe expanding, but that the expansion was accelerating [75]. The rate of expansion is consistent with the existence of a cosmological constant and in modern cosmology this mysterious substance is termed dark energy. Its nature is unclear. Quantum field theory provides a candidate substance that behaves like a cosmological constant -the vacuum energy of standard model particles - but radically overestimates its size. If the vacuum energy is taken to be around the Planck mass then it is roughly one hundred and twenty orders of magnitude

greater than the observed cosmological constant value [60]. This can be partially remedied if the vacuum energy is taken to be around the weak scale, as would be predicted by supersymmetry [49], but the vacuum energy is still sixty orders of magnitude too large. Our current working model relies on almost exactly cancelling out this vacuum energy: a level of fine tuning that is theoretically unsatisfying.

We will introduce the standard model of cosmology [12] in section 1.2. This model uses General Relativity to describe the universe on the largest scales and passes all observational constraints. However its failure to explain the cosmological constant problem, along with other issues detailed in section 1.3, means that it is, at best, incomplete. This has spawned the consideration of a number a rival gravitational theories in the hope that some of the model's problems can be addressed. To be a viable candidate, any theory must pass a range of tests from laboratory experiments to observations of the cosmos, from the dynamics of the solar system to the strong gravity regime of black holes and neutron stars. This thesis discusses various proposed gravitational theories that modify General Relativity in a range of physical scenarios. Observations of the solar system are particularly stringent and so various mechanisms have been developed to suppress (or screen) the effects of the modification in the solar system whilst still allowing meaningful modifications on a cosmological scale. We will consider only theories with such a screening mechanism. Before we discuss modifying gravity, we recapitulate the fundamental features of General Relativity and the standard model of cosmology.

We will first introduce General Relativity in section 1.1 before moving on to discuss in section 1.2 how this is used to formulate the standard model of cosmology. We will then motivate modifying gravity in section 1.3 and introduce specific models of modified gravity in section 1.4. In section 1.5 we will discuss the three main mechanisms for screening the deviations of the predictions of these models from General Relativity in the solar system. As

chapter 2 discusses black holes, we will review black holes in these theories in section 1.6. The chapter will conclude with a summary of the thesis in section 1.7.

1.1 General Relativity

General Relativity [46] was born in 1915 as a theory of gravity that unified Newtonian gravity [70] and Special Relativity [44].

Special Relativity (1905) postulates that the laws of physics are invariant under Lorentz transformations. In particular this means that the previously distinct notions of time and space are not separate, and can differ from observer to observer. This is incompatible with Newtonian gravity which relies upon global notions of time and space.

Additionally, in Newtonian gravity there are two distinct notions of mass; the inertial mass, which is the mass in $F = ma$ and which quantifies the response of an object to an external force; and the gravitational mass, which is the strength with which an object couples to an external gravitational field. These can be measured to be very close in value, but Newtonian theory provides no explanation to this. The weak equivalence principle (WEP) states that the two masses are equal, a principle that guided Einstein in his search for a new gravitational theory and a principle that is indeed made manifest by the geometrical nature of General Relativity.

Furthermore, although Newtonian gravity describes the dynamics of the solar system well up to around one part in ten thousand, it cannot explain the precession of the perihelion of Mercury. Famously, the Newtonian calculation is incorrect by around 43 arc-seconds per century. The motion of bodies differs in General Relativity to Newtonian gravity, and that General Relativity provided an explanation [45] for the missing 43 arc-seconds per century was further evidence of its validity.

Today General Relativity still stands as a theory consistent with all observational data, despite the fact that modern day technology provides a number of precise observational probes that were not available in Einstein's time.

The Einstein-Hilbert action of General Relativity is

$$S = \int dx^4 \sqrt{-g} \left(\frac{M_{Pl}^2}{2} R - \Lambda \right) + S_m(\psi^{(i)}, g_{\mu\nu}) \tag{1.1}$$

where $\psi^{(i)}$ are the matter fields and varying this action gives rises to Einstein's field equations[1]

$$G_{\mu\nu} + \Lambda g_{\mu\nu} = \frac{8\pi G}{c^4} T_{\mu\nu} \tag{1.2}$$

where

$$G_{\mu\nu} = R_{\mu\nu} - \frac{1}{2} R g_{\mu\nu} \tag{1.3}$$

is the Einstein tensor,

$$R_{\mu\nu} = \partial_\lambda \Gamma^\lambda_{\mu\nu} - \partial_\nu \Gamma^\lambda_{\mu\lambda} + \Gamma^\lambda_{\rho\lambda} \Gamma^\rho_{\mu\nu} - \Gamma^\rho_{\mu\lambda} \Gamma^\lambda_{\nu\rho} \tag{1.4}$$

is the Ricci tensor and

$$R = g_{\mu\nu} R^{\mu\nu} \tag{1.5}$$

is the Ricci scalar. The Christoffel symbols are

$$\Gamma^\lambda_{\mu\nu} = \frac{1}{2} g^{\lambda\rho} (\partial_\nu g_{\rho\mu} + \partial_\mu g_{\rho\nu} - \partial_\rho g_{\nu\mu}) \tag{1.6}$$

and the energy momentum tensor is defined to be

$$T_{\mu\nu} = \frac{-2}{\sqrt{-g}} \frac{\delta S_m}{\delta g^{\mu\nu}}. \tag{1.7}$$

[1] We have re-introduced the speed of light here, but for the remainder of the thesis will work in units with $c = \hbar = 1$ unless otherwise stated.

We discussed above the WEP, which can be restated as "uncharged free-falling test particles should follow the same trajectory if they have the same initial position and velocity". The Einstein equivalence principle (EEP) goes further. It states that "WEP is valid, and to free falling observers the laws of special relativity hold locally and are independent of position or velocity". These hold in General Relativity because all matter fields are minimally coupled to a single metric. We will follow the calculation of Ref. [84] to demonstrate below that the diffeomorphic invariance (which is essentially the absence of a preferred coordinate system) of the matter action leads to the conservation of the energy momentum tensor, which in turn means that test particles follow geodesics of the metric to which they are coupled, and thus WEP is ensured. Diffeomorphic invariance of the matter action says that

$$\pounds_\xi S_m = \frac{\delta S_m}{\delta g^{\mu\nu}} \pounds_\xi g^{\mu\nu} + \frac{\delta S_m}{\delta \psi^{(i)}} \pounds_\xi \psi^{(i)} = 0 \tag{1.8}$$

where $\pounds_\xi$ denotes the Lie derivative with respect to ξ^μ. The field equations of the matter fields are

$$\frac{\delta S_m}{\delta \psi^{(i)}} = 0 \tag{1.9}$$

and for a diffeomorphism

$$\delta g^{\mu\nu} = \nabla^{(\mu} \xi^{\nu)}. \tag{1.10}$$

Thus using eqs. (1.7), (1.9) and (1.10) in eq. (1.8) gives us

$$T_{\mu\nu} \nabla^\mu \xi^\nu = 0. \tag{1.11}$$

Integrating over a space on the boundary of which $\xi^\mu = 0$, gives

$$\int dx^4 \sqrt{-g} T^{\mu\nu} \nabla_\mu \xi_\nu = 0. \tag{1.12}$$

Integrating this by parts gives

$$\int dx^4 \sqrt{-g} \nabla_\mu T^{\mu\nu} \xi_\nu = 0 \tag{1.13}$$

because that boundary term vanishes. Furthermore ξ^μ is arbitrary away from the boundary, thus the only way eq. (1.13) can be satisfied is if the energy momentum tensor is conserved:

$$\nabla_\mu T^{\mu\nu} = 0. \tag{1.14}$$

We have shown that the energy momentum tensor is conserved. We now show that this leads to the geodesic motion of test particles.

Consider the energy momentum of a test particle, which we take to be an infinitesimal volume element of a pressureless fluid. This is given by

$$T^{\mu\nu} = \rho u^\mu u^\nu \tag{1.15}$$

where ρ is the mass density of the fluid and u^μ is its four-velocity. Taking the covariant derivative of this gives

$$\nabla_\mu(\rho) u^\mu u^\nu + \rho \nabla_\mu(u^\mu) u^\nu + \rho u^\mu \nabla_\mu(u^\nu) = 0. \tag{1.16}$$

Due to the normalisation of the four velocity, $u^\nu u_\nu = -1$, we have that

$$u_\nu \nabla_\mu(u^\nu) = \nabla_\mu(u^\nu u_\nu)/2 = 0. \tag{1.17}$$

Thus contracting eq. (1.16) with u_ν gives

$$\nabla_\mu(\rho) u^\mu + \rho \nabla_\mu(u^\mu) = 0. \tag{1.18}$$

The first two terms in eq. (1.16) cancel, which implies that four velocity of the fluid elements obey

$$u^\mu \nabla_\mu (u^\nu) = 0 \tag{1.19}$$

which is precisely the geodesic equation. Thus test particles follow geodesics of the metric and, in turn, WEP is respected.

At any point in spacetime we can take $g = \eta$, and then minimal coupling ensures that the matter Lagrangian will locally reduce to that of Minkowski space, thereby ensuring EEP is respected. The fact that the WEP and the EEP are ensured by minimal coupling of the matter fields to a single metric will be significant when we come to attempting to modify gravity in a viable way.

The above justifies the form of the matter Lagrangian in General Relativity. Lovelock's theorem [66] justifies the choice of the Einstein-Hilbert term for the gravitational sector. It says that the term is the unique choice given diffeomorphic invariance, second order field equations for the metric, a four dimensional spacetime, and no fields other than the metric appearing in the gravitational sector. Thus the form of eq. (1.1) is justified, with the constant in front of the Einstein-Hilbert term chosen such that the weak field limit recovers Newtonian gravity.

1.2 Cosmology

To describe cosmology we need to specify both our theory of gravity and the matter content of the universe. As we have said, the standard model of cosmology uses General Relativity and we have briefly reviewed some of its features above. We now move on to discuss cosmology. This will involve finding the form of the metric on cosmological scales, specifying the matter content of the universe and then solving eq. (1.2) to find the cosmological evolution of the universe.

The cosmological principle states that on the largest scales the universe is isotropic and homogeneous. This implies that, on the largest scales, the metric of the universe can be written as

$$ds^2 = -dt^2 + a^2(t)\gamma_{ij}dx^i dx^j \tag{1.20}$$

where $\gamma_{ij}dx^i dx^j$ is the metric for an isotropic, homogeneous 3-space. In particular spatial slices must have constant curvature, which means, in polar coordinates, they must take the form

$$\gamma_{ij}dx^i dx^j = \frac{dr^2}{1-kr^2} + r^2 d\theta^2 + r^2 sin^2\theta d\phi^2 \tag{1.21}$$

where $1/k$ has units of length squared, and k is zero, positive or negative for zero curvature, positive curvature or negative curvature respectively. Thus our metric is given by

$$ds^2 = -dt^2 + a^2(t)(\frac{dr^2}{1-kr^2} + r^2 d\theta^2 + r^2 sin^2\theta d\phi^2). \tag{1.22}$$

This metric is unchanged by the transformation

$$\begin{aligned} a &\to \lambda a \\ r &\to r/\lambda \\ k &\to \lambda^2 k. \end{aligned} \tag{1.23}$$

This freedom is used to set the value of the scale factor, a, to one at the present time, $a(t_0) = 1$.

Now that we have the form of the metric which describes the universe on the largest scales, we need to discuss how it evolves with time. The standard model of cosmology uses General Relativity, and therefore we can plug eq. (1.22) into the left-hand side of eq. (1.2). If one performs this calculation [12] one finds that the only non-zero components of the

Einstein tensor are

$$G^0{}_0 = 3((\dot{a}/a)^2 + k/a^2) \tag{1.24}$$

$$G^i{}_j = (2\ddot{a}/a + (\dot{a}/a)^2 + k/a^2)\delta^i_j. \tag{1.25}$$

We now need to specify the right-hand side of eq. (1.2). That is, specify the types of matter that make up the universe.

Homogeneity and isotropy of the energy momentum tensor implies that it must be of the form

$$T^\mu{}_\nu = (\rho + P)U^\mu U_\nu - P\delta^\mu_\nu \tag{1.26}$$

where U^μ is the four velocity of the fluid particle, and we identify ρ and P as the mass density and pressure of the fluid in its rest frame, respectively.

Most of the constituents of the total energy momentum have a constant equation of state, $\omega = P/\rho$. We use the value of ω to categorise the different constituents.

Matter is defined to be a substance with $\omega = 0$ and radiation is defined to have $\omega = 1/3$. Matter accounts for just over 30% of the universe's present day energy budget. Around 15% of this matter is protons, neutrons and electrons, collectively termed baryons by cosmologists, but the other 85% is termed "cold dark matter". Very little is known about cold dark matter, but it appears to be non-relativistic (cold) and not to interact with photons (dark). Its presence can be inferred from its gravitational effects, such as its effect on the rotation curves of galaxies [76]. The main component of radiation is photons, however for most of their history neutrinos have also behaved like radiation.

Finally we have that dark energy has $\omega = -1$. It is standard practice to move the second term on the left-hand side of eq. (1.2) onto the right-hand side. It can then be interpreted as a constituent of the energy momentum with $\omega = -1$.

The standard model of cosmology is known as ΛCDM as it supposes the existence of dark energy, Λ, and cold dark matter, CDM.

It follows from the conservation of the energy momentum tensor that

$$\dot{\rho} + 3\frac{\dot{a}}{a}(\rho + P) = 0. \tag{1.27}$$

This implies that

$$\rho \propto a^{-3(1+\omega)} \tag{1.28}$$

and so, denoting today's value with a subscript zero, we have

$$\rho_m = \rho_{m,0}/a^3 \tag{1.29}$$

$$\rho_r = \rho_{r,0}/a^4 \tag{1.30}$$

$$\rho_\Lambda \equiv M_{Pl}^2 \Lambda = \rho_{\Lambda,0} \tag{1.31}$$

where the subscripts m, r and Λ denote matter, radiation and dark energy.

Now that we have described the matter content of the universe we are in a position to write down the Friedmann equations. These are the equations that govern the evolution of the scale factor of the universe and are attained by substituting eq. (1.26) into eq. (1.2), which using eqs. (1.24) and (1.25) gives

$$(\frac{\dot{a}}{a})^2 = \rho/3M_{Pl}^2 - k/a^2 \tag{1.32}$$

$$\frac{\ddot{a}}{a} = -(\rho + 3P)/6M_{Pl}^2. \tag{1.33}$$

It is usual to write eq. (1.32) in terms of the Hubble parameter $H = \dot{a}/a$ and to break the energy density up into its constituent parts. We define the density parameters to be

$$\Omega_m = \rho_{m,0}/3H_0^2 M_{Pl}^2 \tag{1.34}$$

$$\Omega_r = \rho_{r,0}/3H_0^2M_{Pl}^2 \tag{1.35}$$

$$\Omega_\Lambda = \rho_{\Lambda,0}/3H_0^2M_{Pl}^2 \tag{1.36}$$

$$\Omega_k = -k/H_0^2. \tag{1.37}$$

Using eqs. (1.34) to (1.37) and eqs. (1.29) to (1.31), eq. (1.32) can be re-written as

$$H^2/H_0^2 = \Omega_r/a^4 + \Omega_m/a^3 + \Omega_k/a^2 + \Omega_\Lambda. \tag{1.38}$$

The observed values of the density parameters [12] are

$$\Omega_m \approx 0.32 \tag{1.39}$$

$$\Omega_r \approx 10^{-4} \tag{1.40}$$

$$\Omega_\Lambda \approx 0.68 \tag{1.41}$$

$$|\Omega_k| \lesssim 10^{-2}. \tag{1.42}$$

Because of the different dependencies of the terms in eq. (1.38) on the scale factor, different energy momentum constituents have dominated at different times in the history of the universe, as depicted in fig. 1.1. A period of radiation dominance preceded a matter dominated period and it now appears that the universe is exiting the matter dominated period and entering a dark energy dominated epoch.

1.3 Motivations for Modifying Gravity

As we have summarised in the previous section the universe is observationally consistent with gravity described by General Relativity and a ΛCDM matter content. Why then do we wish to modify gravity?

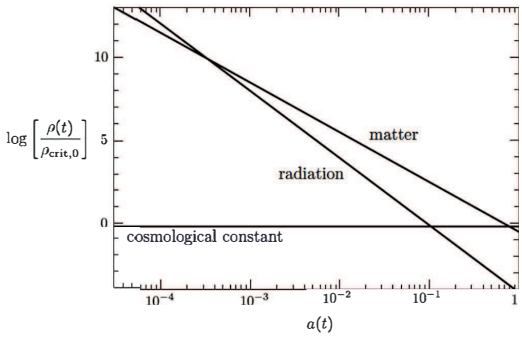

Fig. 1.1 Relative sizes of energy density during the universe's history. Figure from Ref. [12]

There are multiple motivations, but the most pressing seems to be what is known as "the cosmological constant problem". Essentially, this is the (large) disparity between the observed value of the cosmological constant and the value one would expect from considering the vacuum energy of standard model fields.

We have already shown that we observe dark energy to compose around seventy percent of the present day energy budget. That is

$$\Lambda_{obs} \sim 10^{-120} M_{Pl}^4. \tag{1.43}$$

However we have not ascribed the physical source of this energy momentum. In fact, the vacuum energy of standard model particles does provide a source of energy momentum with equation of state equal to minus one. However the theoretical size of the cosmological constant, Λ_{theory}, that the vacuum energy would provide is radically different from Λ_{obs}. The problem is least troublesome if we assume super-symmetry [49], for which particles with masses below the weak scale contribute to Λ_{theory}, but particles with masses above the weak scale do not because above this scale contributions from fermions and bosons cancel each other out. However, even making this assumption, one would expect [60]

$$\Lambda_{theory} \sim 10^{-60} M_{Pl}^4. \tag{1.44}$$

The cosmological constant problem is the fact that Λ_{theory} and Λ_{obs} differ by at least sixty orders of magnitude. One is left with the unsatisfying solution that the bare cosmological constant in the Lagrangian must be fine-tuned to at least sixty decimal places in order to (almost) cancel out the vacuum energy and give the observed cosmological constant value. There is no justification for doing this, other than to give the observed value.

The cosmological constant problem is sometimes split into two: the "old cosmological constant problem" and the "new cosmological constant problem". The old problem can be phrased as "why do we not observe the gravitational effect of the vacuum energy?" The new problem is "why does the cosmological constant take the value that it does?" Proposed solutions to the old problem include anthropic string theory arguments [88] and arguments that, in the absence of matter or radiation, Minkowski space solutions exist despite the non-zero vacuum energy; this is known as self-tuning [32, 31, 35]. The new problem is often addressed by pre-supposing that the old problem has been solved, and the cosmological constant due to the vacuum energy is exactly zero. A mechanism is then proposed that generates a cosmological constant of the observed value.

A related problem in cosmology is known as the coincidence problem. This is the problem that the present day energy densities of matter and dark energy are of the same order of magnitude. We showed in eqs. (1.29) and (1.31) that matter and dark energy scale differently with the scale factor. Therefore that we happen to exist within, on cosmological time scales, the small time window in which the two energy densities are of similar size appears to be a coincidence.

No quantum description of gravity exists but string theory [49] attempts to provide a possible answer . A generic problem with string theories is that scalar fields remain at low energies, and Kaluza-Klein theories have a scalar related to the size of a compactified fifth dimension. This provides further motivation for looking at scalar fields in a gravitational context, in addition to attempting to address existing problems in cosmology.

Although many modified gravity models were spawned by an attempt to address the cosmological constant problem, or other problems in cosmology, no compelling answer has been found. The field of modified gravity now fulfils a wider brief of attempting to explore the ways in which gravity can be modified or extended, in a plausible, observationally viable way. At the very least, these modified gravity models provide inspiration for finding novel ways of testing General Relativity that would not have been thought of otherwise.

1.4 Theories of Modified Gravity

1.4.1 Equivalence Principles

In section 1.1 we discussed the importance of the equivalence principles to Einstein during his development of General Relativity. In this section we first discuss the equivalence principles in the context of modified gravity and then move on to describe scalar-tensor theories.

We specified at the end of section 1.1 the four conditions that pin down the Einstein-Hilbert action as unique for the gravitational sector. As Ref. [84] describes, relaxing any of these assumptions will generically lead to more degrees of freedom. In a theory that contained higher derivatives, more derivatives of the field would need to be specified in the initial data. A theory that is not diffeomorphically invariant can be made so by adding in extra fields and choosing them to transform in a certain way. These fields are called Stuckelberg fields and this is known as the Stuckelberg trick [87]. Finally, we would expect a higher dimensional theory to have an effective four dimensional theory which, in order to differ from General Relativity, would have to violate one of the other three requirements.

Thus extending General Relativity usually involves adding in extra degrees of freedom. However note that the argument given in section 1.1 that WEP and EEP hold for General Relativity relies only on the fact that matter fields are minimally coupled to a single metric, and (in the frame of this metric) assumes nothing about the gravitational sector. Thus scalar-

tensor theories are simple extensions to General Relativity in which a scalar is added to the gravitational sector[2] and matter fields minimally coupled to the metric, so WEP and EEP are automatically satisfied.

We now briefly comment on the third equivalence principle. The strong equivalence principle (SEP) extends EEP such that massive gravitating objects follow the same trajectories, as well as test particles. This holds in General Relativity but it is violated in scalar-tensor theories. This is because the charge to mass ratio of objects can vary, which affects how objects fall in an external field. The details vary between particular scalar-tensor theories, but in all theories a black hole falls differently to a test particle, which is one of the reasons that the study of black holes maybe a fruitful area to test scalar-tensor theories against General Relativity. It has been used [58, 80] to analyse the offset of supermassive black holes from the centre of their host galaxy.

1.4.2 Scalar-Tensor Theories

The action of a scalar-tensor theory can be written in the Jordan frame as

$$S = \int dx^4 \sqrt{-\tilde{g}} \left(\tilde{F}(\phi)\tilde{R} + \tilde{G}(\phi, \nabla\phi, \nabla\nabla\phi) \right) + S_m(\psi^{(i)}, \tilde{g}_{\mu\nu}). \tag{1.45}$$

The first part of the action is the gravitational sector, which includes non-minimal coupling of the scalar to the Ricci scalar, together with a function to make the scalar dynamical. The second term is the matter sector. In this frame the energy momentum tensor is conserved, for exactly the same reasoning as in General Relativity, and test particles move on geodesics of $\tilde{g}_{\mu\nu}$. It is useful to make a conformal transformation $\tilde{g}_{\mu\nu} = A^2(\phi) g_{\mu\nu}$, such that the non-minimal coupling of the scalar is removed. This means that the field equations look like General Relativity, with the scalar contributing to the energy momentum of the

[2] this is a frame-dependent statement that is true in the Jordan frame

matter fields. In this frame the action takes the form

$$S = \int dx^4 \sqrt{-g} \left(\frac{M_{Pl}^2}{2} R + G_E(\phi, \nabla\phi, \nabla\nabla\phi) \right) + S_m(\psi^{(i)}, A^2(\phi) g_{\mu\nu}). \tag{1.46}$$

The removal of the non-minimal coupling comes at the cost that the scalar now appears in the matter sector. This means that the energy momentum tensor is not conserved and the scalar mediates a "fifth force" between standard model fields. At the end of section 1.1 we argued from the action that the conservation of the energy momentum tensor led to geodesic motion. Now we are in the Einstein frame, conservation of the energy momentum tensor is replaced by

$$\nabla_\mu T^{\mu\nu} = g_{\alpha\beta} T^{\alpha\beta} \frac{dlnA}{d\phi} \nabla^\nu \phi. \tag{1.47}$$

A similar argument to that of section 1.1 then gives that, instead of geodesic motion, the four velocity of a test particle is given by

$$u^\mu \nabla_\mu u^\nu = \frac{\beta}{M_{Pl}} \nabla^\mu \phi \tag{1.48}$$

where

$$\beta = M_{Pl} \frac{dlnA}{d\phi}. \tag{1.49}$$

The term on the right-hand side of eq. (1.48) is interpreted as a fifth force which causes the particle to deviate from geodesic motion.

Observations, such as those in the solar system, place constraints upon the strength of this force, and so screening mechanisms are needed to reduce the strength of the force in high density environments, whilst allowing it to compete with gravity on the largest scales.

1.4.3 Couplings to Matter

We showed in section 1.4.1 that the coupling of matter to a single metric was sufficient to ensure that the WEP was satisfied and in eq. (1.46) we assumed that this metric was conformally related to the Einstein metric. This is a standard assumption that most models make; it is covariant and ensures that a vector that is timelike, null or spacelike with respect to one metric is likewise with respect to the other. However in Ref. [13] Bekenstein showed that a more general relationship between the two metrics is permitted. In a theory that obeys causality, the Jordan frame metric can, in the most general case, take the form

$$\tilde{g}_{\mu\nu} = A^2(g_{\mu\nu} + B\partial_\mu\phi\partial_\nu\phi/M^4) \tag{1.50}$$

where the additional term is called a disformal factor, and $B > 0$. Furthermore, A and B can be functions of both ϕ and $(\partial\phi)^2$. Disformal factors occur naturally in some theories [40, 41] and it has even been suggested that a disformal screening mechanism exists [65]. We will discuss the effects of disformal couplings within K-mouflage theories in chapter 3 but for the rest of the thesis we will presume a conformal-only coupling. For conformally coupled fields there are three classes of screening mechanism, which we shall introduce in the next section.

1.5 Screening Mechanisms

Deviations from the inverse square law potential can be parameterised by the addition of a Yukawa interaction, giving a potential of the form

$$V(r) = -\frac{G_N m}{r}(1 + \alpha e^{-r/\lambda}). \tag{1.51}$$

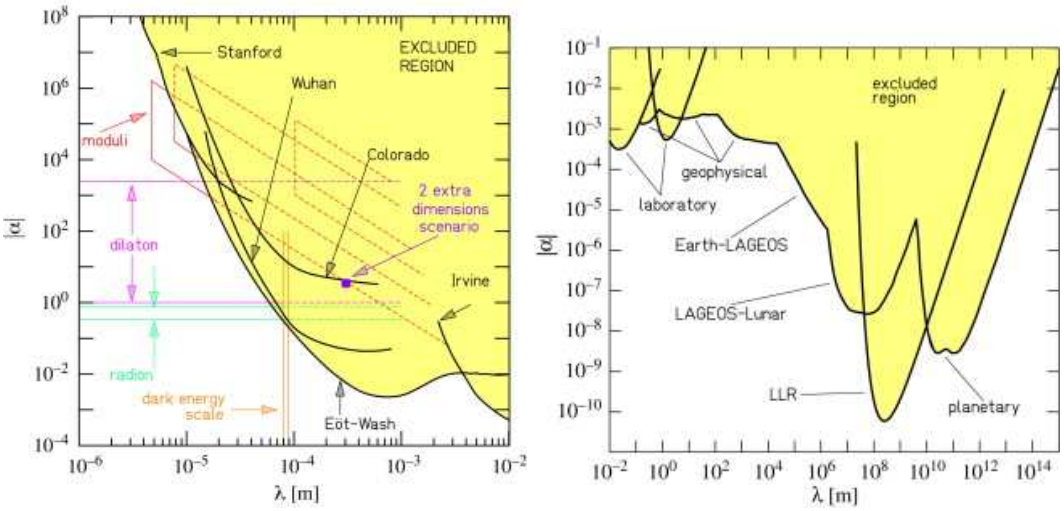

(a) $\lambda \leq 1cm$ (b) $\lambda \geq 1cm$

Fig. 1.2 Constraints on Yukawa couplings. Figure from Ref. [6]

A raft of solar system tests can then be used to constrain the $\alpha - \lambda$ parameter space, the results of which are shown in fig. 1.2. To suppress the deviations from Newtonian gravity the second term in eq. (1.51) must be small. One way to achieve this is to have λ large, or equivalently, for the scalar to be heavy, and fig. 1.2a shows that if this is the case, α does not need to be small.

However if λ is not large, then to suppress deviations from Newtonian gravity α must be to be small. For scalar-tensor theories without a screening mechanism

$$\alpha = 2\beta^2 \tag{1.52}$$

and so β must be fine tuned. Therefore to avoid fine-tuning β to be small, any scalar must either be sufficiently heavy, or have a screening mechanism. The Chameleon mechanism allows the scalar to be sufficiently heavy on solar system scales for β to be unconstrained, whilst also allowing the scalar to become sufficiently light on cosmological scales to influence cosmology. In contrast K-mouflage and Galileon theories use non-linearities in the kinetic structure to suppress the field in the solar system.

Screening mechanisms, can broadly be separated into three classes. Those that are potential based, the most widely studied of these is known as the Chameleon mechanism which screens in regions of high Newtonian potential; those which screen when the Newtonian gravitational force is sufficiently large, such as K-mouflage theories; and those that screen when the curvature exceeds a certain value, such as Galileon theories. We now review these mechanisms.

1.5.1 Chameleons

Chameleon models were first considered in Ref. [61, 62, 25]. They are usually formulated in the Einstein frame, in which the action is

$$S = \int dx^4 \sqrt{-g} \left(\frac{M_{Pl}^2}{2} R - \frac{1}{2} \nabla_\mu \phi \nabla^\mu \phi - V(\phi) \right) + S_m(\psi^{(i)}, A^2(\phi) g_{\mu\nu}) \tag{1.53}$$

where typically

$$V(\phi) = \Lambda_c^{n+4} / \phi^n \tag{1.54}$$

and

$$A(\phi) = exp(\beta \phi / M_{Pl}). \tag{1.55}$$

One usually takes $\beta > 0$ and n a positive integer, although negative n behaviours have also been considered. The key to the Chameleon mechanism is that the mass of the scalar is environmentally dependent. In dense environments the field becomes heavy, and mediates only a short range force, whereas the scalar becomes light in sparse environments and mediates a long range force. This means that the effects of the scalar can be screened in the relatively dense solar system but not at cosmological densities.

The field equation for the scalar derived from eq. (1.53) is

$$\Box \phi = V'(\phi) - \beta T / M_{Pl}. \tag{1.56}$$

This motivates the definition of

$$V_{eff}(\phi) = V(\phi) + \rho lnA(\phi) \tag{1.57}$$

where we have replaced the trace of the energy momentum tensor with the matter density, and in so doing have assumed that the matter is non-relativistic. Now eq. (1.56) can be recast so that the source term is given as the derivative of an effective, density dependent, potential;

$$\Box\phi = V'_{eff}(\phi;\rho). \tag{1.58}$$

One can check that the effective mass of the Chameleon,

$$m^2_{eff}(\rho) = \frac{\partial^2 V_{eff}(\phi_{min})}{\partial\phi^2} \tag{1.59}$$

where ϕ_{min} obeys $V'_{eff}(\phi_{min}) = 0$, is indeed an increasing function of the mass density, for a potential and coupling function of the form of eqs. (1.54) and (1.55) and n positive. This mechanism can be seen in graphically in fig. 1.3. The component of the effective potential that depends on matter is a straight line with a gradient proportional to the matter density. Therefore increasing this gradient pushes the minimum of the effective potential to a lower value of ϕ, and thus increases the curvature around the minimum of the effective potential.

To calculate the profile that a static spherically symmetric object sources one must solve eq. (1.58). Under these assumptions eq. (1.58) becomes a second order ordinary differential equation which needs two boundary conditions to solve. Imposing regularity at the origin and that the field approaches the minimum of the effective potential at spatial infinity will then specify the solution entirely. The full solution would need to be found numerically but good estimates can be found which we detail below.

The heavy mass of the Chameleon field means that, for a dense object embedded in a sparse environment, the field sits at the minimum of the effective potential for almost the

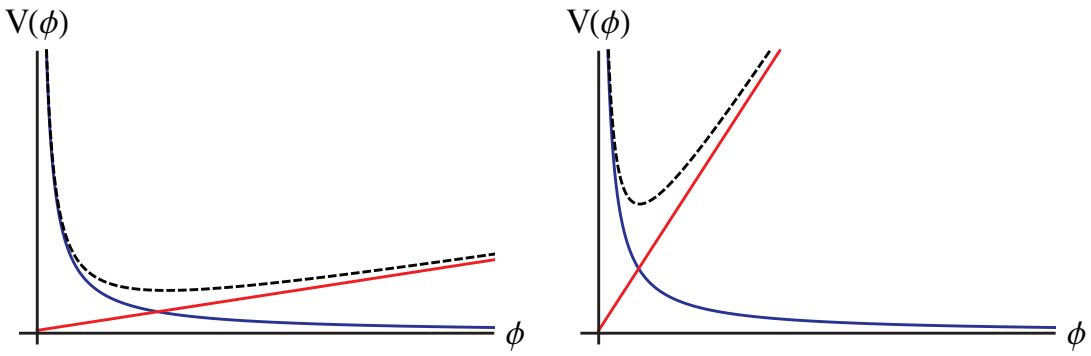

Fig. 1.3 Graphical demonstration of the Chameleon mechanism. Low density environment on the left. High density on the right. Blue line shows the bare potential and red line shows the contribution from matter coupling. The dotted line is the effective potential. Figure from Ref. [28].

entirety of the interior of the object, and therefore only a thin shell of the object sources an external field. As the mass of the entire object sources the gravitational field, the fifth force will be suppressed relative to the gravitational force.

We now follow Ref. [28] to explain how to calculate the thickness of the shell.

Consider a static spherically symmetric source of density ρ_{obj} and radius R embedded in a background of density ρ_{bg} where $\rho_{obj} \gg \rho_{bg}$. Then eq. (1.58) becomes

$$\frac{1}{r^2}\frac{d}{dr}(r^2\frac{d\phi}{dr}) = V'(\phi) + \beta\rho/M_{Pl} \tag{1.60}$$

where we have restricted to the case of a constant β. Restoring the dependence of β on ϕ does not change the argument provided the dependence is sufficiently weak, as is normally assumed.

We first linearise eq. (1.60) about $\bar{\phi}$ the minimum of the effective potential at the background density. Outside the object this amounts to

$$\frac{1}{r^2}\frac{d}{dr}(r^2\frac{d\phi}{dr}) = m_0^2(\phi - \bar{\phi}) \tag{1.61}$$

where $m_0^2 = V''(\bar{\phi})$. Inside the object eq. (1.60) becomes

$$\frac{1}{r^2}\frac{d}{dr}(r^2\frac{d\phi}{dr}) = m_0^2(\phi - \bar{\phi}) + \beta(\rho_{obj} - \rho_{bg})/M_{Pl}. \tag{1.62}$$

In practice the second term will dominate over the first and so eq. (1.62) will become

$$\frac{1}{r^2}\frac{d}{dr}(r^2\frac{d\phi}{dr}) = \beta(\rho_{obj} - \rho_{bg})/M_{Pl} \approx \beta\rho_{obj}/M_{Pl}. \tag{1.63}$$

Deep inside the object ϕ will simply take the value ϕ_{obj} where $V_{eff}(\phi_{obj};\rho_{obj}) = 0$. We then assume that the field remains at $\phi = \phi_{obj}$ up to a radius r_*, which we call the screening radius. Integrating eq. (1.63) from the screening radius gives

$$\frac{d\phi}{dr} = \frac{\beta(M(r) - M(r_*))}{4\pi M_{Pl} r^2} \tag{1.64}$$

where $M(r)$ is the mass enclosed in a sphere of radius r. Integrating eq. (1.64) then gives

$$\phi - \phi_{obj} = \frac{\beta M(r_*)}{4\pi M_{Pl}}(\frac{1}{r} - \frac{1}{r_*}) + \int_{r_*}^{r} dr \frac{\beta M(r)}{4\pi M_{Pl} r^2}. \tag{1.65}$$

Applying integration by parts on the second term then gives

$$\phi - \phi_{obj} = -\frac{\beta(M(r) - M(r_*)}{4\pi M_{Pl} r} - \int_{r_*}^{r} dr' 4\pi\rho_{obj} r'. \tag{1.66}$$

Outside the object the solution to eq. (1.61) is given by

$$\phi - \bar{\phi} \propto e^{-m_0 r}/r. \tag{1.67}$$

The coefficient can be found using eq. (1.64) to match the derivative of the scalar at the surface of the scalar. Assuming that $m_0 R \ll 1$, this gives that the exterior solution is

$$\phi - \bar{\phi} = -\frac{\beta(M(R) - M(r_*))}{4\pi M_{Pl} r} \tag{1.68}$$

which is indeed the solution to the Poisson equation sourced by only the shell outside of the screening radius.

To find the screening radius we evaluate both eqs. (1.66) and (1.68) at R and subtract one from the other. This gives an implicit formula for r_*:

$$\bar{\chi} = \frac{\bar{\phi}}{2\beta M_{Pl}} = \int_{r_*}^{R} dr' r' \rho_{obj} \tag{1.69}$$

where we used that $\phi_{obj}/\bar{\phi} \ll 1$. The eq. (1.69) can be re-written in terms of the Newtonian potential,

$$\bar{\chi} + \Phi_N(r_*) = -r_* \Phi_N'(r_*). \tag{1.70}$$

Because $\Phi_N'(r) > 0$ the right-hand side of eq. (1.70) is always negative. Therefore to have a solution one must have $\bar{\chi} < -\Phi_N(r_*) \approx GM/R$. The object will be fully screened if $\bar{\chi} \ll GM/R$, but unscreened if $\bar{\chi} > GM/R$.

Despite the screening mechanism, the Chameleon models are now well constrained by a combination of laboratory and astrophysical observations [28]. The exclusion zones for $n = 1$ Chameleon theories, in terms of $M_c = M_{pl}/\beta$ and Λ_c are displayed in fig. 1.4.

1.5.2 Galileons

Galileons first appeared in the Dvali-Gabadedze-Porrati (DGP) braneworld scenario [42]. In braneworld scenarios the observable four dimensional universe exists on what is known as a brane within a higher dimensional space. In DGP the Galileon describes the brane

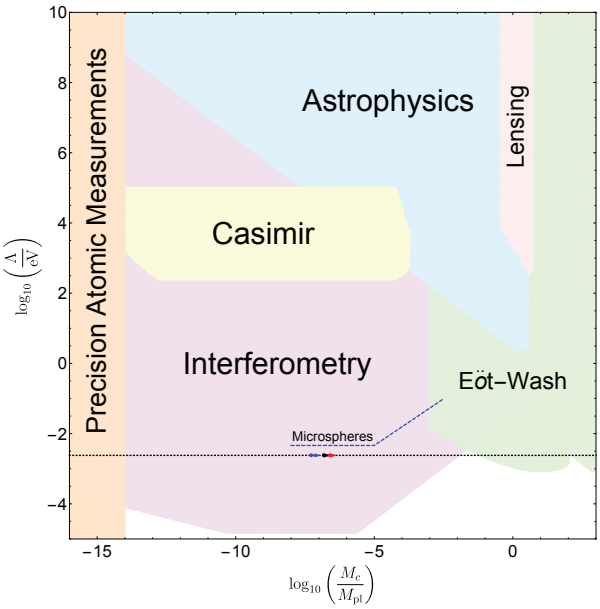

Fig. 1.4 Current bounds on $n = 1$ Chameleon models. Figure from Ref. [28]

bending of a four dimensional brane in five dimensional Minkowski space. Galileon scalars have a shift symmetry $\phi(x) \to \phi(x) + c + b_\mu x^\mu$ which is inherited from Galilean invariance of the higher theory, and gives them their name. Galileons have been used to attempt to address cosmic acceleration [33, 82, 47] and inflation [8, 64, 26] and also appear as the longitudinal polarisation in limits of massive gravity [89, 50]. Further to having the shift symmetry, Galileons are required to have second order equations of motion. This is in order to avoid the Ostrogradski ghost that appears generically in field equations with higher order derivatives [92]. In four dimensions there are in fact only five possible Galileon terms:

$$L_1 = \phi, \tag{1.71}$$

$$L_2 = \frac{1}{2}(\partial\phi)^2, \tag{1.72}$$

$$L_3 = \Box\phi(\partial\phi)^2, \tag{1.73}$$

$$L_4 = \frac{1}{4}(\partial\phi)^2\left((\Box\phi)^2 - (\partial_\mu\partial_\nu\phi)^2\right), \tag{1.74}$$

and

$$L_5 = \frac{1}{3}(\partial\phi)^2\big((\Box\phi)^3 + 2(\partial_\mu\partial_\nu\phi)^3 - 3\Box\phi(\partial_\mu\partial_\nu\phi)^2\big). \tag{1.75}$$

This gives an Einstein frame action of

$$S = \int dx^4\sqrt{-g}\left(\frac{M_{Pl}^2}{2}R + \Sigma_{i=1}^5 c_i L_i\right) + S_m(\psi^{(i)}, A^2(\phi)g_{\mu\nu}). \tag{1.76}$$

To covariantise the Galileon, for the first three terms the usual prescription $\eta_{\mu\nu} \to g_{\mu\nu}$ and $\partial_\mu \to \bigtriangledown_\mu$ suffices. However, for the quartic and quintic terms, non-minimal couplings between the metric and scalar are required to ensure second order equations of motion for both the metric and the scalar, giving

$$L_4 = \frac{1}{4}(\bigtriangledown\phi)^2\big((\Box\phi)^2 - (\bigtriangledown_\mu\bigtriangledown_\nu\phi)^2 - \frac{1}{4}(\bigtriangledown\phi)^2 R\big) \tag{1.77}$$

and

$$L_5 = \frac{1}{3}(\bigtriangledown\phi)^2\big((\Box\phi)^3 + 2(\bigtriangledown_\mu\bigtriangledown_\nu\phi)^3 - 3\Box\phi(\bigtriangledown_\mu\bigtriangledown_\nu\phi)^2 - 6G_{\nu\rho}\bigtriangledown_\mu\phi\bigtriangledown^\mu\bigtriangledown^\nu\phi\bigtriangledown^\rho\phi\big). \tag{1.78}$$

Upon covariantising the shift symmetry $\phi \to \phi + c$ remains but the symmetry $\phi \to \phi + b_\mu x^\mu$ is lost. Galileons exhibit screening through what is known as the Vainshtein mechanism. The field is screened when the second derivative of the field gets large compared with some energy scale, usually inherited from a higher theory.

We now demonstrate the Vainshtein mechanism for the cubic Galileon in Minkowski space. The Lagrangian for the cubic Galileon in Minkowski space can be written as

$$\mathscr{L} = -\frac{1}{2}(\partial\phi)^2 - \frac{\alpha_3}{\mathscr{M}^3}\Box\phi(\partial\phi)^2 + \frac{\beta}{M_{Pl}}\phi T. \tag{1.79}$$

For a static, spherically symmetric field around a point particle of mass M, eq. (1.79) gives an scalar equation of

$$\frac{\phi'(r)}{r\mathscr{M}^3}+\alpha_3(\frac{\phi'(r)}{r\mathscr{M}^3})^2=\frac{\beta M}{4\pi M_{Pl}\mathscr{M}^3 r^3}. \tag{1.80}$$

The left-hand side of eq. (1.80) is a polynomial in $\phi'(r)/r\mathscr{M}^3$. Therefore far away from the object, when the right-hand side is small, the first term dominates and

$$\phi'(r)\approx\frac{\beta M}{4\pi M_{Pl}r^2} \tag{1.81}$$

which is of gravitational strength. Close to the object the right-hand side will be large and so the second term will dominate. This will give

$$\phi'(r)\approx(\frac{\beta M\mathscr{M}^3}{4\pi\alpha_3 M_{Pl}r})^{1/2}. \tag{1.82}$$

Because this scales like $\sim 1/\sqrt{r}$ and the Newtonian force scales like $\sim 1/r^2$, the fifth force will be suppressed relative to gravity. The transition between the dominance of the different terms happens at the Vainshtein radius, within which we have screening. The Vainshtein radius is given by

$$r_v=(\frac{\beta M\alpha_3^{1/2}}{M_{Pl}\mathscr{M}^3})^{1/3}. \tag{1.83}$$

For β and α_3 order unity, and $\mathscr{M}^3=M_{Pl}H_0^2$ the Vainshtein radius of the Sun is much larger than the solar system, and so the solar system is a screened environment. As the right hand side of eq. (1.80) $\sim\nabla^2\Phi_N$ and, in the Newtonian limit $R\sim\nabla^2\Phi_N$, the screening operates in regions of higher curvature.

In part, interest in Galileons was developed because, on top of exhibiting a screening mechanism, they also exhibit self-accelerating solutions [71] that dispense with the need for

a cosmological constant. However these solutions have now been constrained by both various observations [63, 67, 73] and theoretical considerations [7, 39]. Self-accelerating cubic Galileons have now been ruled out [74]. This is due to their effect on the red shifting of photons; specifically cubic Galileon theories predict a negative integrated Sachs-Wolfe effect that is in conflict with observations. Another particularly stringent constraint comes from gravitational waves. Upon covariantisation, non-minimal couplings between the quartic and quintic Galileons and the metric must be introduced to maintain second order equations of motion, which implies that gravitational waves and electromagnetic waves can travel at different speeds. The first direct detection of gravitation waves [1, 2] added a new tool with which to probe modified gravity theories. Recently a binary neutron star merger [4, 3] was observed. Both electromagnetic waves and gravitational waves were measured arriving at Earth within seconds of each other after having travelled around 40Mpc across the universe. Consequently the speeds of gravitational waves and electromagnetic waves in these theories must be extremely close and this heavily constrains the parameters of the theories [79]. However, the cubic Galileon is unaffected as gravitational and electromagnetic waves always travel at the same speed in this theory.

1.5.3 K-mouflage

K-mouflage theories are similar to, but less studied than, Galileon theories. The main difference is that the screening takes place when the first derivative of the field is made large, as opposed to the second as is the case for Galileons. They were introduced in Ref. [10] as a theory with an inherent screening mechanism and then made more relevant to cosmology in Ref. [22]. These theories are formulated in the Einstein frame. The theories are usually taken to be without a potential, and the canonical kinetic term in the Lagrangian, $-\frac{1}{2}(\partial\phi)^2$, is replaced by the function $\mathscr{M}^4K(\chi)$ where $\chi = -\frac{1}{2\mathscr{M}^4}(\partial\phi)^2$, $\mathscr{M}$ is some energy scale, and the field is coupled to matter. This gives an action of

$$S = \int dx^4 \sqrt{-g} \left(\frac{M_{Pl}^2}{2} R + \mathscr{M}^4 K(\chi) \right) + S_m(\psi^{(i)}, A^2(\phi) g_{\mu\nu}). \tag{1.84}$$

In this thesis we will simplify our analysis by considering only polynomial $K(\chi)$. Furthermore we will restrict $K(\chi)$ to the form

$$K(\chi) = -1 + \chi + ... \tag{1.85}$$

where the ellipsis denotes higher order powers of χ. This restriction is made so that a canonical scalar with cosmological constant is recovered in the weak field limit. In the weak field regime the canonical term dominates, but in high density regions the non-linear terms become dominant and so screen the field. This can be seen explicitly in Minkowski space around a point mass. Take the illustrative example of $K(\chi) = -1 + \chi - \chi^2$. For this the Lagrangian is

$$\mathscr{L} = -\mathscr{M}^4 - \frac{1}{2}(\partial\phi)^2 - \frac{1}{4\mathscr{M}^4}(\partial\phi)^4 + \frac{\beta}{M_{Pl}}\phi T \tag{1.86}$$

where $T = -M\delta^{(3)}(x)$. As we did for the Galileon, we impose staticity and spherical symmetry. Then, the equation of motion derived is

$$\phi'(r) + \frac{1}{\mathscr{M}^4}\phi'(r)^3 = \frac{\beta M}{4\pi M_{Pl} r^2}. \tag{1.87}$$

At large r the field is simply

$$\phi'(r) = \frac{\beta M}{4\pi M_{Pl} r^2} \tag{1.88}$$

and hence the fifth force, which is proportional to $\nabla^\mu \phi$, is of gravitational strength. However at small r, the gradient of the field is

$$\phi'(r) = \left(\frac{\beta M \mathscr{M}^4}{4\pi M_{Pl} r^2}\right)^{\frac{1}{3}} \tag{1.89}$$

and so is suppressed relative to gravity. This transition happens at the K-mouflage radius,

$$R_K = (\frac{\beta M}{4\pi M_{Pl}\mathscr{M}^2})^{1/2}. \tag{1.90}$$

For example if we take $\beta = 1$ and $\mathscr{M}^4 = H_0^2 M_{pl}^2$ - natural choices as this has β of order unity and $\mathscr{M}$ around the dark energy scale - the K-mouflage radius of the Sun is approximately $10000\,AU$ and hence the solar system (around $100\,AU$ in extent) is screened. This is the essence of the K-mouflage mechanism: non-linearities suppress the scalar around massive objects such as the Sun and so solar system tests can be passed while still allowing the scalar to be a significant player on cosmological scales. Despite screening, constraints do still exist as discussed in Ref. [11]. In particular K-mouflage models' predictions of a deviation from the Newtonian potential in the Earth-Moon system are used to constrain the matter coupling, relatively independently of the functional form of $K(\chi)$, to have $|A(\phi) - 1| \lesssim 0.1$. Unlike Galileons, the right-hand side of eq. (1.87) $\sim \nabla\Phi_N$ and so K-mouflage models screen in regions of high Newtonian gravitational force.

The cosmological behaviour of K-mouflage models was considered in Ref. [23] and the parameters of the theory were constrained by imposing that background cosmological evolution was matter dominated at early times and that the universe has entered a dark energy dominated era. Interestingly Ref. [15], which further constrained the theory using the CMB power spectrum, found that significant constraints could be imposed upon forms of K-mouflage theories that exactly reproduced the same expansion history as ΛCDM, which they termed "K-mimic" theories. Screening of the solar system is a necessary but not sufficient condition for a viable theory because the solar system tests are so accurate that they may still be able to pick up the small deviations from General Relativity that exist in a screened environment. Bounds on the fifth force from the Cassini Probe and the anomalous perihelion of the Moon's orbit from lunar ranging were used in Ref. [11] to constrain K-mouflage further. K-mouflage theories have also been considered in Ref. [24].

1.6 Black Holes and Scalar Fields

Black holes are one of the numerous environments in which modified gravity theories must be tested. Black holes will form through gravitational collapse, a time-dependent process, however we expect them to settle down to a time-independent solution. Thus it is of interest to try to classify all stationary black hole solutions. In General Relativity a Kerr-Newman black hole is the most general stationary black hole (modulo some assumptions of analyticity) [52]. It is described by only three numbers - it's charge, angular momentum and mass. Wheeler termed this the "no-hair" theorem of black holes.

1.6.1 No-Hair Theorem

In scalar-tensor theories there are numerous no-hair theorems, but no general, all encompassing one. Standard scalar-tensor theories do have a no-hair theorem. We will now follow Ref. [83] to review the no-hair argument.

By standard scalar-tensor theory we mean those for which the action, in the Einstein frame, can be written as

$$S = \int dx^4 \sqrt{-g} \left(\frac{M_{Pl}^2}{2} R - \frac{1}{2} (\partial \phi)^2 - V(\phi) \right) + S_m(\psi^{(i)}, A^2(\phi) g_{\mu\nu}). \tag{1.91}$$

This gives rise to the vacuum equations of motion

$$\Box \phi = V'(\phi) \tag{1.92}$$

$$M_{Pl}^2 G_{\mu\nu} = \nabla_\mu \phi \nabla_\nu \phi - g_{\mu\nu} \nabla_\mu \phi \nabla^\mu \phi / 2 - V(\phi). \tag{1.93}$$

We multiply eq. (1.92) by $\sqrt{-g} V'(\phi)$ and integrate over a region $\mathscr{V}$, bounded by part of the black hole event horizon, a timelike 3-surface at infinity, and two spacelike surfaces, one of which lies a unit parameter distance of the timelike killing vector field to the future of the

other. This gives

$$\int_{\mathscr{V}} dx^4 \sqrt{-g} \left(V'(\phi) \Box \phi - V'(\phi)^2 \right) = 0. \tag{1.94}$$

We integrate by parts on the first term of eq. (1.94) to give

$$\int_{\partial \mathscr{V}} dx^3 \sqrt{|h|} n_\mu \nabla^\mu \phi V'(\phi) - \int_{\mathscr{V}} dx^4 \sqrt{-g} \left(V''(\phi) \nabla^\mu \phi \nabla_\mu \phi + V'(\phi)^2 \right) = 0 \tag{1.95}$$

where n_μ is the unit normal to the boundary and h is the determinant of the induced metric on the boundary. The contributions from the surfaces at the horizon and infinity vanish[3] and contributions from the other two surfaces exactly cancel each other. This leaves

$$S = \int_{\mathscr{V}} dx^4 \sqrt{-g} \left(V''(\phi) \nabla^\mu \phi \nabla_\mu \phi + V'(\phi)^2 \right) = 0. \tag{1.96}$$

$V''(\phi) > 0$ is required for stability and so, assuming this, the integrand is non-negative, so we must have $\phi = \phi_0$, a constant that satisfies $V'(\phi) = 0$.

Considering the right-hand side of eq. (1.93), the scalar energy momentum tensor of this solution is $-V(\phi_0) g_{\mu\nu}$ and so asymptotic flatness requires further that $V(\phi_0) = 0$. If this is the case, eq. (1.93) becomes simply the vacuum equations for General Relativity. By Wheeler's no-hair theorem, the black hole must therefore be a Kerr-Newman black hole.

1.6.2 Evasions of the No-Hair Theorems

We now discuss possible evasions of the above argument. The first point is a subtle one. In the above argument we assumed axis-symmetry, but Hawking's rigidity theorem assumes the weak energy condition. If this holds for the energy momentum of the scalar then this is

[3] The contribution from the surface at infinity vanishes because ϕ tends to a constant as $r \to \infty$. The contribution from the surface at the horizon vanishes because, by Hawking's rigidity theorem [51], the spacetime will be axis-symmetric. The normal to the horizon is a linear combination of the two killing vectors. Because the scalar is assumed to respect the symmetries of the spacetime this implies that the integrand vanishes.

fine. If it does not then the axis-symmetry would have to be assumed additionally, and so stationary non-axis-symmetric solutions are not excluded.

Secondly we could alter the boundary conditions. For cosmological applications this may be particularly relevant as boundary conditions can be used to try to embed the solution in a cosmological setting. It has been shown that hair can be created as a result of time-evolving boundary conditions, albeit suppressed by ratios of the relevant cosmological and system timescales [55].

Also it was assumed above that the scalar field obeyed the same symmetries as the metric. However this is not implied by the equations of motion. For example theories with a shift symmetry $\phi \to \phi + c$ have only derivatives appearing in the field equations, and hence applying symmetries to the scalar itself is overly restrictive.

In this thesis we will exclusively consider real scalar fields, as is assumed in the argument of section 1.6.1. However considering complex fields around a black hole is an active area of research. In some instances [14, 72] no-hair theorems have been extended to cover theories with complex fields, however it has also been shown that stationary hairy black holes do exist [53, 54].

A further change one could make would be to add matter around the exterior of the black hole. In this case eq. (1.92) is replaced by

$$\Box\phi = V'(\phi) - A'(\phi)T_E/A(\phi) \tag{1.97}$$

where T_E is the trace of the Einstein frame energy momentum tensor. Now for any hairless solution to exist we require $V'(\phi)$ and $A'(\phi)$ to have zeroes that coincide. If this is the case then the General Relativity solution $\phi = \phi_0$ will exist, but it may not be unique. Around compact objects it has been shown that the General Relativity solutions are energetically preferable up to a certain threshold of compactness, beyond which non-trivial scalar field profiles are energetically preferred - a phenomenon known as spontaneous scalarisation.

This phenomenon can also be observed in black holes with external matter. Ref. [29] showed that the density of external matter can affect whether or not the General Relativity solution is energetically favoured.

1.6.3 Additional No-Hair Theorems

In this thesis we look at theories with non-canonical kinetic terms which therefore cannot be written in the form of eq. (1.91). They do not have a general no-hair theorem - although for vacuum, static, spherically symmetric solutions one is given in Ref. [59] and one for another special case is given in Ref. [48]. The argument of Ref. [59] goes as follows and applies to any theory with a shift symmetry $\phi \to \phi + c$. This symmetry means that the equations of motion can be written as a conserved current

$$\bigtriangledown_\mu J^\mu = 0. \tag{1.98}$$

We take the metric to be

$$ds^2 = -f dt^2 + f^{-1} dr^2 + R(r)^2 d\Omega^2 \tag{1.99}$$

with the event horizon at a zero of $f = f(r)$. By staticity and spherical symmetry J^r is the only non-zero component of J^μ and so eq. (1.98) implies that

$$R(r)^2 J^r = Constant. \tag{1.100}$$

Scalars must be smooth on the event horizon, thus $J^2 = J^{r2}/f$ implies that J^r vanishes on the horizon and so by eq. (1.100) everywhere. The final part of the proof shows that, for a

solution that decays at infinity, $J^r = 0$ implies $\phi'(r) = 0$ everywhere[4]. This part of the proof essentially holds because at large r we are in the weak field limit, and the theory looks like a canonical scalar, $J^r = f(r)\phi'$. A constant ϕ field then means that the energy momentum of the scalar field vanishes, and so the black hole solution coincides with that of General Relativity.

1.7 Outline of the Thesis

In chapter 2 we will consider black holes with external matter in K-mouflage and Galileon theories. We will first consider those that have settled down to a time-independent solution. To simplify our calculation we will consider a spherically symmetric exterior matter distribution and scalar field. We then compute the fifth force of the resultant scalar field and consider its effect on a stellar mass object falling into a supermassive black hole. In the second part of chapter 2 we relax the assumption of time-independence. To ease calculation we assume that the scalar has only a linear time-dependence, which allows the metric to remain static. We find an exact vacuum black hole solution for K-mouflage theory. We then add matter to this set-up and revisit the physical effects considered previously. We also discuss the effect of an accretion disk on the supermassive black hole argument [58]. This uses the fact that, in Galileon theories, a linear gradient will penetrate a galaxy because linear gradients are unsuppressed by the Vainshtein mechanism. As black holes do not couple to the field, but ordinary matter does, the supermassive black hole at the centre of galaxies will be offset.

In chapter 3 we consider the background cosmological evolution of K-mouflage with a disformal coupling to matter. We show that the addition of a disformal coupling leads to significantly different behaviour to the conformal-only case and attain necessary conditions

[4][85] shows this is actually not true if a term of the form ϕG, where G is the Gauss-Bonnet invariant, appears in Lagrangian, but this term does not appear for Galileons or K-mouflage. If the term does appear, then hairy black hole solutions do exist.

for an observationally viable cosmological evolution. For the majority of the chapter we consider the $A = 1$ case. In this case large portions of the parameter space are shown to produce viable backgrounds, with only percent level deviations from ΛCDM. We then explore further the effect of introducing ϕ dependence to A and conclude the chapter with an analysis of disformal couplings in the context of the black holes that we looked at in chapter 2.

Often we assume the source masses in our set-ups are spherically symmetric and it is in this context that the screening mechanisms are usually demonstrated. However in many physical set-ups this assumption will not hold true and in chapter 4 we consider how the screening of K-mouflage theories depends on the shape of the source masses. We find that they do indeed depend considerably on the shape of the source mass. Planar shapes, for which screening is entirely absent for Galileons, are found to have the most powerful screening which persists arbitrarily far from the planar object. The shape dependence is compared with that of the D-BIon, another theory with a screening mechanism, which was considered in Ref. [17].

We suggest a new form of Chameleon potential in chapter 5 which is logarithmic, as opposed to the standard power-law potential. We constrain the parameter space by considering two solar system tests, measurements from the Cassini probe and Lunar Ranging.

The thesis concludes with final remarks in chapter 6 in which we summarise and discuss our results.

Chapter 2

Black Holes with External Matter

2.1 Introduction

The standard cosmological model of ΛCDM within a framework of General Relativity is in good agreement with all of our current data [34, 60]. There do, however, remain open questions about gravity and considering whether modifying gravity can provide answers to some of these questions is an active area of research. The use of a cosmological constant requires unsatisfactory fine tuning [30] and many modified gravity theories attempt to find self-accelerating solutions so that one can do away with the cosmological constant altogether. At the other end of the scale a generic feature of string theories [49] that attempt to provide a quantum gravity theory is that scalar fields remain in the low energy limit. These issues have led to much research exploring how one can modify General Relativity in a way that is consistent with all observational data. Satisfactory answers to these problems have yet to be found and the field of modified gravity now has a wider brief: to elucidate the nature of gravity, even if the theories at hand do not directly provide a solution to the cosmological constant problem or quantum gravity. This can still help us to build an understanding of the behaviour or issues that any future candidate theory may have. At the very least it is only by attempting to modify General Relativity that we can either find other theories that

are equally adept at passing all the observational tests, or demonstrate how unique General Relativity is as a theory that does so.

As discussed in chapter 1, modifications to gravity must be screened on solar system scales. The screening mechanisms that we consider in this chapter, K-mouflage and Galileon theories, replace the usual kinetic term with something more exotic, and the non-linearities near a source object then suppress the field close to the object.

Given a gravitational theory we should consider its implications in a raft of different regimes to allow us to use observations to constrain, or perhaps even verify, the theory at hand. One such regime is the high curvature regime. Consideration of our theories in this environment is particularly pertinent given that we now live in the age of direct gravitational wave detections [4, 3, 1, 2] that provide an effective probe of this regime. Neutron stars and black holes provide two such high curvature environments: in this chapter we consider black holes.

A starting point for examining scalar fields around black holes is to consider the no-hair theorems [48, 59] which tell us that the scalar field around a black hole is trivial and the solutions simply coincide with those of General Relativity. However this is not the end of the story. These theorems rely on assumptions that may not be accurate in a real astrophysical environment. Firstly these theorems consider vacuum solutions, but astrophysical black holes will have an accretion disk which, as the scalar couples to matter, we would expect to source the scalar field. Furthermore many of them, including Ref. [59] which applies directly to the specific theories we are considering, rely upon a time-independent scalar in an asymptotically flat spacetime. Our universe is certainly not asymptotically flat and a scalar that has something to do with the expansion of the universe may well have significant time-dependence.

In this chapter we will show that breaking the assumptions detailed above does indeed lead to non-trivial scalar profiles. This important result establishes that, in realistic scenarios

the results of the no-hair theorems do not hold. We then go on to quantify the physical effects that these non-trivial profiles will cause. Due to the simplifying assumptions that we have made, these calculations are not concrete predictions of the physical effects. They are instead an attempt to gain an approximate understanding of the size of the physical effects generated.

Due to the nature of the black holes as astrophysical objects that do not emit light, their nature is challenging to probe. Consequently, the study of accretion disks has, in part, developed as a tool to probe the strong gravity regime of black holes. The physical processes involved in accretion disks are many and complex. A comprehensive treatment of accretions disks would include analysis of electromagnetic fields generated by the accretion disk, radiation emitted, and viscous fluid effects [5]. In the simplest case these effects can be omitted and the accretion disk modelled as a perfect fluid. Even in this case there are multiple analytical accretion disk models. The dynamics of these types of accretion disk can be categorised by the importance of pressure and speed of rotation. So called "slim" and "thick" disks have high pressure and rotate quickly, whereas thin disks rotate quickly but have low pressures. Slowly rotating accretion disks are known as "Bondi flows", due to the work of Bondi [18] on spherically symmetric accretion, which can be seen as a limiting case of slow rotation. For the purposes of this thesis we make assumption that the accretion disk pressureless and spherically symmetrically, corresponding to the physical situation of slow rotation with freely falling particles.

In this chapter we introduce the models that we are working with in section 2.2. In section 2.3 we consider a static set up with external matter, and consider its physical effects in section 2.4. In section 2.5 we consider time-dependent scalars, both in vacuum and in combination with external matter. Following that, section 2.6 revisits the physical effects in the light of the results of section 2.5. In section 2.7 we consider the black hole offset

argument of Ref. [58] when black holes have an accretion disk. We conclude the chapter with some remarks in section 2.8.

2.2 Models

The two models that we consider are K-mouflage and Galileon scalar-tensor theories of gravity. In this section we will introduce the models and review their salient features.

2.2.1 K-mouflage

The first type of model we consider is the K-mouflage theories of gravity. These were introduced in Ref. [10] as a theory with an inherent screening mechanism. They were then rediscovered and made more relevant to cosmology in Ref. [22]. In these theories the canonical kinetic term in the Lagrangian, $-\frac{1}{2}(\partial\phi)^2$, is replaced by the function $\mathscr{M}^4K(\chi)$ where $\chi = -\frac{1}{2\mathscr{M}^4}(\partial\phi)^2$, and the field is coupled to matter. Thus in the Einstein frame, the K-mouflage action is

$$S = \int dx^4\sqrt{-g}\left(\frac{M_{Pl}^2}{2}R + \mathscr{M}^4K(\chi)\right) + S_m(\psi^{(i)}, A^2(\phi)g_{\mu\nu}) \tag{2.1}$$

where $\chi = -\frac{1}{2\mathscr{M}^4}(\partial\phi)^2$, $K(\chi) = \sum_{n=1}^{N} a_n\chi^n$ and $\mathscr{M}$ is some energy scale. As we are interested in cosmology, we will take this to be the dark energy scale, $\mathscr{M}^4 = H_0^2M_{Pl}^2$.

K-mouflage fields are screened when the first derivative of the field becomes large. In the weak field regime the canonical term dominates, but in high density regions the non-linear terms become dominant and so screen the field.

The coupling to matter is constrained to $|A(\phi) - 1| \lesssim 0.1$ [11] by bounds derived from lunar ranging experiments. This means that in practice we can take

$$A(\phi) = 1 + \frac{\beta\phi}{M_{Pl}} \tag{2.2}$$

and work to first order in $\frac{\beta\phi}{M_{Pl}}$. Note also that the Lagrangian is unchanged by flipping the sign of both ϕ and β, thus we can assume, without loss of generality, that $\beta > 0$.

2.2.2 Galileons

Galileons are the second model that we have looked at. They first appeared in the decoupling limit of the Dvali-Gabadedze-Porrati (DGP) braneworld scenario [42] in which they describe the brane bending of a four dimensional brane in five dimensional Minkowski space. Ref. [29] then argued that any infrared modification to gravity due to a scalar which decouples from matter at short scales (and is therefore screened) must be a Galileon. Galileons have since cropped up in attempts to address both late time cosmic acceleration [33, 47, 68] and inflation [26, 36] and in a plethora of differing theories such as massive gravity [40] and Kaluza-Klein compactifications of Lovelock actions [90].

Galileon scalars in Minkowski space have two defining characteristics. The first is a $\phi(x) \to \phi(x) + c + b_\mu x^\mu$ shift symmetry which is inherited from Galilean invariance of the higher theory, and gives them their name. The second is that they have second order equations of motion [34]. This is in order to avoid the Ostrogradski ghost that appears generically in field equations with higher order derivatives. In fact, in four dimensions the Galileon must be a linear combination of five terms: $L_1 = \phi$, $L_2 = \frac{1}{2}(\partial\phi)^2$, $L_3 = \Box\phi(\partial\phi)^2$, a quartic and a quintic term.

The Galileon can be covariantised. For the first three terms the usual prescription $\eta_{\mu\nu} \to g_{\mu\nu}$ and $\partial_\mu \to \bigtriangledown_\mu$ suffices. However, for the quartic and quintic terms, non-minimal couplings between the metric and scalar are required to ensure second order equations of motion for both the metric and the scalar. Upon covariantising the shift symmetry $\phi \to \phi + c$ remains but the symmetry $\phi \to \phi + b_\mu x^\mu$ is lost. Thus the Einstein frame action that we will

use in this thesis is

$$S = \int dx^4 \sqrt{-g} \left(\frac{M_{Pl}^2}{2} R + \sum_{i=1}^{5} c_i L_i \right) + S_m(\psi^{(i)}, A^2(\phi) g_{\mu\nu}) \tag{2.3}$$

where the L_i are the covariantised versions of the five Galileon terms spoken about previously and the scalar is coupled to matter, just as it was for K-mouflage.

Galileons exhibit screening through what is known as the Vainshtein mechanism. The field is screened when the second derivative of the field becomes large compared with some energy scale, usually inherited from a higher theory. Beyond the Vainshtein radius the field is canonical, but non-linear interactions suppress the gradient of the field within the Vainshtein radius, and hence it is screened.

2.3 Field Profiles in Static Case

Astrophysical black holes are not surrounded by a vacuum, but accrete matter in a disk around them, thus the assumptions of the no-hair theorem do not apply and we investigate how this matter will affect the scalar profile. Observable black holes will have long since finished their formation process and should have settled down to a steady solution. Our interest is therefore restricted to stationary black hole solutions. We focus further upon static solutions as these are the ones covered by the no-hair theorem of Ref. [59], though later we will relax this assumption and consider solutions with some time-dependence. The dynamics within the accretion disk can be complicated in themselves, however as this is a first calculation we do not consider these internal accretion disk dynamics and instead consider the salient features that can be captured with a spherically symmetric matter distribution. That is that within the innermost stable orbit, and beyond a finite distance (that we take to be fifty Schwarzschild radii), there is indeed no matter, but in-between these two radii we have a non-zero matter distribution. The features that we find may well extend to beyond the

simple case that we have considered here. For example Ref. [38] considered Chameleons, another class of scalar-tensor theories with a screening mechanism, around a black hole with an accretion disk in a spherically symmetric set-up similar to ours. The authors followed up with another paper [37] in which they considered Chameleons with a more realistic disk shaped accretion disk, on the background of a spinning black hole and in fact found results similar to those of the first paper. We will consider both stellar mass black holes, as these have been observed directly through gravitational waves [1], and supermassive black holes, such as the one that is believed to reside at the centre of our galaxy and has already been discussed in the context of Galileon theories [58]. We argue that the back-reaction of the scalar and matter on the background metric should be negligible, and so our calculation amounts to solving the equations of motion for the theories on a fixed Schwarzschild background. We consider K-mouflage models first, and then Galileon models.

2.3.1 K-mouflage

A natural choice if we are interested in cosmological scales is to take $\mathscr{M}^4 = M_{Pl}^2 H_0^2$ in (2.1) and set $a_1 = 1$ so that we have a canonical scalar at leading order. We take the scalar field to be on a Schwarzschild background, that is

$$ds^2 = -f(r)dt^2 + f(r)^{-1}dr^2 + r^2 d\Omega^2 \tag{2.4}$$

where $f(r) = 1 - r_s/r$ and r_s is the Schwarzschild radius of the black hole. We neglect the back-reaction of the matter and the scalar field upon the background metric, which should be reasonable provided the mass of the black hole is much larger than that of the matter, and given that $\mathscr{M}$ is small. Varying the action with respect to ϕ gives the equation of motion

$$\frac{1}{\sqrt{-g}}\partial_\mu(\sqrt{-g}\partial^\mu\phi K'(\chi)) = \frac{dlnA(\phi)}{d\phi}\rho_E \tag{2.5}$$

where $\rho_E = -g^{\mu\nu}T_{\mu\nu}$ and $T_{\mu\nu}$ is the Einstein frame energy momentum. We take $A(\phi) = 1 + \frac{\beta\phi}{M_{Pl}}$, where β is a constant that we expect to be of order unity. As discussed previously, $A(\phi) \approx 1$. The matter densities in the Jordan and Einstein frames differ by a factor of $A(\phi)^4$ and a further definition that is sometimes used in the Einstein frame is $\rho_E A^{-1}(\phi)$ because this is non-relativistically conserved [19]. However all these definitions agree to first order in $\frac{\beta\phi}{M_{Pl}}$. We only work to first order in this quantity, and so the right-hand side of eq. (2.5) becomes $\frac{\beta\rho}{M_{Pl}}$ where

$$\rho = \rho_0(H(r-r_0) - H(r-r_1)) \tag{2.6}$$

$r_1 > r_0$, ρ_0 is a constant and H the Heaviside function. The inner edge of the accretion disk, r_0, can be taken to be the innermost stable orbit and the outer edge to be at some point r_1, which we take to be $50r_s$. We then choose the disk to be of constant density to ease calculation. We can integrate eq. (2.5) to give

$$YK'(-\frac{Y^2}{2}) = \frac{\beta M(r)}{4\pi r^2\sqrt{f(r)}M_{Pl}\mathscr{M}^2} = R(r) \tag{2.7}$$

where this equation defines $R(r)$. We have defined the dimensionless quantity

$$Y = \sqrt{f(r)}\phi'(r)/\mathscr{M}^2 \tag{2.8}$$

and

$$M(r) = \begin{cases} 0 & r \leq r_0 \\ \frac{4\pi\rho_0}{3}(r^3 - r_0^3) & r_0 \leq r < r_1 \\ \frac{4\pi\rho_0}{3}(r_1^3 - r_0^3) & r_1 \leq r \end{cases} \tag{2.9}$$

is the mass of the accretion disk that is enclosed in a sphere of radius r, thus $M_{acc} = M(r_1)$. We will refer to the regions with $r < r_0$, $r_0 < r < r_1$ and $r_1 < r$ as regions I, II and III respectively. Note that the equation in region III is the same as that for a point mass of mass

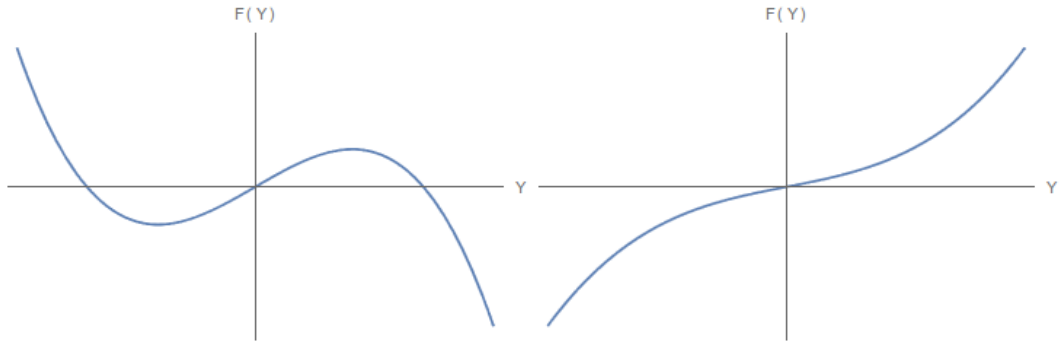

(a) $F(Y) = Y - \frac{1}{2}Y^3$ (b) $F(Y) = Y + \frac{1}{2}Y^3$

Fig. 2.1 $F(Y)$ for quadratic K-mouflage for different choices of the sign of the quadratic term

M_{acc}. This makes sense because M_{acc} is the scalar charge of the system. The behaviour of the scalar depends on the function

$$F(Y) = YK'(-\frac{Y^2}{2}) = \sum_{n=1}^{N} a_n(-\frac{1}{2})^{n-1}Y^{2n-1}. \tag{2.10}$$

Not all forms of $F(Y)$ have solutions. We consider Fs which are monotonic for $Y \geq 0$. This means that F is invertible and so we can write Y, and in turn ϕ', uniquely as a function of r. Note that F has a unique zero, $Y = 0$. This means that immediately we have that in region I $\phi'(r) = 0$ and therefore no fifth force.

For asymptotic flatness we require that $\phi' \to 0$ as $r \to \infty$. This is indeed that case because $R(r) \to 0$ and so F, and in turn Y, tends to zero as $r \to \infty$. In fact as $R(r) \sim \beta M_{acc}/4\pi M_{Pl}\mathscr{M}^2 r^2$ for large r, and $F(Y) \sim Y$ for small Y, we recover the $\phi' \sim \beta M_{acc}/4\pi M_{Pl} r^2$ behaviour of a canonical field around an object of charge $Q = M_{acc}$.

Thus, assuming that we have an invertible F, the scalar gradient will be zero in region one, its value will grow inside the accretion disk, up to $r = r_1$, where the scalar gradient will begin to fall off back to zero at $r = \infty$. We can write the gradient of the scalar explicitly as

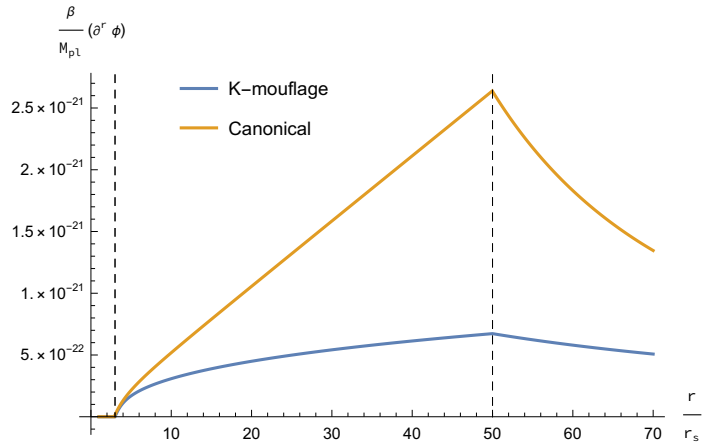

Fig. 2.2 Profiles for K-mouflage (orange) and canonical (blue) fields for $K(\chi) = \chi - \frac{1}{2}\chi^2$ with $\beta = 1$ and $M_{BH} = 10M_{\odot}$. Vertical dashed lines denote inner and outer edge of accretion disk.

$$\phi'(r) = \frac{\mathscr{M}^2}{\sqrt{f(r)}} F^{-1}(R(r)) \approx \begin{cases} \dfrac{\beta M(r)}{4\pi r^2 f(r) M_{Pl}} & \text{unscreened} \\ \left(\dfrac{\beta M(r)}{N a_N 4\pi r^2 f(r) M_{Pl}}\right)^{\frac{1}{2N-1}} \left(\dfrac{-2\mathscr{M}^4}{f(r)}\right)^{\frac{N-1}{2N-1}} & \text{screened} \end{cases} \tag{2.11}$$

where the unscreened region is the one in which the χ term in $K(\chi)$ dominates, and conversely the screened region is one in which the highest power of $K(\chi)$, $a_N\chi^N$, dominates. Inside the accretion disk, and once r/r_0 is reasonably large, then $M(r) \sim r^3$, and so in the unscreened region $\phi'(r) \sim r$, and in the screened region $\phi'(r) \sim r^{\frac{1}{2N-1}}$. This can be seen in fig. 2.2 which gives the profile for quadratic K-mouflage.

Note it is the requirement of asymptotic flatness that restricts the form $F(Y)$ can take. Any F for which there is a Y_* such that $F(Y_*) = 0$, and which is an increasing function of Y for $Y_* \leq Y$, will solve (2.7), but the gradient of the field will not tend to zero at large r. Further solutions do exist for some non-monotonic Fs for some matter distributions. They are however non-generic and we do not consider them here.

In figure fig. 2.2 we can see that the K-mouflage field is indeed screened relative to a canonical field. Screening depends on the magnitude of $R(r)$. If $R(r) \ll 1$ then Y is small and so $Y \gg Y^n$ for $n > 1$. This means the first term of $F(Y)$ dominates and we simply have $Y \approx R(r)$: an approximately canonical field. However if $R(r) \gg 1$ then $Y^n \gg Y$ for $n > 1$ and so the largest power of Y dominates. This gives that $Y \approx R(r)^{\frac{1}{2N-1}} \ll R(r) = Y_{canonical}$ and so the field is screened. As $R(r)$ is largest at $r = r_1$ we evaluate it here. We choose cosmological values of our free parameters to get an explicit form for $R(r)$. We take $r_0 = 3r_s$, $r_1 = 50r_s$, $\rho_0 = 10^{21} H_0^2 M_{Pl}^2, \mathscr{M}^4 = H_0^2 M_{Pl}^2$ giving $R(r_1) \approx 2 \times 10^5 \beta M_{BH}/M_\odot$. We expect β to be of order unity and thus we have screening for all astrophysical sizes of black holes.

2.3.2 Galileons

We consider the same physical set up, with the same matter distribution and $A(\phi)$, for the Galileon as we did for K-mouflage. Due to the shift symmetry of the Galileons the field equations can be written in terms of a Noether current

$$\bigtriangledown_\mu J^\mu = \frac{\beta \rho}{M_{Pl}}. \tag{2.12}$$

Ref. [86] gives the current for Horndeski theories. Horndeski theories are, by definition, the most general scalar-tensor theories with second order equations of motion, and were first written down by Horndeski in 1974 [56]. Galileon theories are the subset of Horndeski theories with the additional requirement of a shift symmetry. The Galileon current can be found by making the replacements $K(X) = X, G_3(X) = X, G_4(X) = X^2$ and $G_5(X) = X^2$ in the current given in Ref. [86]. The eq. (2.12) can then be integrated easily to give the scalar equation of motion. Setting the term in the Lagrangian proportional to L_1 to zero and

relabelling constants, this is

$$f(r)\phi'(x)(c_2+c_3\frac{\phi'}{r}(2-\frac{3r_s}{2r})+c_4\phi'^2\frac{f}{r^2}+c_5\phi'^3\frac{r_s}{r^3}(4-\frac{7r_s}{r}+\frac{2r_s^2}{r^2}))=\begin{cases}0 & r<r_0\\ \frac{\beta M(r)}{4\pi M_{Pl}r^2} & r_0\leq r<r_1\\ \frac{\beta M_{acc}}{4\pi M_{Pl}r^2} & r_1\leq r.\end{cases} \tag{2.13}$$

The constants here are dimensional. Replacing them by dimensionless α_i multiplied by the appropriate power of some energy scale $\mathscr{M}$ and normalising c_2 to match the canonical scalar gives us

$$\frac{J^r}{r\mathscr{M}^3}=\begin{cases}0 & r<r_0\\ \frac{\beta M(r)}{4\pi M_{Pl}\mathscr{M}^3r^3} & r_0\leq r<r_1\\ \frac{\beta M_{acc}}{4\pi M_{Pl}\mathscr{M}^3r^3} & r_1\leq r\end{cases} \tag{2.14}$$

where

$$J^r=f(r)\phi'(1+\alpha_3\frac{\phi'}{r\mathscr{M}^3}(2-\frac{3r_s}{2r})+\alpha_4(\frac{\phi'}{r\mathscr{M}^3})^2f(r)+\alpha_5(\frac{\phi'}{r\mathscr{M}^3})^3\frac{r_s}{r}(4-\frac{7r_s}{r}+\frac{2r_s^2}{r^2})). \tag{2.15}$$

We saw that for K-mouflage we could cast the equation of motion in terms of a function, F, of a single variable Y. This cannot be done for Galileons but we can write the equation of motion as $F(Y(r),r)=R(r)$ with $Y=\frac{\phi'}{r\mathscr{M}^3}$ where F is a polynomial in Y with coefficients that have r dependence. Nevertheless, if $F(Y(r),r)$ is monotonically increasing in Y for all $r>r_s$ then we can invert F to get a unique solution for the gradient of the field. Just as was the case for the K-mouflage field, this solution will vanish in region I and asymptotically decay like a canonical field at large r. For example, for the cubic Galileon $F(Y)=f(r)Y(1+\alpha Y(2-\frac{3r_s}{2r}))$; if $\alpha>0$ then $\frac{\partial F}{\partial Y}>0$ for all $r>r_s$ and so F is invertible, and a unique solution exists.

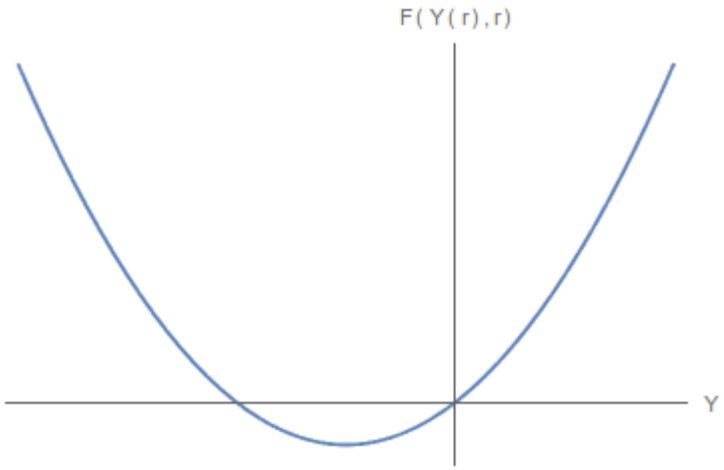

Fig. 2.3 $F(Y(r),r)$ for cubic Galileon. Shape is independent of the specific value to which explicit dependence on r is fixed.

Whether other generic solutions exist for Galileons is less clear than it was for K-mouflage. However as the polynomial coefficients are constant to first order in r_s/r, their r dependence does not seem strong enough to qualitatively change the behaviour that would occur for an F with constant coefficients, in which there would be no other generic solutions.

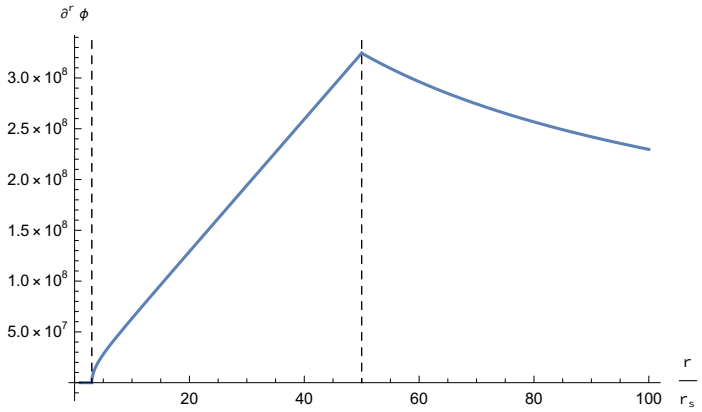

Fig. 2.4 Profile for the cubic Galileon with $\alpha_3 = 1$, $\alpha_4 = \alpha_5 = 0$ and $\beta = 1$, in units with $r_s = 1$. Vertical dashed lines denote inner and outer edge of accretion disk.

Thus, as for the K-mouflage model, the field will be constant in region I, react to the matter and grow in region II and then decay back down to a constant as $r \to \infty$. Inside the

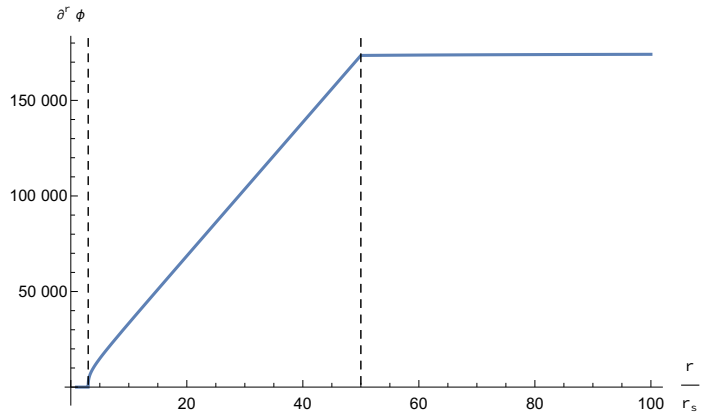

Fig. 2.5 Profile for the quartic Galileon with $\alpha_4 = 1$, $\alpha_3 = \alpha_5 = 0$ and $\beta = 1$, in units with $r_s = 1$. Vertical dashed lines denote inner and outer edge of accretion disk.

disk the right-hand side of eq. (2.14) can be written as

$$E(1-(\frac{r_0}{r})^3) \tag{2.16}$$

where $E = \frac{\beta\rho_0}{3M_{Pl}\mathscr{M}^3}$. If E is small then $\frac{\phi'}{r\mathscr{M}^3}$ must be small and so the canonical term dominates i.e. we have no screening. If $E > 1$ then there will be a radius beyond which screening will occur. Note this is different to the standard Vainshtein radius of an object within which non-linear effects occur. This radius is given by

$$r_v = r_0(1-E^{-1})^{-1/3}. \tag{2.17}$$

We can see that for $E < 1$ there is no Vainshtein radius, for $E = 1$ the Vainshtein radius is infinite, and, for large E,

$$r_v \approx r_0 \tag{2.18}$$

and so almost the entire disk is screened. This is in contrast to the K-mouflage model. In eq. (2.7) the right-hand side is approximately linear in r. This means that for any density of the accretion disk, there will be screening provided r_1 is large enough.

We can evaluate E for cosmological values of the parameters $\rho_0 = 10^{21} M_{Pl}^2 H_0^2$ and $\mathscr{M}^3 = H_0^2 M_{Pl}$ giving $E \approx 10^{21}/3$. Thus $r_v \approx r_0$ and the scalar is screened for almost the entirety of the accretion disk. Note that this is independent of the mass of the black hole.

The fig. 2.4 shows the profile for a cubic Galileon, with the sign of α_3 chosen such that a solution exists. Inside the matter the $\phi'(r)$ quickly becomes roughly linear in r. This is because here we have $Y^2 \approx E$. At $r = 50 r_s$ we enter into region III, and have $Y^2 \sim r^{-3}$ and so $\phi' \sim r^{-1/2}$. The scalar stays in the non-linear regime well beyond the extent of the graph. It will transition back at around the Vainshtein radius, R_v, of the accretion disk, given by $\beta M_{acc}/4\pi M_{Pl} \mathscr{M}^3 R_v^3 = 1$ which for our system is $R_v \approx 5 \times 10^8 r_s$.

Similarly fig. 2.5 shows the profile for the quartic Galileon, with α_4 chosen to be positive so that a solution exists. As for the cubic Galileon the profile quickly becomes linear in region II. However in region III we have that $Y^3 \sim r^{-3}$ and hence $\phi'(r)$ stays constant. Again this will persist until the Vainshtein radius is approached.

2.4 Physical Effects

2.4.1 Strength Versus Gravity

The most obvious physical effect to consider is the size of the fifth force. We will see that this is small compared to the gravitational force. There are two reasons for this. The first is that, as we have seen, the scalar is screened relative to a canonical scalar. The second is that even the canonical scalar force is suppressed relative to the gravitational force. For an object composed of non-compact matter, that is an object whose mass does not receive a significant contribution from its gravitational binding energy, this is not the case. However our object is a black hole with an accretion disk, and the black hole's mass is entirely of gravitational origin. The gravitational field is sourced by the mass density of the object but the scalar is sourced by the trace of the energy momentum tensor. For non-compact objects these are

$F_\phi(r_1)/F_{con}(r_1)$	K-mouflage		Galileon		
	N=2	N large	cubic	quartic	quintic
$M_{BH} = 10M_\odot$	10^{-1}	10^{-2}	5×10^{-11}	2×10^{-14}	4×10^{-16}
$M_{BH} = 10^7M_\odot$	10^{-4}	10^{-6}	5×10^{-11}	2×10^{-14}	4×10^{-16}

Table 2.1 Values of the ratio of fifth force of various theories to that of a canonical scalar field, evaluated at r_1.

$F_\phi(r_1)/F_N(r_1)$	K-mouflage		Galileon		
	N=2	N large	cubic	quartic	quintic
$M_{BH} = 10M_\odot$	10^{-19}	10^{-20}	5×10^{-29}	2×10^{-32}	4×10^{-34}
$M_{BH} = 10^7M_\odot$	10^{-10}	10^{-12}	5×10^{-17}	2×10^{-20}	4×10^{-22}

Table 2.2 Values of the ratio of fifth force of various theories to that of gravity evaluated at r_1.

approximately equal and so the scalar force is of gravitational strength. However the black hole does not contribute to the energy momentum tensor, but does source the gravitational field, and hence the gravitational force is much stronger than the canonical scalar force in the case that we are considering. Evaluating at the outside edge of the accretion disk, the ratio between the canonical scalar and gravitational force is

$$\frac{\beta\phi'_{con}(r_1)}{M_{pl}F_N(r_1)} \approx 2\beta^2\frac{M_{acc}}{M_{BH}+M_{acc}}. \tag{2.19}$$

We expect β to be of order unity, so that we get order unity alterations to gravity at cosmological scales, and our initial assumptions that the back-reaction of the matter on the Schwarzschild metric is small enforces that $M_{acc} \ll M_{BH}$. Thus this ratio is small. Multiplying this quantity by the ratios in table 2.1 gives the ratios of the scalar force to gravitational force displayed in table 2.2. For each table we have calculated the quantities for typical sizes of solar mass black hole and supermassive black hole.

2.4.2 Classical Energy Estimate

Further to the fifth force strength calculation we can consider energy. We consider a stellar mass object in-spiralling toward a supermassive black hole with an accretion disk. We can then use the scalar profile that we have calculated as that of the supermassive black hole, and take the stellar mass object to follow the path of a test particle. We wish to consider whether the energy loss due to the scalar is comparable to that due to the quadrupole of General Relativity. The work done by the fifth force gives an energy loss of

$$\dot{\xi}_{\phi} = \dot{r}\frac{\beta m_t}{M_{pl}}\phi' \tag{2.20}$$

where m_t denotes the mass of the in-falling object. The energy loss in General Relativity can be approximated by the quadrupole

$$\dot{\xi}_{GR} = \left\langle \frac{8m_t^2 G^3 M_{BH}^2}{15c^5 r^4}(12v^2 - 11\dot{r}^2) \right\rangle \tag{2.21}$$

where the angled brackets denote the time averaging an orbital period. We approximate $\dot{r}$ by first evaluating both the quadrupole and classical Newtonian energy, E, on a Newtonian circular orbit, $\dot{r} = 0$ and $v^2 = \frac{GM_{BH}}{r}$. This gives

$$\dot{\xi}_{GR}(r) = \frac{32m_t^2 G^4 M_{BH}^3}{5c^5 r^5} \tag{2.22}$$

$$E(r) = \frac{-Gm_t M_{BH}}{2r}. \tag{2.23}$$

We then equate the quadrupole with the change of energy

$$\dot{\xi}_{GR}(r) = \frac{d}{dt}E(r) = \frac{GM_{BH}m_t}{r^2}\dot{r}. \tag{2.24}$$

To show that the approximation of circular motion is valid we show that rate of change of orbit radius is small compared to the speed of orbit,

$$\frac{\dot{r}}{v} = \frac{16\pi^2}{5}(\frac{r_s}{r})^2\frac{m_t}{M_{BH}}. \tag{2.25}$$

As we are considering a stellar mass object falling into a supermassive black hole, this is indeed small. We now evaluate the ratio of the work done by the fifth force with that of the quadrupole of General Relativity:

$$\frac{\dot{\xi}_{\phi_c}}{\dot{\xi}_{GR}} = \frac{\beta\phi'(r)}{2M_{pl}F_N}. \tag{2.26}$$

We see that this is nothing other than half the ratio of the fifth force to Newtonian gravitational force. As we have already seen the scalars are screened and this ratio is small. This means that we expect the work done by the fifth force to be a small effect on the in-spiralling motion.

2.5 Field Profiles with Time-Dependence

No-hair theorems make several assumptions and we have seen in section 2.3 that adding matter to the exterior of the black hole, as would exist in an astrophysical situation in the form of an accretion disk, is sufficient to generate a non-zero scalar profile outside the black hole. Further to the absence of matter, Ref. [59] also assumes staticity of both the scalar and the metric and asymptotic flatness. However in a cosmological setting we do not have asymptotic flatness and there will at least be the time-dependence associated with the expansion of the universe. In this section we consider the scalar profiles of asymptotically de Sitter solutions in the absence of matter, and then add matter to these solutions. It is complicated to consider fully time-dependent solutions so we add only linear time-dependence

to the scalar, and keep the metric static. As only derivatives appear in the scalar equation of motion, this means that they remain easily solvable ordinary differential equations. As in section 2.3, we will again consider both solar mass and supermassive black holes.

We first present a novel set of exact black hole K-mouflage solutions with a de Sitter-Schwarzschild metric and then consider the scalar profile generated by a spherically symmetric matter distribution on this background. For Galileons we review the vacuum, asymptotically de Sitter solutions found in Ref. [9], and then consider the matter on top of this, in the test field limit.

2.5.1 K-mouflage

Exact Black Hole Solution

First we demonstrate that exact de Sitter-Schwarzschild black hole solutions exist in K-mouflage theories. The field equations without matter are:

$$M_{Pl}^2(G_{\alpha\beta}+\Lambda_{bare}g_{\alpha\beta}) = g_{\alpha\beta}\mathscr{M}^4K(\chi)+K'(\chi)\partial_\alpha\phi\partial_\beta\phi \tag{2.27}$$

$$\frac{1}{\sqrt{-g}}\partial_\mu(\sqrt{-g}\partial^\mu\phi K'(\chi)) = 0. \tag{2.28}$$

If $K'(\chi)$ has a zero, χ_0, then setting $\chi=\chi_0$ solves eq. (2.28) and eq. (2.27) becomes

$$M_{Pl}^2G_{\alpha\beta}+(M_{Pl}^2\Lambda_{bare}-\mathscr{M}^4K(\chi_0))g_{\alpha\beta} = 0 \tag{2.29}$$

which is solved by a de Sitter-Schwarzschild metric

$$ds^2 = -(1-\frac{r_s}{r}-H^2r^2)dt^2+(1-\frac{r_s}{r}-H^2r^2)^{-1}dr^2+r^2d\Omega^2 \tag{2.30}$$

with an effective cosmological constant

$$\Lambda_{eff} = 3H^2 = \Lambda_{bare} - \mathscr{M}^4 K(\chi_0)/M_{Pl}^2. \tag{2.31}$$

If $K(\chi)$ has coefficients of order unity then we expect χ_0 and $K(\chi_0)$ to be roughly of order unity. Taking $\mathscr{M}^4 \sim H_0^2 M_{Pl}^2$, the dark energy scale, then gives a contribution to the effective cosmological constant of order H_0^2. This metric is Schwarzschild for $H = 0$ and de Sitter for $r_s = 0$. It has a black hole horizon near $r = r_s$ and a cosmological horizon near $r = \frac{1}{H}$. From now on we denote $f(r) = 1 - \frac{r_s}{r} - H^2 r^2$. Note that this solution does not exist for a canonical scalar as the $K'(\chi_0) = 0$ condition can be imposed, since for a canonical scalar $K'(\chi) \equiv 1$.

In the special case where $r_s = 0$ we have de Sitter space. We can use the co-ordinate relations

$$\tau = t + \frac{1}{2H} ln|1 - H^2 r^2| \tag{2.32}$$

and

$$\rho = re^{-Ht}(1 - H^2 r^2)^{-\frac{1}{2}} \tag{2.33}$$

to rewrite the metric in the more familiar "cosmological" coordinates, as opposed to the "Schwarzschild-like" coordinates of eq. (2.30). In these coordinates the metric takes the form

$$ds^2 = -d\tau^2 + e^{2H\tau}(d\rho^2 + \rho^2 d\Omega^2). \tag{2.34}$$

We now find the black hole solution explicitly, denoting $\chi_0 = -\frac{C}{2\mathscr{M}^4}$. We take an ansatz of

$$\phi = qt + \psi(r). \tag{2.35}$$

The $\chi = \chi_0$ condition then gives

$$\psi'(r) = \pm \frac{q}{f(r)} (1 + \frac{C}{q^2}(1 - \frac{r_s}{r} - H^2 r^2))^{1/2} \tag{2.36}$$

with the positivity of the square root imposing that $q^2 \geq -C$. Any solution to eq. (2.36) is an exact black hole solution. However one should note that in the case $C = -q^2$ we have that

$$\psi'(r) = \pm\frac{q}{f(r)}(\frac{r_s}{r} + H^2r^2)^{1/2} = \frac{\pm qHr}{1-H^2r^2} + O(r_s/r) \tag{2.37}$$

$$\psi(r) = \mp\frac{q}{2H}ln|1-H^2r^2| + O(r_s/r). \tag{2.38}$$

Using eq. (2.32) we can see that when the minus sign is chosen in eq. (2.37), this particular solution tends toward the isotropic, homogeneous de Sitter solution that is linear in comoving time:

$$\phi = q\tau. \tag{2.39}$$

If the plus sign is chosen, then the solution tends toward an inhomogeneous de Sitter solution:

$$\phi = q\tau - \frac{q}{H}ln|1-H^2e^{2H\tau}\rho^2|. \tag{2.40}$$

As the time coordinate blows up at the horizon, we need consider regularity at the future horizon of the black hole. To do this we trade our time coordinate for the ingoing Eddington Finkelstein coordinate $v = t + r^*(r)$, where r^* is the tortoise coordinate defined by $\frac{dr^*}{dr} = 1/f$, which covers the future horizon of the black hole. We have that

$$\phi = qt + \psi(r) \tag{2.41}$$

$$\phi = qv + \psi(r) - qr^*. \tag{2.42}$$

This implies that for ϕ to be regular at the horizon (at which v is finite), $\psi(r) - r^*$ must be regular, which differentiating gives

$$\psi'(r) \sim \frac{q}{f} \tag{2.43}$$

at the horizon. At the horizon $\frac{r_s}{r} + H^2 r^2 = 1$ and so this is only possible if the plus sign is chosen in eq. (2.37). This means that solutions regular at the horizon with the asymptotics of eq. (2.40) exist, as do solutions that are not regular at the horizon but have the asymptotics of eq. (2.39). However solutions do not exist which are both regular at the horizon and, far from the black hole, approach cosmological solutions that are linear in comoving time.

Adding Matter

We now solve the scalar equation of motion for the same accretion disk as used in the previous sections, on the de Sitter-Schwarzschild background found above:

$$\frac{1}{\sqrt{-g}}\partial_\mu(\sqrt{-g}\partial^\mu\phi K'(\chi)) = \frac{\beta}{M_{Pl}}\rho(r). \tag{2.44}$$

As $\sqrt{-g}g^{tt}\partial_t\phi K'(\chi)$ is independent of t then the equation of motion is just an ordinary differential equation in r, which we can integrate

$$f(r)\psi'(r)K'(\frac{q^2}{2\mathscr{M}^4 f(r)} - \frac{f(r)}{2\mathscr{M}^4}\psi'(r)^2) = \frac{\beta}{4\pi r^2 M_{Pl}}M(r) \tag{2.45}$$

where $f(r) = 1 - \frac{r_s}{r} - H^2 r^2$ and $M(r) = 4\pi\int^r dr' r'^2\rho(r')$ is the baryonic mass contained within a sphere of radius r.

We now focus only on quadratic K-mouflage, $K'(\chi) = 1 - c\chi$, with $C = -q^2$. The requirement that $K'(\frac{q^2}{2\mathscr{M}^4}) = 0$ implies that $c = \frac{2\mathscr{M}^4}{q^2}$. We define $Y = \frac{\sqrt{f(r)}\psi'(r)}{\mathscr{M}^2}$ and re-write eq. (2.45) as

$$F(Y,r) = YK'(\frac{q^2}{2\mathscr{M}^4 f(r)} - \frac{1}{2}Y^2) = \frac{\beta}{4\pi r^2\sqrt{f(r)}M_{Pl}\mathscr{M}^2}M(r). \tag{2.46}$$

This function is displayed in fig. 2.6. Matter will drive the value of F to beyond the value of the local maxima and so our solution must have $Y \geq Y_+$, where $Y_+ = \frac{|q|}{\mathscr{M}^2}(\frac{1}{f} - 1)^{\frac{1}{2}}$

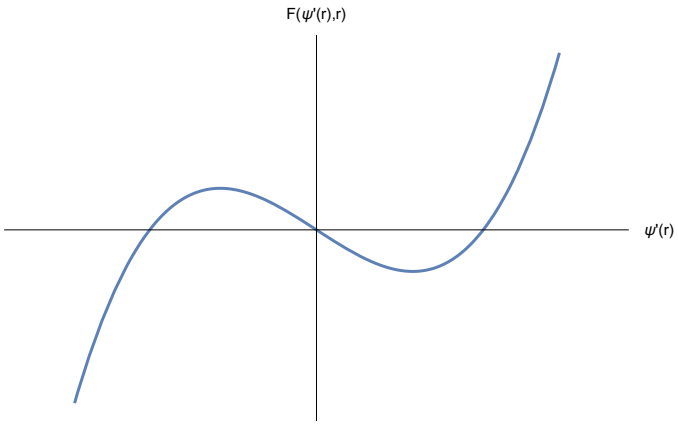

Fig. 2.6 Shape of F for $K(\chi) = \chi - \chi^2$

is the positive zero of F. F is invertible on this branch and so we have a unique solution which, at large r, relaxes back to the solution that exists in the absence of matter. This is $Y = Y+$. As in the static case F is zero in region I and so

$$\psi'(r) = \frac{|q|}{f(r)}\left(\frac{r_s}{r} + H^2 r^2\right)^{1/2} \tag{2.47}$$

in region I. This means that if $q > 0$ we have a solution which is regular at the horizon with the asymptotics of eq. (2.40) and if $q < 0$ we have a solution with the asymptotics of eq. (2.39) that is not regular at the horizon.

We now describe the features of this solution.

As in the static case the solution in region I is exactly as if there were no matter at all. In this respect the matter does not effect the scalar field here at all. However we do now have a non-trivial scalar profile given by $\psi'_+(r) = \frac{|q|}{f}\left(\frac{r_s}{r} + H^2 r^2\right)^{\frac{1}{2}}$. We will consider the physical effects of this later.

We assume $r_s \ll 1/H$ and consider region II, where $f(r) \approx 1$. In this case we have

$$\frac{c}{2} Y^3 \approx \frac{\beta M(r)}{4\pi M_{Pl} \mathscr{M}^2 r^2}. \tag{2.48}$$

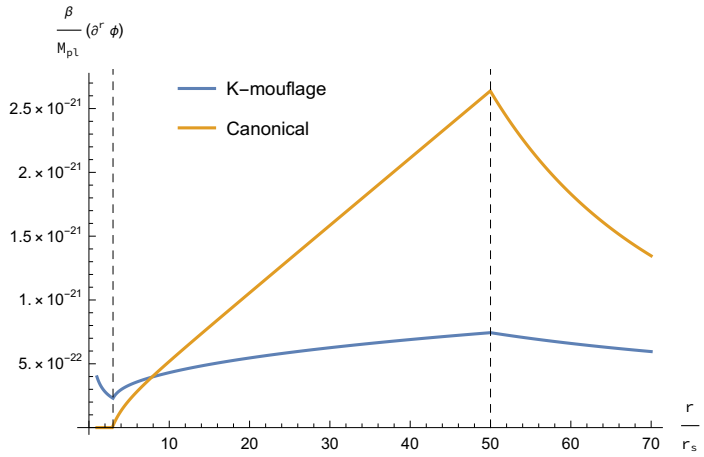

Fig. 2.7 K-mouflage de Sitter-Schwarzschild solution versus the canonical field on a Schwarzschild background in units with r_s=1. Vertical dashed lines denote inner and outer edge of accretion disk.

When the right-hand side is large, which it is for almost the entirety of region II, this coincides with the solution for the static case. In particular, the physical effects which were calculated in the static case on the border of regions II and III will remain the same for the time-dependent case.

In region III, the solution tends to one of the cosmological solutions, which one depending on the choice of sign of q. For the solution regular at the horizon, we must have $q > 0$, and the asymptotics of eq. (2.40).

In fig. 2.7 we show the K-mouflage de Sitter-Schwarzschild solution versus the canonical field on a Schwarzschild background. For the majority of the disk the K-mouflage force is the same as that of the Schwarzschild case, however in region I we now have a non-zero force.

2.5.2 Galileon

The Black Hole Solution

Ref. [9] found exact cubic Galileon black hole solutions with $\phi = qt + \psi(r)$ in static coordinates, which tend to isotropic cosmological solutions far from the black hole. We fix

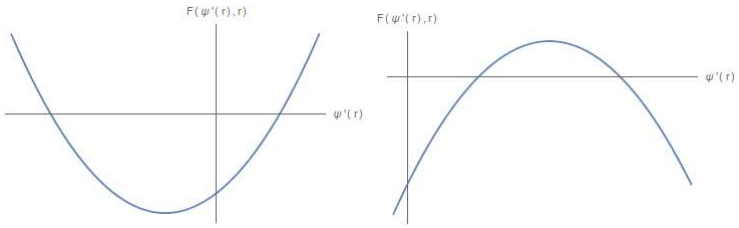

Fig. 2.8 $F(\psi'(r),r)$ for cubic Galileon, in the vicinity of the black hole (left) and for $r \gtrsim \sqrt{\frac{2}{3}}\frac{1}{H}$ (right)

$c_3 = \frac{1}{3qH}$ so that cosmological solutions exist. In the test field limit these solutions have a de Sitter-Schwarzschild metric. In this case the field equation is

$$f(r)\psi' + \frac{c_3 f(r)\psi'^2}{r}(2 - \frac{3r_s}{2r} - 3H^2r^2) - \frac{c_3 q^2(\frac{r_s}{r^2} - 2H^2r)}{2f(r)} = 0. \tag{2.49}$$

There are two solutions to this quadratic equation. However one of them blows up when $2 - \frac{3r_s}{2r} - 3H^2r^2 = 0$. It is the other one that we want.

Adding matter

We add matter to this test field case, for which the integrated equation of motion is

$$F(\psi'(r),r) = f(r)\psi' + \frac{c_3 f(r)\psi'^2}{r}(2 - \frac{3r_s}{2r} - 3H^2r^2) - \frac{c_3 q^2(\frac{r}{r^2} - 2H^2r)}{2f(r)} = \frac{\beta M(r)}{4\pi M_{Pl} r^2}. \tag{2.50}$$

That the matter drives F to high positive values implies that we must have $q > 0$. We again take the solution that does not blow up when $2 - \frac{3r_s}{2r} - 3H^2r^2 = 0$ to attain a unique solution which relaxes back to the matter-less solution at large r. The zero of F taken implies that in region I $\psi'(r) \sim \frac{|q|}{f(r)}$ as $f(r) \to 0$, which implies that the solution is indeed regular at the future event horizon because we have chosen that $q > 0$, for exactly the same reason as in the K-mouflage case.

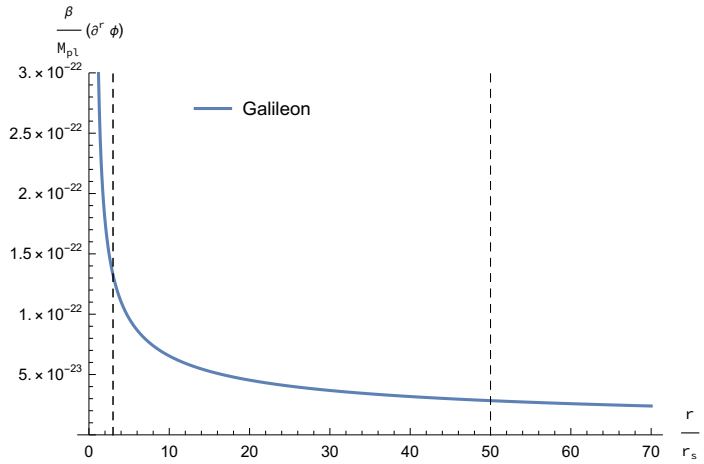

Fig. 2.9 Fifth force for Galileons with a black hole of mass $10M_\odot$ in units with $r_s = 1$. Vertical dashed lines denote inner and outer edge of accretion disk.

The figs. 2.9 and 2.10 show the profile for stellar mass and supermassive black holes respectively. The fig. 2.9 shows the profile for a black hole with $M_{BH} = 10M_\odot$, in which we have taken a cosmological value of $q = H_0 M_{Pl}$. This figure shows that the introduction of the matter has little effect on the gradient of the Galileon field. For the K-mouflage field the presence of the accretion disk was noticeable due to the sharp changes in gradient of the fifth force profile at the accretion disk edges. However no such change is noticeable for the Galileon. This is because the ratio of the third term on the left hand-side of eq. (2.50) and the right hand-side is roughly $\frac{M_{BH}}{M_{acc}}$ which we have assumed to be large so that we can neglect the back-reaction of matter. Thus the field profile for the Galileon in the presence of matter is similar to that of the Galileon field in the absence of matter. If we ignore the back-reaction of the matter for a large black hole, fig. 2.10 shows the profile for a black hole with $M_{BH} = 10^{10}M_\odot$, and therefore has $M_{BH} \ll M_{acc}$. Now in region II the matter term in eq. (2.50) dominates over the third term on the right hand-side. Consequently the fifth force coincides with that of the static case. This is because the third term in F can be dropped and, as we are in the vicinity of the black hole, $Hr \ll 1$. This means F reduces to that of the static, Schwarzschild background case. However, as before, there remains a nonzero force in region I.

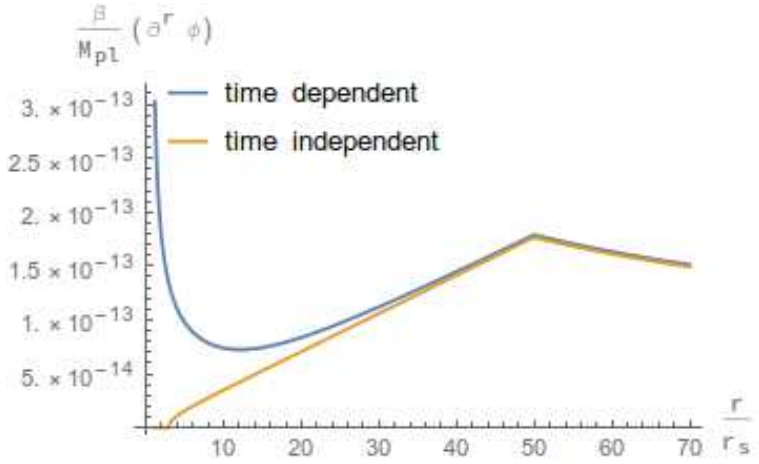

Fig. 2.10 Fifth force for Galileons with a black hole of mass $10^{10}M_{\odot}$ in units with r_s=1

2.6 Physical Effects Revisited

We now quantify the effect that adding the time-dependence to the solutions has had on the fifth force. For K-mouflage we have already seen that the fifth force at r_1 is approximately the same as that of the static case. We have also seen that there is now a fifth force in region I. We thus evaluate this at r_0. We take $q = H_0 M_{Pl}$ in eq. (2.47). This gives us a ratio of fifth force to Newtonian gravity of

$$F_\phi(r_0)/F_N(r_0) = 4 \times 10^{-22}(M_{BH}/M_\odot) \tag{2.51}$$

which is again small for even the largest of black holes.

For Galileons we see that the Galileon term dominates for all sizes of black holes, giving a similar force ratio to that of K-mouflage:

$$F_\phi(r_0)/F_N(r_0) = 2 \times 10^{-22}(M_{BH}/M_\odot). \tag{2.52}$$

We saw that for large black holes that the Galileon scalar profile was similar, around r_1, to that of the static case. However for small black holes it was different. In this case the

profile was similar to the vacuum profile, for which the ratio of the forces is

$$F_\phi(r_1)/F_N(r_1) = 10^{-23}(M_{BH}/M_\odot). \tag{2.53}$$

In all cases the fifth force is highly suppressed relative to the Newtonian gravitational force.

2.7 Supermassive Black Hole Offset

It has been discussed in Ref. [58] that supermassive black holes in Galileon theories should be offset from the centre of the galaxy. This is because the non-relativistic equation of motion for an object in an externally sourced scalar field is

$$\ddot{\vec{x}} = -\nabla\Phi_N(\vec{x}) - \frac{\beta Q}{M_{Pl}M}\nabla\phi_{ext} \tag{2.54}$$

where M and Q are the mass and scalar charge of the object respectively. Black holes have no scalar charge and so do not couple to external scalar gradients which are generated by large scale structure, whereas the ordinary matter in the galaxy does. The black hole is therefore offset from the centre of the galaxy such that the ordinary gravitational attraction of constituents of the galaxy on the black hole is balanced by the scalar fifth force. A similar effect has been discussed in Ref. [80] in the context of scalar gradients generated by galaxy clusters. Both Ref. [58] and Ref. [80] focus on Galileon theories. Whether such an effect is present in K-mouflage theories is unclear. The key difference is that K-mouflage theories do not have the shift symmetry in the gradient of the field and so linear gradients are suppressed, unlike in Galileon theories. Thus one would expect the host galaxy to suppress the external gradient field and consequently, at the centre of the galaxy, it makes little difference whether an object couples to this field or not.

We note however that it is the entire black hole and accretion disk system that is offset, and this does have a scalar charge; namely the mass of the accretion disk. This means that the black hole and accretion disk feel a fifth force and therefore the offset is reduced. An offset is still present because the scalar charge, M_{acc}, does not equal the total mass, $M_{acc}+M_{BH}$. The displacement, r, of an object of scalar charge Q and mass M in an external scalar gradient can be found by equating the fifth force with the additional gravitational force due to the offset from the galactic centre. An object of scalar charge Q and mass M falls according to eq. (2.54). Therefore a test mass (which has $Q=M$) at the galactic centre (which is the minimum of the Newtonian potential) will have an equation of motion

$$\ddot{\vec{x}}_0 = -\frac{\beta}{M_{Pl}}\nabla\phi_{ext}. \tag{2.55}$$

The relative acceleration between the galactic centre and the object is zero and we take $\nabla\Phi_N(\vec{x}_1) = Gm(r)/r^2$, where $m(r)$ is the mass contained within a sphere of radius r centred on the galactic centre. Thus

$$\frac{Gm(r)}{r^2} = (1-\frac{Q}{M})\frac{\beta}{M_{Pl}}|\nabla\phi_{ext}|. \tag{2.56}$$

As we can see black holes (with $Q=0$) have the maximum displacement, and non-compact objects (with $Q=M$) are not displaced. If we assume, as in Ref. [58], that the background density is constant, then $m(r)\sim r^3$ and so the displacement increases linearly with $|\nabla\phi_{ext}|$. Putting $Q=M_{acc}$ and $M=M_{acc}+M_{BH}$ then gives us that the offset calculated in Ref. [58] would be reduced by a factor of

$$1+\frac{M_{acc}}{M_{BH}}. \tag{2.57}$$

In table 2.3 approximate values of this ratio are shown for various values of M_{BH}, where, to calculate the mass of the accretion disk, we have assumed a disk-like accretion disk fifty Schwarzschild radii wide, and a tenth of a Schwarzschild radius deep. We can see that for

$M_{BH}/M_{\odot}$	1	10	10^6	10^9
$M_{acc}/(M_{BH}+M_{acc})$	10^{-19}	10^{-17}	10^{-7}	10^{-1}

Table 2.3 Approximate values of the fractional offset reduction for various values of M_{BH}

small black holes, such as the one in our own galaxy, the difference is slight, however for the larger black holes the difference is increased.

2.8 Discussion and Conclusion

In this chapter we have performed exploratory calculations to investigate the Galileon and K-mouflage scalar profiles that can be generated by a black hole with an accretion disk. In static setups, with no external matter, no-hair theorems [59] tell us that no scalar gradients exist. However this setup is not truly representative of astrophysical black holes and we have therefore considered setups in which some of the stipulations of the no-hair theorems have been relaxed. We first investigated a static setup with an accretion disk, then a time-dependent setup in vacuum, and finally a time-dependent setup with an accretion disk.

In section 2.3 we considered the profiles generated by a spherically symmetric accretion disk, on a Schwarzschild background, with an r-dependent scalar. We showed that for both theories the scalar gradient was zero inside of the inner edge of the accretion disk, grew inside the disk, and then decayed to zero at large r. This is very much in contrast to the potential based screening mechanisms investigated in Ref. [38]. In these the gradient was pinned to zero within the relatively dense accretion disk, but attained non-zero values inside of the inner edge of the disk. We evaluated the ratio of the scalar fifth force to gravitational force at the outer edge of the accretion disk, with the values displayed in table 2.1. They are small for two reasons. Firstly the scalar screening mechanisms work as usual, and secondly the mass of the black hole contributes to the gravitational force, but not the scalar force.

In section 2.5 we reviewed the time-dependent Galileon black hole solutions of Ref. [9], and found exact vacuum black hole K-mouflage solutions. The solutions have a Schwarzschild-de Sitter metric and a scalar with linear time-dependence. For K-mouflage theories we found that the fifth force strength coincided with that of the time-independent calculation at the outer edge of the accretion disk. However there is now a force inside of the inner edge of the disk, albeit a small one. For the Galileon we found that the addition of the accretion disk had little affect on the vacuum profile, and that the force was always small.

We also considered how the addition of an accretion disk alters the argument of Ref. [58] that supermassive black holes are offset from the centre of their host galaxy in Galileon theories. We argue that this effect should not be seen in K-mouflage theories, but that in Galileon theories the addition of the disk should reduce the offset distance by a factor of

$$1 + M_{acc}/M_{BH}. \tag{2.58}$$

Further to considering purely the ratio of the fifth force to the gravitational force, we considered how the work done by this fifth force would affect an object in-spiralling towards the black hole due to the loss of energy via quadrupole radiation. We found that this was suppressed by the same ratio as the fifth force to gravitational force.

Chapter 3

K-mouflage Theories with a Disformal Coupling

In the previous chapter we discussed Galileon and K-mouflage theories around a black hole with external matter. The coupling to matter of both the Galileon and K-mouflage was via a conformal coupling factor. Here we extend our study of K-mouflage models to include an analysis of K-mouflage theories with an additional, disformal coupling to matter. These couplings were first discussed by Bekenstein in Ref. [13] in which he argued that the most general form of the metric to which matter couples is of the form

$$\tilde{g}_{\mu\nu} = A^2(g_{\mu\nu} + B\partial_\mu\phi\partial_\nu\phi/M^4) \tag{3.1}$$

where M is an energy scale and B is referred to as the disformal factor. Despite this the majority of the literature focuses on conformal couplings to matter. In the first part of the chapter we consider the background cosmological behaviour of the K-mouflage with a disformal term and at the end of the chapter we reconsider the set-up of chapter 2 with the addition of the disformal term.

3.1 Background to Disformal Couplings

In scalar-tensor theories one has the freedom to change frames which amounts to defining a new metric in terms of the old metric and the scalar field. Matter fields couple minimally to the Jordan frame metric, $\tilde{g}_{\mu\nu}$, so it is this metric on which the matter dynamics take place. For example test particles follow the geodesics of this metric. One can change frames to write the Lagrangian in terms of another metric. Typically one chooses to write in terms of the Einstein metric, $g_{\mu\nu}$, which is the one for which the gravitational sector Lagrangian can be written as a standard Einstein-Hilbert term. These two metrics differ, and conventionally they are taken to be related by a conformal factor, $\tilde{g}_{\mu\nu} = A^2 g_{\mu\nu}$. However Ref. [13] argued that, although this was the simplest relation one could have a more general relation; that if the theory was to obey causality and the weak equivalence principle then the relation between the two metrics could only be a conformal factor plus a term comprised of the outer product of the derivatives of the scalar

$$\tilde{g}_{\mu\nu} = A^2(g_{\mu\nu} + B\partial_\mu\phi\partial_\nu\phi/M^4) \tag{3.2}$$

where M is some energy scale and, in the most general case, A and B can be functions of both ϕ and $(\partial\phi)^2$. This additional term is referred to as a "disformal coupling". Disformal couplings can occur naturally, in for example massive gravity [40] or braneworld scenarios [41], but have been investigated less in the literature, particularly so in theories with a screening mechanism. It was shown in Ref. [77] that the non-relativistic limit of standard scalar-tensor theories is unaltered by the addition of a disformal term. A related fact is that, when expanded in powers of $1/M^4$, the first order term in the matter Lagrangian is proportional to

$$\partial_\mu\phi\partial_\nu\phi T_E^{\mu\nu} \tag{3.3}$$

which vanishes for a static field and non-relativistic source;

$$T_E^{00} = -\rho_E \tag{3.4}$$

$$T_E^{0i} = T_E^{ij} = 0 \tag{3.5}$$

$$\partial_t \phi = 0. \tag{3.6}$$

In fact Ref. [20] showed that the matter Lagrangian, with no conformal coupling and a constant disformal coupling, vanishes for all orders in $1/M^4$ and so no classical force is produced. Quantum effects will produce a fifth force [20] but, nevertheless, standard fifth force experiments are ill-suited to constraining a disformal coupling. Thus alternative physics has had to be considered such as coupling to photons [21] and collider constraints [20].

Given that static set-ups are ill-suited to constraining disformal couplings, it is natural to consider time-dependent situations. This is what we do in this chapter, firstly with regard to the background evolution of the universe, and secondly in the time-dependent black hole solutions discussed at the end of chapter 2.

3.1.1 Disformal Cosmologies

In this chapter we consider the cosmologies of theories with a disformal coupling to matter and K-mouflage kinetic structures. So far, the literature has focussed on disformal couplings in theories with a canonical kinetic term [77, 78], that is extending actions of the form eq. (1.91) to include a disformal coupling, or theories with Galileon kinetic structures [95]. One problem that can occur when calculating the cosmologies of disformal theories is that the determinant of the Jordan frame metric becomes singular, which happens when the square root in the middle term of eq. (3.24) becomes zero. Numerical studies [94] have shown that cosmological solutions slow down as the singularity is approached and this was dubbed "a natural resistance to pathology". In Ref. [78] it was clarified that the singularity

actually only occurs the infinite future. Nevertheless, it was still argued that cosmological solutions that evolve toward this singularity are not viable because fifth forces diverge as the singularity is approached. Ref. [78] further characterised the late time behaviour of disformal cosmologies. It was found that viable models that avoid the singularity do exist, but that the disformal term does not affect these end states, and therefore that disformal cosmologies in standard scalar-tensor theories are of limited interest in terms of their late time cosmological behaviour.

3.2 Background Cosmological Evolution

The background cosmological evolution of K-mouflage with a conformal-only coupling to matter has been considered in Ref. [23]. There it was found that solutions screened at early times existed and that these exhibited tracker behaviour. These solutions had $\phi \to 0$ and $\chi \to \infty$ as $t \to 0$. Although the scalar energy density blows up at early times, it does so slower than matter, and so the universe is matter-dominated. This is despite the fact that the equation of state of the scalar is not minus one, and can even diverge at a specific time point in the evolution of the universe . As t increases, χ decreases. Dependent upon the functional form of $K(\chi)$ solutions are discussed where $\chi \to 0$ at late time, or when χ tends to a non-zero value. The final fate of the universe is found to be a de Sitter universe. In between the early and late times where the behaviour is indistinguishable from ΛCDM, percent level differences between the Hubble rate and that of ΛCDM are found. The differences are greatest for red shifts of around $1 \leq z \leq 5$.

Our goal in this part of the chapter is to find solutions of this theory that demonstrate ΛCDM-like behaviour. We consider the matter-era onwards and so our criteria amount to having matter domination at early times, transitioning to a dark energy dominated universe, and having the correct equation of state for this dark energy during the dark energy dominated era.

3.2.1 Preliminaries

Our action is the same as the K-mouflage action of chapter 2. It is

$$\int dx^4\sqrt{-g}\left(\frac{M_{Pl}^2}{2}R+\mathscr{M}^4K(\chi)\right)+S_m(\tilde{g}_{\mu\nu}) \tag{3.7}$$

where $\chi=-(\partial\phi)^2/2\mathscr{M}^4$, $\mathscr{M}$ is an energy scale, S_m is the matter Lagrangian. The difference is in the form of the Jordan frame metric, $\tilde{g}_{\mu\nu}$, which is related to the Einstein frame metric, $g_{\mu\nu}$, via the equation

$$\tilde{g}_{\mu\nu}=A^2(\phi)(g_{\mu\nu}+\frac{B}{M^4}\partial_\mu\phi\partial_\mu\phi) \tag{3.8}$$

where $B>0$ is a constant. B is called a disformal factor and it is the introduction of this term in the context of K-mouflage cosmology that is novel. As before we assume $K(\chi)$ is of the form

$$K(\chi)=-1+\chi+... \tag{3.9}$$

where the ellipsis denotes higher powers of χ. When χ is small $K(\chi)\approx-1+\chi$. However when χ is large the higher powers of χ will dominate. For the purposes of this work we only consider $K(\chi)$ to be a polynomial of χ. This means that for large χ, taking the highest power to be n, we have that $K(\chi)\sim\chi^n$. For the purposes of generating numerical plots we take

$$K(\chi)=-1+\chi+k_0\chi^n \tag{3.10}$$

as this is a simple function that has the qualitative features of $K(\chi)$ that we desire. The equations derived from varying the Einstein metric are unaffected by the way in which matter is coupled to the metric, and they are simply the usual GR-like equations

$$M_{Pl}^2G_{\mu\nu}=T^E_{\mu\nu}+T^\phi_{\mu\nu} \tag{3.11}$$

where $T^E_{\mu\nu}$ is the Einstein frame energy-momentum tensor and $T^\phi_{\mu\nu}$ is the energy momentum associated to the scalar. Explicitly we have

$$T^\phi_{\mu\nu} = \mathscr{M}^4 K(\chi) g_{\mu\nu} + K'(\chi)\partial_\mu\phi\partial_\nu\phi. \tag{3.12}$$

All modifications to gravity appear in the equation of motion derived from varying the scalar, which gives

$$\frac{1}{\sqrt{-g}}\partial_\mu(\sqrt{-g}\partial^\mu\phi K'(\chi) - \sqrt{-g}T_E^{\mu\nu}\partial_\nu\phi B/M^4) = -T_E^{\mu\nu}g_{\mu\nu}A'(\phi)/A(\phi) - T_E^{\tau\nu}\partial_\tau\phi\partial_\nu\phi(A'(\phi)B/AM^4). \tag{3.13}$$

3.2.2 Cosmological Equations

We look for homogeneous isotropic cosmological solutions. This amounts to having

$$ds^2 = -dt^2 + a(t)^2 d\Sigma^2 \tag{3.14}$$

$$\phi = \phi(t). \tag{3.15}$$

In this work we are focusing on the matter-dominated era onwards. We assume a spatially flat universe and ignore contribution to the Einstein frame energy momentum other than matter. That is we take

$$T_E^{00} = \rho_E \tag{3.16}$$

$$T_E^{0i} = T_E^{jk} = 0. \tag{3.17}$$

Combining these assumptions leaves us with the standard Friedmann-like equations with a contribution of the scalar energy momentum

$$3M_{Pl}^2 H_E^2 = \rho_E + \rho_\phi \tag{3.18}$$

$$-2M_{Pl}^2\dot{H}_E = \rho_E + \rho_\phi + p_\phi \tag{3.19}$$

with

$$\rho_\phi = -\mathscr{M}^4 K(\chi) + 2\chi K'(\chi) \tag{3.20}$$

$$p_\phi = \mathscr{M}^4 K(\chi). \tag{3.21}$$

These equations are the same as for the conformal case, however the evolution equation for the scalar is modified to become

$$\frac{d}{dt}(a^3\dot{\phi}K'(\chi) + a^3\rho_E\dot{\phi}B/M^4) = \rho_E A'(\phi)/A(\phi) - \rho_E\dot{\phi}^2 A'(\phi)B/AM^4. \tag{3.22}$$

The Einstein frame energy momentum is not conserved and therefore the Einstein frame matter density does not obey the usual evolution equation of matter. However the Jordan frame energy momentum is conserved because in this frame the modifications to General Relativity appear in the gravitational sector. Therefore the usual argument that the diffeomorphic invariance of the matter Lagrangian implies the conservation of the energy momentum follows through. We use this fact to substitute out the Einstein frame matter density in favour of a matter density that is conserved (with respect to Einstein frame time). To do this we must consider the relation between the two frames. We take the Jordan frame metric to be

$$\tilde{ds}^2 = -d\tilde{t}^2 + \tilde{a}(\tilde{t})^2 d\Sigma. \tag{3.23}$$

We can now use eq. (3.8), along with eq. (3.14) and eq. (3.15) to give the relations

$$d\tilde{t} = A\sqrt{1 - B(\partial_t\phi)^2/M^4}dt = \frac{A}{\sqrt{1 + B(\partial_{\tilde{t}}\phi)^2/M^4}}dt \tag{3.24}$$

$$a(t) = \tilde{a}(\tilde{t})/A. \tag{3.25}$$

We include the relation between $d\tilde{t}$ and dt in both Einstein frame time and Jordan frame time for completeness, but will use exclusively the first equality of eq. (3.24). We will also require the relation between the Einstein and Jordan frame energy momentum tensors [95]

$$T_E^{\mu\nu} = A^6\sqrt{1-2BX/M^4}\tilde{T}^{\mu\nu} \tag{3.26}$$

where $X = -g^{\mu\nu}\partial_\mu\phi\partial_\nu\phi/2$. From eq. (3.26) we can calculate the relation between the matter densities of the two frames:

$$\rho_E = T_E^{tt} = A^6\sqrt{1-B(\partial_t\phi)^2/M^4}\tilde{T}^{tt} = A^6\sqrt{1-B(\partial_t\phi)^2/M^4}\tilde{T}^{\tilde{t}\tilde{t}}(\frac{dt}{d\tilde{t}})^2 = A^4\tilde{\rho}/\sqrt{1-B(\partial_t\phi)^2/M^4} \tag{3.27}$$

where tilded quantities are those in the Jordan frame. As stated above conservation of the Jordan frame energy momentum implies the usual conservation equation for matter

$$\frac{d}{d\tilde{t}}(\tilde{a}^3\tilde{\rho}) = 0 \tag{3.28}$$

which, re-written in terms of Einstein frame quantities is

$$\frac{d}{dt}(a^3\rho_E/A\sqrt{1-2BX/M^4}) = 0. \tag{3.29}$$

This motivates us to define the quantity

$$\hat{\rho} = \rho_E/A\sqrt{1-2BX/M^4} \tag{3.30}$$

which obeys the usual matter conservation equation in the Einstein frame,

$$\dot{\hat{\rho}} = -3H_E\hat{\rho}, \tag{3.31}$$

and so

$$\hat{\rho}_0 = \hat{\rho} a^3 \tag{3.32}$$

is a conserved quantity. We also define

$$\rho_{eff} = \rho_\phi + \hat{\rho}(A\sqrt{1-2BX/M^4} - 1) \tag{3.33}$$

and use eq. (3.32) and eq. (3.33) to re-write eqs. (3.18) to (3.22) into the final form that we shall use

$$3M_{Pl}^2 H_E^2 = \hat{\rho} + \rho_{eff} \tag{3.34}$$

$$-2M_{Pl}^2 \dot{H}_E = \hat{\rho} + \rho_{eff} + p_\phi \tag{3.35}$$

$$\rho_\phi = -\mathscr{M}^4(K(\chi) - 2\chi K'(\chi)) \tag{3.36}$$

$$p_\phi = \mathscr{M}^4 K(\chi) \tag{3.37}$$

$$\omega_\phi = p_\phi/\rho_{eff} \tag{3.38}$$

$$\frac{d}{dt}(a^3\dot{\phi}K'(\chi) + \hat{\rho}_0\rho_0\dot{\phi}A\sqrt{1-2B\chi}B/\mathscr{M}^4) = -\beta(\phi)\hat{\rho}_0(1-2B\chi)^{3/2}/M_{Pl} \tag{3.39}$$

where $\beta(\phi) = M_{Pl}A'(\phi)/A(\phi)$ and we have set $M = \mathscr{M}$, which is without loss of generality because the difference can be absorbed into B.

3.2.3 Early Time Limit

A physically realistic universe must be matter-dominated at early times. This can be achieved if $\rho_{eff}/\hat{\rho}$ and $p_\phi/\hat{\rho}$ are both small. In this case eqs. (3.34) and (3.35) become

$$3M_{Pl}^2 H_E^2 \approx \hat{\rho} \tag{3.40}$$

$$-2M_{Pl}^2 \dot{H}_E \approx \hat{\rho} \tag{3.41}$$

which is solved by

$$a \approx (3\hat{\rho}_0 t^2/4M_{Pl})^{1/3}. \tag{3.42}$$

We now consider the conditions required to have a matter-dominated universe, that is, one with $a^3 \sim t^2$. Integrating eq. (3.39) gives that at early time

$$-\hat{\rho}_0\dot{\phi}A\sqrt{1-2B\chi}B/\mathscr{M} \approx -\hat{\rho}_0\dot{\phi}(0)A(\phi(0))\sqrt{1-2B\chi(0)}B/\mathscr{M} - \beta\hat{\rho}_0(1-2B\chi(0))^{3/2}t/M_{Pl}. \tag{3.43}$$

Unlike conformally coupled K-mouflage, which has $\dot{\phi} \to \infty$ at early times, we are free to choose the initial value of $\dot{\phi}$. Whatever this is chosen to be, ρ_ϕ and p_ϕ will be fixed to an initial, finite value therefore, because $\hat{\rho} \to \infty$ as $t \to 0$, both $\rho_\phi/\hat{\rho}$ and $p_\phi/\hat{\rho}$ will tend to zero as $t \to 0$. From eq. (3.33) at early time $\rho_{eff}/\hat{\rho} \approx A\sqrt{1-2B\chi} - 1$, therefore to ensure matter domination we must choose initial conditions such that

$$A(\phi(0))\sqrt{1-2B\chi(0)} \approx 1. \tag{3.44}$$

This condition will be sufficient to ensure that at early times the right-hand sides of eqs. (3.34) and (3.35) will be dominated by matter and the scale factor will have the correct dependence upon time.

In the above argument we have shown that eq. (3.44) is sufficient to have $a^3 \sim t^2$ at early time. However, this is the Einstein frame scale factor and what we really need in order to have a matter-dominated universe is for the Jordan frame quantities to obey the equivalent relation, that is $\tilde{a}^3 \sim \tilde{t}^2$. We now show that this is indeed the case. To do this we need to calculate the relation between the Hubble rates, $H_E \equiv \frac{d}{dt}ln(a(t))$ and $\tilde{H} \equiv \frac{d}{d\tilde{t}}ln(\tilde{a}(\tilde{t}))$, which, using eqs. (3.24) and (3.25), is

$$H_E = \frac{d\tilde{t}}{dt}(\tilde{H} - \frac{d}{d\tilde{t}}ln(A)) \tag{3.45}$$

$$H_E = A\sqrt{1-2B\chi}\tilde{H} - \beta\dot{\phi}/M_{Pl}. \tag{3.46}$$

Given eq. (3.44), that H_E diverges as $t \to 0$ and that $\dot{\phi}(0)$ is finite, we have that, at early time, $t \approx \tilde{t}$ and $H_E \approx \tilde{H}$ and so we do indeed have early time matter domination.

3.2.4 Late Time Limit

Our universe appears to be entering an era of accelerated expansion driven by a dark energy with equation of state of minus one. We therefore impose that, in addition to early time matter domination, any solution that we find must have this behaviour in the large t limit. That is, we seek a late time de Sitter solution, with $\dot{H_E} = 0$ and $a \sim exp(H_E t)$. Because $\rho \to 0$ as $t \to \infty$, at late times we must have

$$\rho_{eff} + p_\phi = 2\mathscr{M}^4 \chi K'(\chi) \approx 0. \tag{3.47}$$

Thus $\dot{\phi}$ must tend towards either zero or a zero of $K'(\chi)$. Integrating eq. (3.39) and taking t to be large gives late time behaviour of

$$\dot{\phi}K'(\chi) \approx -\beta_\infty \hat{\rho}_0 (1-2B\chi_\infty)^{3/2} t/M_{Pl}a^3 \tag{3.48}$$

where $\chi_\infty = \lim_{t\to\infty}\chi$ and we assume that $\beta_\infty = \lim_{t\to\infty}\beta$ is finite. The right-hand side of this equation tends to zero and so $\dot{\phi}$ tending to either zero or a zero of $K'(\chi)$ appear to both be valid asymptotic behaviour of solutions to eq. (3.39). Indeed Ref. [23] has discussed solutions of both these forms for conformally coupled matter. However, as we did for the early time behaviour, we must ensure that de Sitter solutions in the Einstein frame correspond to de Sitter solutions in the Jordan frame. Consider first those solutions which have $\dot{\phi} \to \dot{\phi}_\infty \neq 0$. We evaluate eq. (3.46) on this solution and differentiate. Using eq. (3.24)

this gives

$$0 = \dot{H}_E = \frac{d}{dt}(A\sqrt{1-2B\chi_\infty})\tilde{H} + (A\sqrt{1-2B\chi_\infty})^2\frac{d}{d\tilde{t}}\tilde{H} + \beta'(\phi)\dot{\phi}_\infty^2/M_{Pl} \tag{3.49}$$

which, evaluating eqs. (3.33), (3.34) and (3.46) on these solutions and substituting in, gives

$$\frac{d}{d\tilde{t}}\tilde{H} = -(\beta\dot{\phi}_\infty(\mathscr{M}^2\sqrt{-K(\chi_\infty)/3} + \beta\dot{\phi}_\infty) + 2M_{Pl}\mathscr{M}^4\beta'(\phi)\chi_\infty)/A^2M_{Pl}^2(1-2B\chi_\infty). \tag{3.50}$$

For this to be zero we require the numerator to be zero. If β tends to a non-zero constant then this cannot happen, unless the zero of $K(\chi)$ is chosen specifically so that the value of $\dot{\phi}$ is such that the numerator is zero. Alternatively the functional form of β could be chosen specifically to force the numerator to be zero. These cases are highly contrived and we will not consider them here but will return to the $\beta = 0$ case later.

For the left-hand side of eq. (3.50) to tend to zero one could also have the denominator blow up. However upon inspection of eq. (3.46) this will correspond to $\tilde{H} \to 0$ which we discount as unphysical. Although we cannot rule out the possibility that there will be physically acceptable solutions in the Jordan frame that appear unphysical in the Einstein frame, these would be difficult to find. We therefore limit ourselves to looking for solutions in the Einstein frame that appear physical, and ensuring that the differences between the two frames are small enough that physical behaviour can be inferred from the Einstein frame.

For the reasons explained above we will discount the solutions with asymptotic behaviour $\dot{\phi} \to \dot{\phi}_\infty \neq 0$ and will require $\dot{\phi} \to 0$ as $t \to \infty$. This gives satisfactory physical behaviour, which using eqs. (3.35) to (3.37), (3.46) and (3.48) is

$$\phi \approx \phi_\infty \tag{3.51}$$

$$\dot{\phi} \approx -\beta(\phi_\infty)\hat{\rho}_0 t/M_{Pl}a^3 \tag{3.52}$$

$$\rho_{eff} \approx \mathscr{M}^4 \tag{3.53}$$

$$p_\phi \approx -\mathscr{M}^4 \tag{3.54}$$

$$H_E \approx \mathscr{M}^2/M_{Pl}\sqrt{3} \tag{3.55}$$

$$a(t) \sim exp(\mathscr{M}^2 t/M_{Pl}\sqrt{3}) \tag{3.56}$$

$$\tilde{H} \approx \mathscr{M}^2/A(\phi_\infty)M_{Pl}\sqrt{3} \tag{3.57}$$

$$\tilde{a}(\tilde{t}) \sim exp(\mathscr{M}^2\tilde{t}/A(\phi_\infty)M_{Pl}\sqrt{3}). \tag{3.58}$$

Recall that standard scalar-tensor theories with a disformal coupling [78] have late time cosmological behaviour that is independent of the disformal coupling. Although eqs. (3.51) to (3.58) do not depend on the disformal coupling explicitly, they do depend on ϕ_∞. And unlike standard scalar-tensor theories, in which ϕ_∞ is the minimum of a potential and therefore independent of B, in K-mouflage models ϕ_∞ is dependent on B.

3.2.5 $A = 1$ Case

Before considering the more general case we will take some time to discuss the more tractable case in which $A = 1$. This case is made particularly simple as there is no explicit dependence on ϕ, only on its derivatives. As a consequence of Noether's theorem, this means that eq. (3.39) takes the form of a conservation equation:

$$\frac{d}{dt}(a^3\dot{\phi}K'(\chi) + \hat{\rho}_0\dot{\phi}\sqrt{1-2B\chi}B/\mathscr{M}^4) = 0. \tag{3.59}$$

Revisiting the late time behaviour discussed above, all of eqs. (3.51) to (3.58) hold true, except eq. (3.52), which instead has

$$\dot{\phi} \sim 1/a^3. \tag{3.60}$$

Early and Late Time Behaviour in this Case

Considering the early time limit in this instance, if we impose eq. (3.44) exactly, then we will have $\dot{\phi}(0) = 0$ and therefore, from eq. (3.59), $\dot{\phi}(t) = 0$ for all time. This is simply a cosmological constant. We instead allow eq. (3.44) to hold approximately and so achieve modifications to gravity. We suppose that we have

$$\lim_{t\to 0} \rho_{eff}/\hat{\rho} = \sqrt{1-2B\chi(0)} - 1 = -\varepsilon \tag{3.61}$$

where ε is small, which amounts to

$$\dot{\phi}(0)/\mathscr{M}^2 = \sqrt{\varepsilon(2-\varepsilon)/B} \approx \sqrt{2\varepsilon/B} \tag{3.62}$$

where we have chosen $\dot{\phi}(0) \geq 0$, which is without loss of generality because eqs. (3.34) to (3.37) and (3.59) are invariant under the inversion $\dot{\phi} \to -\dot{\phi}$.

Behaviour of Solutions

We now integrate the equation of motion and determine the behaviour of $\dot{\phi}$. We then consider our original criteria for a physically realistic solution, and attain constraints from these restrictions.

We integrate eq. (3.59) and rearrange to find for an implicit equation for $\dot{\phi}$:

$$\dot{\phi} = \frac{B\hat{\rho}_0\dot{\phi}(0)\sqrt{1-2B\chi(0)}/\mathscr{M}^4}{a^3K'(\chi) + B\hat{\rho}_0\sqrt{1-2B\chi}/\mathscr{M}^4}. \tag{3.63}$$

Initially a is small, the second term of the denominator will dominate over the first and so $\dot{\phi}$ will remain fixed at its initial value. This will remain the case until the first term has

become significant in size relative to the second term. We define this time t_{tr} by the equation

$$a^3(t_{tr}) = B\hat{\rho}_0\sqrt{1-2B\chi(0)}/10\mathscr{M}^4K'(\chi(0)). \tag{3.64}$$

At the time t_{tr}, $\dot{\phi}$ will have reached around ninety percent of its original value, and will, from then on, decrease further. We take t_{tr} as a ball park figure that denotes the time at which $\dot{\phi}$ starts to vary significantly from its original value.

If we reach a point where the first term of the denominator does dominate then we have that

$$a^3\dot{\phi}K'(\chi) \sim constant. \tag{3.65}$$

We have that a^3 is increasing with time and have imposed that $\dot{\phi}K'(\chi)$ is an increasing function of $\dot{\phi}$. Therefore eq. (3.65) implies that $\dot{\phi}$ must be decreasing with time, which in turn means that $a^3K'(\chi)$ is increasing. This means that once the first term of the denominator starts to dominate, it will continue to do so. Thus t_{tr} denotes a transition time, before which $\dot{\phi}$ is approximately constant and after which $\dot{\phi}$ starts to decrease. Once the first term of the denominator starts to dominate eq. (3.63) is then approximated by

$$a^3\dot{\phi}K'(\chi) \approx B\hat{\rho}_0\dot{\phi}(0)\sqrt{1-2B\chi(0)}/\mathscr{M}^4. \tag{3.66}$$

As a increases with time, $\dot{\phi}$ will eventually decrease towards zero.

We have now established that $\dot{\phi}$ remains constant early at early times. At some point, as defined by eq. (3.64), $\dot{\phi}$ will begin to decrease, and the dynamics will transition from $\dot{\phi}$ being approximately constant, to $\dot{\phi}$ decreasing and finally asymptoting toward the behaviour of eqs. (3.51), (3.53) to (3.58) and (3.60). Note also that, because $\dot{\phi}$ is decreasing, $\sqrt{1-2B\chi}$ will increase from its original value to unity. It is this quantity that vanishes for the pathological, singular behaviour previously seen in disformal cosmologies, and therefore the problem of singularity in the Jordan frame is not an issue for these solutions.

Constraining these Solutions

We now consider the third criterion of the requirements that we stated at the beginning of the chapter. That is that the equation of state of scalar energy momentum is approximately minus one during the dark energy dominated era.

Firstly, we consider the equation of state. From eqs. (3.33) and (3.36) to (3.38) we have

$$\omega_\phi = -1 + \frac{2\chi K'(\chi) + \hat{\rho}(\sqrt{1-2B\chi}-1)/\mathscr{M}^4}{-K(\chi) + 2\chi K'(\chi) + \hat{\rho}(\sqrt{1-2B\chi}-1)}. \tag{3.67}$$

We wish to have $\omega_\phi \approx -1$ and for this to be achieved we must have $\chi \lesssim 1$. The time at which the universe will leave the matter-dominated era and enter the dark energy dominated era will be given by

$$\hat{\rho} \sim \rho_{eff}. \tag{3.68}$$

As we have already stated, to ensure the correct equation of state for the scalar energy momentum at the time of transition between the matter and dark energy dominated eras, χ must already be small and so eq. (3.68) amounts to

$$\hat{\rho} \approx \mathscr{M}^4. \tag{3.69}$$

This gives us our definition of the time, t_{DE}, at which the universe transitions between eras:

$$a^3(t_{DE}) = \rho_0/\mathscr{M}^4. \tag{3.70}$$

By the time we enter the dark energy dominated era, we require ρ_{eff} to be behaving like a cosmological constant. For this to happen we have two options. The first is simply that the initial value of $\dot{\phi}$ was small, and that t_{tr} is greater than the current age of the universe. This means that $\dot{\phi}$ has been fixed at its initial value for the entire age of the universe and the scalar energy momentum has acted like a cosmological constant. This case is uninteresting

as it is effectively just reproducing a ΛCDM universe. The other option is the one we shall focus on. In this case ρ_{eff} behaves like a cosmological constant because it is already close to the late time asymptotics of eqs. (3.51), (3.53) to (3.58) and (3.60). This means that $\dot{\phi}$ must have the behaviour of eq. (3.60). Thus we require t_{tr} to happen during the matter-dominated era, before the transition is observable as a change in the equation of state of the dark energy. Combining eqs. (3.64) and (3.70) with the requirement that $t_{tr} < t_{DE}$ then gives us the constraint that

$$a^3(t_{tr})/a^3(t_{DE}) \lesssim 1 \implies B\sqrt{1-2B\chi(0)}/K'(\chi(0)) \lesssim 10. \tag{3.71}$$

Re-writing this in terms of ε rather than the initial values of the derivative of the scalar, gives

$$B(1-\varepsilon)/K'(\varepsilon/B) \lesssim 10. \tag{3.72}$$

This constraint will be violated for large B. This is because for large B the initial value of χ will be small, and we will effectively have cosmological constant-like behaviour. The interesting question is whether eq. (3.72) can be violated for small B. Clearly this would require $K'(\varepsilon/B)$ to be small. For the forms of $K(\chi)$, given by eq. (3.10), analysed in our numerical plots, $K'(\chi) \geq 1$ and therefore eq. (3.72) will not be violated. However there is nothing in principal wrong with having $K'(\chi)$ small for large χ, as long as $\dot{\phi}K'(\chi)$ is an increasing function of $\dot{\phi}$.

As we have said, at t_{DE} we must have $\chi \lesssim 1$. We can impose this directly on eq. (3.63) to get a further constraint. This gives

$$\frac{B\dot{\phi}(0)\sqrt{1-2B\chi(0)}/\mathscr{M}^2}{1+B} \lesssim 1. \tag{3.73}$$

Again substituting for initial values gives us the constraint

$$\frac{\sqrt{\varepsilon B}(1-\varepsilon)}{1+B} \lesssim 1. \tag{3.74}$$

In fact, the maximum value of the left hand side of this equation is $1/3\sqrt{3}$ for $\varepsilon = 1/3$ and $B = 1$, so the constraint is always satisfied.

Plotting the Solutions

In the above subsection we have described the behaviour of the solution when $A = 1$ and derived the constraint eq. (3.71). In this subsection we generate a number of plots to see explicitly the level of variation between these models and ΛCDM. We take our form of $K(\chi)$ to be given by eq. (3.10) and so our model is described by the six parameters $(\mathscr{M}, \hat{\rho}_0, B, \varepsilon, K_0, m)$. We will generate plots in which the latter four are varied but we will fix the first two.

We fix $\hat{\rho}_0$ by matching the Hubble rate at early time with that given by ΛCDM. The eqs. (3.34) and (3.61) give that at early time

$$3M_{Pl}^2 H_E^2 \approx \hat{\rho}(1-\varepsilon) \tag{3.75}$$

and so

$$3M_{Pl}^2(1-2B\chi)\tilde{H}^2 \approx \hat{\rho}_0(1-\varepsilon)/a^3. \tag{3.76}$$

Using eq. (3.61) once more gives

$$\tilde{H}^2 \approx \hat{\rho}_0/3M_{Pl}^2(1-\varepsilon)a^3. \tag{3.77}$$

At early times ΛCDM has

$$H^2 \approx H_0^2\Omega_m/a^3 \tag{3.78}$$

and thus we fix

$$\hat{\rho}_0 = 3M_{Pl}^2 H_0^2 \Omega_m (1-\varepsilon). \tag{3.79}$$

We fix $\mathscr{M}$ by imposing the correct present day Hubble rate. Combining eqs. (3.39) and (3.46), imposing that $\tilde{H} = H_0$ and evaluating at $a = 1$ gives

$$3M_{Pl}^2(1-2B\chi_0)H_0^2 = \hat{\rho}_0\sqrt{1-2B\chi_0} - \mathscr{M}^4 K(\chi_0) + 2\chi_0 K'(\chi_0) \tag{3.80}$$

where χ_0 denotes the present day value of χ which can be found by evaluating eq. (3.63) at $a = 1$ and inverting.

For each parameter that we have varied, we have created three plots which depict the difference between the Hubble rate and that of ΛCDM, the value of $\dot{\phi}/\mathscr{M}^2$ and ω_ϕ respectively.

The fig. 3.1 shows how the solutions vary as B is changed. The eq. (3.62) gives the initial value of $\dot{\phi}/\mathscr{M}^2$, which in the $B = 100$ case is approximately 0.01. This means that the behaviour is very close to that of ΛCDM because the scalar just behaves like a cosmological constant. Indeed fig. 3.1c shows that the equation of state is fixed at minus one. The constraint eq. (3.72) is violated for $B = 100$ as this was calculated on the assumption that we did not have this type of behaviour. For $B = 1$ the initial value of $\dot{\phi}/\mathscr{M}^2$ is again small however in this case the left-hand side of eq. (3.72) is roughly 0.9. For this case the dark energy dominated era begins at $z_{de} \approx 0.4$, $z_{tr} \approx 2$ and the initial value of $\dot{\phi}/\mathscr{M}^2$ was small enough that ω_ϕ is already close to one at this time. In both the $B = 1$ and $B = 100$ fig. 3.1b shows that the Hubble rates are extremely close to those of ΛCDM. For the $B = 0.01$ case, the Hubble rates still only differ by maximum of a couple of percent, despite the greater variation in the value of $\dot{\phi}/\mathscr{M}^2$. In this case the constraint eq. (3.72) is easily satisfied. The initial value of $\dot{\phi}/\mathscr{M}^2$ was large, but t_{tr} was reached quickly and the value decreased so that at $z_{de} \approx 0.35$, $\dot{\phi}/\mathscr{M}^2$ is small and $\omega_\phi \approx -1$. In short, in all three cases, $B = 0.01$, $B = 1$

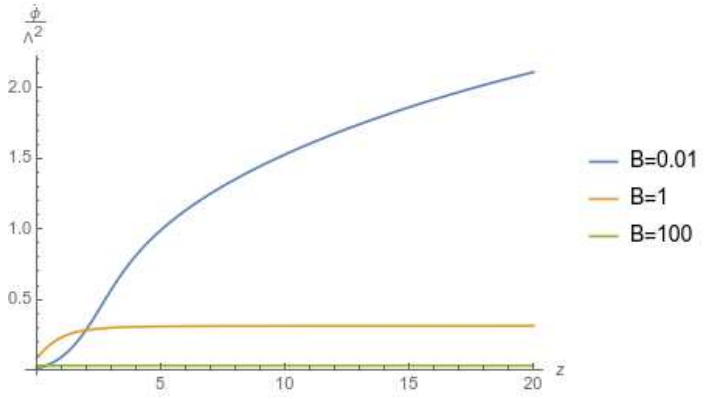

(a) $\dot{\phi}/\mathscr{M}^2$ as a function of z

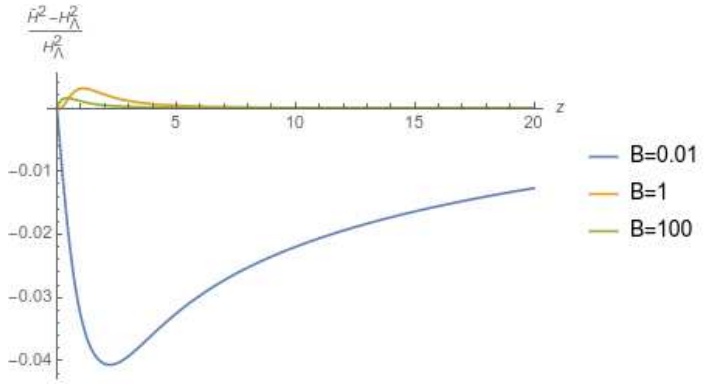

(b) Deviation of the Hubble rate squared from that of ΛCDM

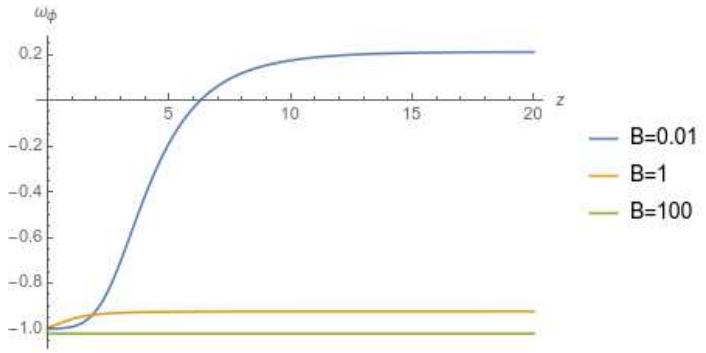

(c) ω_ϕ as a function of z

Fig. 3.1 Variation of solutions with respect to B, with fixed $(\varepsilon, k_0, n) = (0.05, 1, 3)$

and $B = 100$, the Hubble rates are all within percent differences of the ΛCDM Hubble rate despite significant variations in the underlying dynamics of $\dot{\phi}$. The small differences that there are, tend to be larger for smaller B.

In fig. 3.2 the three plots demonstrate the different behaviour for three different values of ε. In each of the three cases $\varepsilon = 0.05$, $\varepsilon = 0.2$ and $\varepsilon = 0.25$ the transition time occurs at $z_{tr} \approx 2$, $z_{tr} \approx 2.5$ and $z_{tr} \approx 2.7$ respectively. Indeed, fig. 3.2a shows that the value of $\dot{\phi}$ stays close to its initial value until around these times. The value then decreases toward zero, and correspondingly, fig. 3.2c show that ω_ϕ tends toward minus one. Observable differences between the models are shown in fig. 3.2b. It is clear that the largest differences occur at late time, when dark energy is becoming roughly equal to matter density - for $\varepsilon = 0.05$, $\varepsilon = 0.2$, and $\varepsilon = 0.25$ the corresponding starts of the dark energy era are at $z_{DE} = 0.35$, $z_{DE} = 0.45$ and $z_{DE} = 0.5$. It is also shown in fig. 3.2b that the larger values of ε give larger deviations from ΛCDM.

The effect of varying n is shown in fig. 3.3. In all three plots the variation of n makes little difference. This is primarily because the initial value of χ is approximately 0.5 and therefore the linear term dominates, which is the same for all three. The small differences displayed in fig. 3.3a and fig. 3.3b show that increasing n increases the value of $\dot{\phi}$ but decreases the deviation from the ΛCDM Hubble rate. However the absolute value of the Hubble rate deviation is small for all three. The equations of state displayed in fig. 3.3c all tend toward minus one. There are significant differences in the far past between the equations of state, however these would not be measurable as they are deep into the matter-dominated era.

In the main body of this work we have assumed $k_0 \sim 1$, however fig. 3.4 shows the differences that relaxing this assumption makes. For $K(\chi)$ of the form eq. (3.10) this means that $K(\chi)$ changes between linear and non-linear behaviour, not at $\chi \approx 1$, but at $\chi \approx k_0^{1/(m-1)}$. Thus increasing k_0 decreases the value of χ for which $K(\chi)$ becomes non-linear. In fig. 3.4a the values of $\dot{\phi}$ for $k_0 = 0.01$ and $k_0 = 1$ are shown to be similar. This is because for both

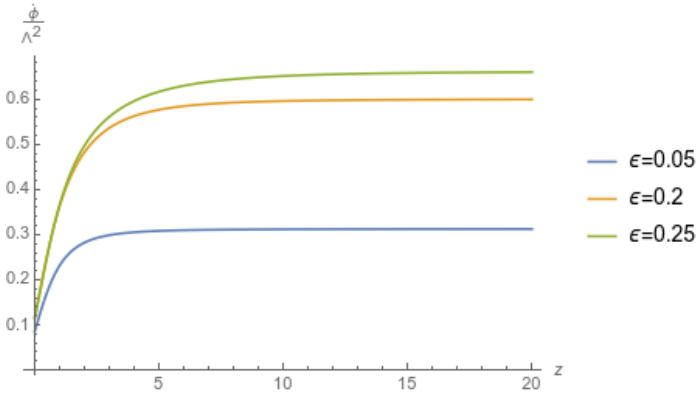

(a) $\dot{\phi}/\mathscr{M}^2$ as a function of z

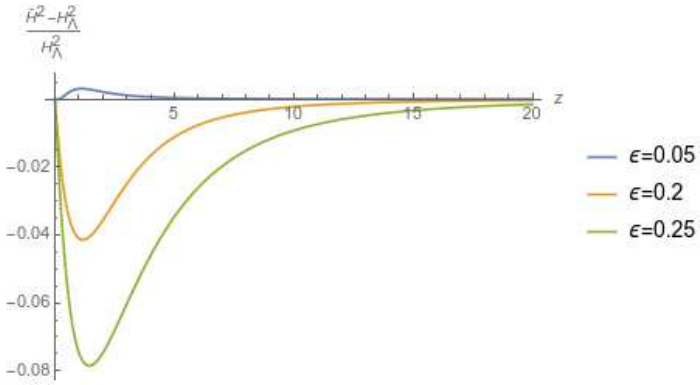

(b) Deviation of the Hubble rate squared from that of ΛCDM

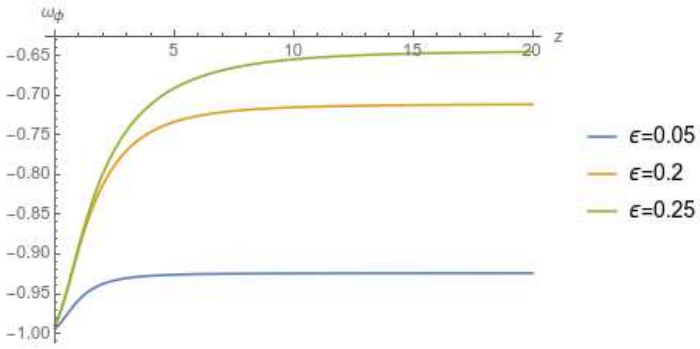

(c) ω_ϕ as a function of z

Fig. 3.2 Variation of solutions with respect to ε, with fixed $(B,k_0,n) = (1,1,3)$

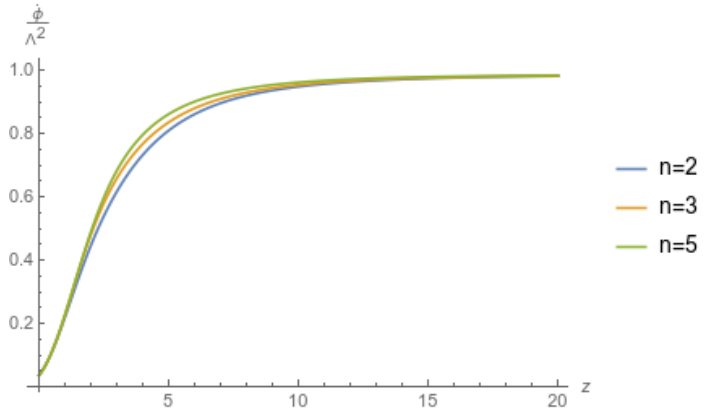

(a) $\dot{\phi}/\mathscr{M}^2$ as a function of z

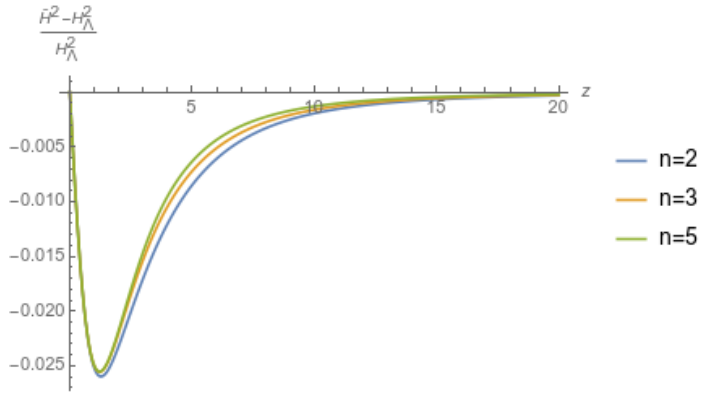

(b) Deviation of the Hubble rate squared from that of ΛCDM

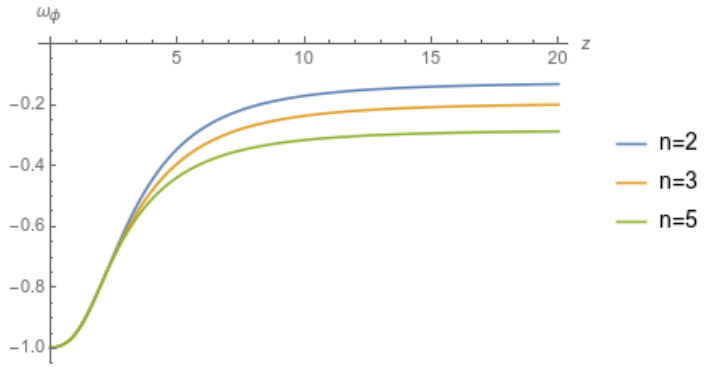

(c) ω_ϕ as a function of z

Fig. 3.3 Variation of solutions with respect to n, with fixed $(B, \varepsilon, k_0) = (0.1, 0.05, 1)$

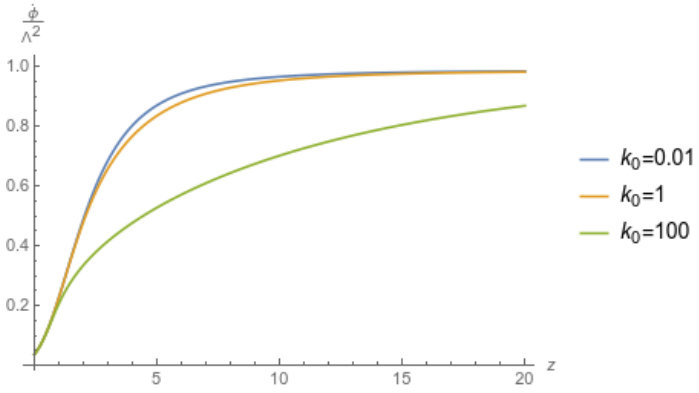

(a) $\dot{\phi}/\mathscr{M}^2$ as a function of z

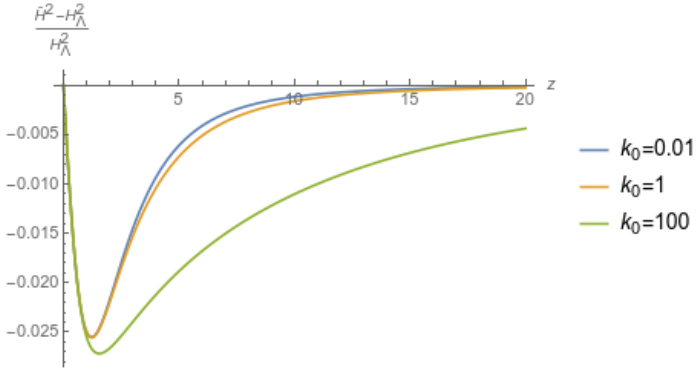

(b) Deviation of the Hubble rate squared from that of ΛCDM

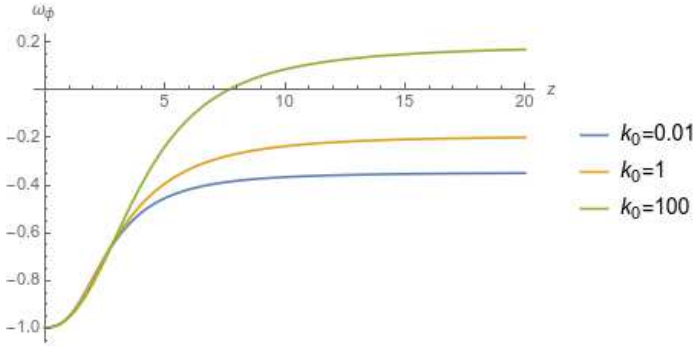

(c) ω_ϕ as a function of z

Fig. 3.4 Variation of solutions with respect to k_0, with fixed $(B,\varepsilon,n) = (0.1, 0.05, 3)$

$K(\chi)$ is behaving linearly, whereas for $k_0 = 100$, behaviour is non-linear and the value of $\dot{\phi}$ decreases more quickly. The initial value of $\dot{\phi}/\mathscr{M}^2 \approx 1$ and therefore the initial value of $K(\chi)$ and $K'(\chi)$ are larger for the smaller value of k_0. This means that despite the fact that $\dot{\phi}$ is suppressed quicker for large k_0, the overall deviation in the Hubble rate from that of ΛCDM is larger, as shown in fig. 3.4b. We seen in fig. 3.4c that all three models converge to $\omega_\phi \approx -1$. However in the distant past they differ, and the equation of state in the $k_0 = 100$ case even changes sign.

Below we discuss the implications of the results displayed in figs. 3.1 to 3.4 on the viability of disformally coupled K-mouflage models but leave a detailed analysis of the observational constraints on the parameter space (B, ε, n, k_0) to future research. Such an analysis would involve ensuring that the deviations of the predicted Hubble rate against red shift of disformal K-mouflage are consistent with observations [93]. These observations constrain the parameters of General Relativity with a ΛCDM matter content to the percent level [81] and figs. 3.1b, 3.2b, 3.3b and 3.4b plot deviations of the disformal K-mouflage Hubble rate from that of General Relativity with a ΛCDM matter content. Thus for our discussion below we consider those models which display a deviation of the squared Hubble rate from that of the ΛCDM model of more than a few percent to be in tension with observations.

In each of figs. 3.1 to 3.4 we have fixed three of (B, ε, n, k_0) and varied the fourth. It is clear that varying some of the parameters has more of an effect than varying others. For example, when varying k_0 or n deviations of the Hubble rate from that of the ΛCDM model were small for all values considered. Thus we would expect observations to only weakly constrain these parameters and for the more stringent constraints to be on B and ε.

In the $B \to \infty$ limit, the model we have investigated coincides with General Relativity with a ΛCDM matter content, and therefore, for sufficiently large B, the model will always be unconstrained. Indeed fig. 3.1 shows that for $B = 100$ ($\varepsilon = 0.05, k_0 = 1, n = 3$) deviations from ΛCDM are minimal. The more interesting question is whether observationally viable

models can occur with B not large. In fact, fig. 3.1b shows that for $B = 1$ ($\varepsilon = 0.05, k_0 = 1, n = 3$) deviations of the Hubble rate from that of General Relativity with a ΛCDM matter content are still small, and even with $B = 0.01$, the maximum deviation between the squared Hubble rates is around four percent, about the level we would expect to be coming into tension with observations.

In fig. 3.2b we see significant variation of the Hubble rate as ε is varied, indicating that ε is amenable to constraint from observation. For $\varepsilon = 0.05$ ($B = 1, k_0 = 1, n = 3$) deviations are small, but for $\varepsilon = 0.2$ deviations of the squared Hubble rates are around four percent and for $\varepsilon = 0.25$ they are up to eight percent. We would expect deviations of eight percent to be ruled out observationally and therefore, on this basis, would expect constraints on ε, for $B = 1, k_0 = 1, n = 3$, to be around $\varepsilon \leq 0.1 - 0.2$.

Models with $\chi \to \chi_* \neq 0$ at Late Time

To conclude the discussion of models with $A = 1$, we will briefly discuss forms of $K(\chi)$ that have late time behaviour of $\chi = \chi_*$ where $K'(\chi_*) = 0$. As discussed in section 3.2.4 these types of solution are generically unsatisfactory because, although the Einstein frame Hubble rate tends to a constant at late time, the Jordan frame Hubble rate does not. However this is not the case when $A = 1$. In this case eq. (3.46) becomes

$$H_E = \sqrt{1 - 2B\chi}\tilde{H} \tag{3.81}$$

and so asymptotically we have that

$$H_E \approx \sqrt{1 - 2B\chi_*}\tilde{H}. \tag{3.82}$$

Therefore, on these solutions, both the Jordan frame Hubble rate and the Einstein frame Hubble rate are constant at late times. Additionally, from eq. (3.67), we still have the equation

of state of the scalar energy tending to minus one. The asymptotics of eqs. (3.51) to (3.58) are replaced by

$$\dot{\phi} \approx \phi_* \tag{3.83}$$

$$\rho_{eff} \approx -\mathscr{M}^4 K(\chi_*) \tag{3.84}$$

$$p_\phi \approx \mathscr{M}^4 K(\chi_*) \tag{3.85}$$

$$H_E \approx \mathscr{M}^2 \sqrt{-K(\chi_*)}/M_{Pl}\sqrt{3} \tag{3.86}$$

$$a(t) \sim exp(\mathscr{M}^2 \sqrt{-K(\chi_*)}t/M_{Pl}\sqrt{3}) \tag{3.87}$$

$$\tilde{H} \approx \mathscr{M}^2 \sqrt{-K(\chi_*)}/M_{Pl}\sqrt{3}\sqrt{1-2B\chi_*} \tag{3.88}$$

$$\tilde{a}(\tilde{t}) \sim exp(\mathscr{M}^2 \sqrt{-K(\chi_*)}/M_{Pl}\sqrt{3}\sqrt{1-2B\chi_*}). \tag{3.89}$$

Note that to ensure that the overall energy density on the right-hand side of eq. (3.34) is positive, necessary because the left-hand side is a square, we must have that $K(\chi_*) < 0$. Consider eq. (3.63) for these solutions. As before $\dot{\phi}$ will initially be fixed to its initial value however, in contrast to the other solutions, there is no analogy of the transition time t_{tr}, because the first term of the denominator in eq. (3.63) will never dominate. Instead $a^3K'(\chi)$ will approach a finite number. Nevertheless, by the time the universe enters the dark energy dominated era the equation of state of the scalar energy density must be close to minus one and therefore χ must be close to χ_* which constrains the parameters in the same way as eq. (3.72) does.

3.2.6 $A = A(\phi)$ Case

Behaviour of Solutions

In sections 3.2.3 and 3.2.4 we showed that when $A = A(\phi)$, we have desirable early and late time behaviour. We now discuss in more detail the evolution of the scalar. The starting point

for this is eq. (3.39). Although we cannot solve it exactly, if $\beta(1-2B\chi)^{3/2}$ varies slowly with time, the solution can be approximated by

$$a^3\dot{\phi}K'(\chi)+\hat{\rho}_0\dot{\phi}A\sqrt{1-2B\chi}B/\mathscr{M}^4=\hat{\rho}_0\dot{\phi}(0)B/\mathscr{M}^4-\beta(\phi)\hat{\rho}_0(1-2B\chi)^{3/2}t/M_{Pl} \quad (3.90)$$

where we have imposed eq. (3.44). We can, as we did for the $A=1$ case, rearrange this to find an implicit equation for $\dot{\phi}$:

$$\dot{\phi}=\frac{\hat{\rho}_0\dot{\phi}(0)B/\mathscr{M}^4-\beta(\phi)\hat{\rho}_0(1-2B\chi)^{3/2}t/M_{Pl}}{a^3K'(\chi)+\hat{\rho}_0A\sqrt{1-2B\chi}B/\mathscr{M}^4}. \quad (3.91)$$

For the $A=1$ case we had the freedom to impose that $\dot{\phi}\geq 0$. For non-constant A this freedom is lost. Instead the field equations, eqs. (3.34), (3.35) and (3.39), are invariant under the transformation $(\beta,\phi)\to(-\beta,-\phi)$. Therefore we can choose either $\beta(\phi(0))$ or $\dot{\phi}(0)$ to be non-negative. In this work we follow convention by setting $\beta>0$. The sign of $\dot{\phi}(0)$ will greatly affect the behaviour of the solution. For example, for $\dot{\phi}(0)>0$, $\dot{\phi}$ will pass through zero and change sign, whereas for $\dot{\phi}(0)<0$ it will stay negative for all time. We define two times. Firstly define

$$t_1=\begin{cases} 2B\dot{\phi}(0)M_{Pl}/\beta\mathscr{M}^4 \text{ for } \dot{\phi}(0)\geq 0 \\ -B\dot{\phi}(0)M_{Pl}/\beta\mathscr{M}^4 \text{ for } \dot{\phi}(0)\leq 0. \end{cases} \quad (3.92)$$

This is the time at which the second term of the numerator starts to dominate over the first. The extra factor of two when $\dot{\phi}(0)>0$ is necessary because when both terms are of the same sign, the numerator is dominated by the second term after the absolute value of the first and second term are equal. When they differ in sign, the numerator is only dominated by the second term when its absolute value is twice that of the first term. In fact, these differences are unimportant as the time is simply a ball park figure for when behaviours change. The

second time, t_2, we define by

$$a^3(t_2) = B\hat{\rho}_0 A(\phi(t_2))\sqrt{1-2B\chi(t_2)}/\mathscr{M}^4 K'(\chi(t_2)). \tag{3.93}$$

This is the time beyond which the first term of the denominator dominates over the second. Depending upon the ordering of these times the behaviour of the solution will vary greatly. For example for $t_1 \ll t_2$, $\dot{\phi}$ will go through a period in which it decreases linearly with time. This is in contrast to the $A = 1$ case, in which the absolute value of the scalar was always decreasing with time. Irrespective of the details of the behaviour of $\dot{\phi}$, as long as matter is dominant it will have little effect on the evolution of the universe.

Constraining the Solutions

What is observationally important is that, as for the $A = 1$ case, the equation of state of the scalar energy momentum has already achieved a value close to minus one before the universe leaves the matter-dominated era and enters the dark energy dominated era. The reasoning is exactly the same for $A = A(\phi)$, and we must once again have t_{DE} given by eq. (3.70) and $K(\chi)$ in the linear regime at this time.

Considering eq. (3.91) at t_{DE} gives

$$\dot{\phi}(t_{DE}) \approx \frac{\dot{\phi}(0)B/\mathscr{M}^4 - \beta(\phi_\infty)t_{DE}/M_{Pl}}{(1+A(\phi_\infty)B)/\mathscr{M}^4}. \tag{3.94}$$

To be in the linear regime, we need $\dot{\phi}/\mathscr{M}^2 \lesssim 1$. This can be achieved if the two terms of the numerator either approximately cancel, or are both individually smaller than the denominator. However in the former case, the derivative of $\dot{\phi}/\mathscr{M}^2$ will still be significant, and so the rate of change of ω_ϕ will be significant. This is not the behaviour that we seek because

we require that ω_ϕ remains close to minus one after t_{DE}. We therefore require that

$$\frac{\dot{\phi}(0)B/\mathscr{M}^2}{1+A(\phi_\infty)B} \lesssim 1 \tag{3.95}$$

and

$$\frac{\beta(\phi_\infty)t_{DE}/M_{Pl}}{(1+A(\phi_\infty)B)/\mathscr{M}^2} \lesssim 1. \tag{3.96}$$

We can estimate t_{DE} by assuming the universe is completely matter-dominated until t_{DE}. Substituting $a(t) = a_0 t^{2/3}$ into eq. (3.40) gives

$$a_0 \approx (3\hat{\rho}_0/4M_{Pl}^2)^{1/3} \tag{3.97}$$

which setting

$$a_0 t_{DE}^{2/3} \approx \hat{\rho}_0/\mathscr{M}^4 \tag{3.98}$$

gives

$$t_{DE} \approx 2M_{Pl}/\sqrt{3}\mathscr{M}^2. \tag{3.99}$$

Substituting this back into eq. (3.96) gives us a constraint in terms of the parameters of the theory

$$\frac{\beta(\phi_\infty)}{(1+A(\phi_\infty)B)} \lesssim 1. \tag{3.100}$$

3.2.7 Beyond $A = A(\phi)$ and Constant B

In this section we will discuss possible functional dependencies of A and B that we have not considered in the main body of the chapter. One particular dependence to mention is when A^2B is constant. This is because it is a matter of convention as to whether the disformal factor is defined as in eq. (3.2), or

$$\tilde{g}_{\mu\nu} = A^2 g_{\mu\nu} + B\partial_\mu\phi\partial_\nu\phi/M^4. \tag{3.101}$$

If we take eq. (3.101) with B constant, the equation of motion is altered. It becomes

$$\frac{d}{dt}(a^3\dot{\phi}K'(\chi)+\hat{\rho}_0\dot{\phi}A\sqrt{1-2B\chi}(B+\chi\partial_\chi B)/\mathscr{M}^4)=-\beta(\phi)\hat{\rho}_0\sqrt{1-2B\chi}/M_{Pl}. \quad (3.102)$$

This is similar to eq. (3.39) with the difference being a factor of $1-2B\chi$ on the right-hand side. Thus although there will be small alterations, it seems that the behaviour would be qualitatively the same.

As mentioned at the start of the chapter one can, in theory have $A=A(\chi,\phi)$ and $B=B(\phi,\chi)$. If we consider only $A=A(\phi)$ then one has an equation of motion of

$$\frac{d}{dt}(a^3\dot{\phi}K'(\chi)+\hat{\rho}_0\dot{\phi}A\sqrt{1-2B\chi}(B+\chi\partial_\chi B)/\mathscr{M}^4)=\hat{\rho}_0A\sqrt{1-2B\chi}(-A'(\phi)/A+\chi(2BA'(\phi)/A+\partial_\phi B)). \quad (3.103)$$

Inspecting this, one can see that, as before, one is free to impose an initial finite value of $\dot{\phi}$. This once again means that the universe will be matter-dominated if the initial conditions are chosen such that

$$A(\phi(0))\sqrt{1-2B\chi(0)}\approx 1. \quad (3.104)$$

Similarly the late time de Sitter universe of eqs. (3.51) to (3.58) will be approached for sufficiently regular A and B. To investigate the different behaviours possible in between these times would require solving of eq. (3.103) which may well be involved. However, in our work we analysed the $A=1$ case because the $\phi\to\phi+c$ shift symmetry occurs when there is no explicit ϕ dependence, meaning that, as a result of Noether's theorem, the equation of motion is of the form of a conservation equation. This symmetry would be preserved if $A=1$ and $B=B(\chi)$ and an analysis of this case would be more tractable.

3.3 Disformal Couplings Around a Black Hole

3.3.1 Recap

In the first part of this chapter we have considered the background cosmological evolution of K-mouflage with a disformal coupling to matter and in chapter 2 we considered K-mouflage theories with a conformal coupling to matter around a black hole. In the second part of this chapter we consider the effect of introducing the disformal coupling that we have analysed in this chapter to the physical set-up of chapter 2.

As we have previously discussed, in the static, non-relativistic limit, the addition of this disformal coupling leaves the field equations unchanged. This is because only the time-time component of the energy momentum tensor is non-zero and it is always contracted with a derivative of the scalar. Therefore if the scalar is time-independent these terms are zero:

$$T^{\mu\nu}\partial_\nu\phi = T^{\mu t}\partial_t\phi = 0. \tag{3.105}$$

Thus to probe disformal couplings one needs to consider time-dependent solutions. The addition of a disformal coupling will have no effect on the time-independent solutions around a black hole that were found in chapter 2, because we did indeed assume that the accretion disk was comprised of non-relativistic matter and the scalar had no time dependence. However, in chapter 2 we also considered a scalar with linear time dependence. The disformal coupling will affect this solution and this set-up therefore provides a probe for the disformal coupling.

What we say will apply equally to Galileons and K-mouflage, and therefore we keep the discussion as general as possible.

3.3.2 Calculation

To start, consider again the action eq. (3.106) where we have not specified with which scalar-tensor theory we are working, and instead denote the scalar sector with a generic term L_ϕ:

$$S = \int dx^4 \sqrt{-g}\big[\frac{M_{Pl}^2}{2}(R - 2\Lambda_{bare}) + L_\phi\big] + S_m(\psi^{(i)}, \tilde{g}_{\mu\nu}). \tag{3.106}$$

As all we have changed is the form of the metric to which matter fields couple, the field equations gained from varying the metric are unchanged in the Einstein frame:

$$M_{Pl}^2(G_{\alpha\beta} + \Lambda_{bare} g_{\alpha\beta}) = T^\phi_{\mu\nu} + T^E_{\mu\nu} \tag{3.107}$$

where $T^\phi_{\mu\nu}$ is the energy momentum tensor of the scalar. For example in the case of K-mouflage we have $T^\phi_{\mu\nu} = g_{\mu\nu}\mathscr{M}^4 K(\chi) + K'(\chi)\partial_\mu\phi\partial_\nu\phi$. All changes occur in the field equation gained from varying the scalar. This is

$$\frac{1}{\sqrt{-g}}\frac{\delta\sqrt{-g}L_\phi}{\delta\phi} = \frac{1}{\sqrt{-g}}\partial_\mu(\sqrt{-g}T_E^{\mu\nu}\partial_\nu\phi B/M^4) - T_E^{\mu\nu}g_{\mu\nu}A'(\phi)/A(\phi) - T_E^{\tau\nu}\partial_\tau\phi\partial_\nu\phi A'(\phi)B/AM^4 \tag{3.108}$$

where, for simplicity, we have taken B to be a constant. As one would expect, given that we have only altered the way that the matter fields couple to the metric, in the case that there is no matter these equations are the same for both disformal and conformal only couplings. In particular, that the vacuum solutions coincide means that the de Sitter-Schwarzschild solutions found in chapter 2 for K-mouflage, and the solutions found in Ref. [9] for Galileons are still valid. Recall that for K-mouflage these solutions were exact, whereas for Galileons they were in the test field limit. Following the same methodology as before, we now add a spherical accretion disk into the picture, and consider the scalar equation of motion on the background of the vacuum solution.

The requirement that the matter is non-relativistic amounts to the conditions:

$$T_E^{0i} = T_E^{ij} = 0 \tag{3.109}$$

$$\rho_E = T_E^{00}. \tag{3.110}$$

Further to this we have that our ansatz for the scalar is

$$\phi = qt + \psi(r) \tag{3.111}$$

and a de Sitter-Schwarzschild background metric:

$$ds^2 = -f(r)dt^2 + 1/f(r)dr^2 + r^2 d\Omega^2 \tag{3.112}$$

$$f(r) = 1 - r_s/r - H^2 r^2. \tag{3.113}$$

Substituting in these quantities, the righthand side of eq. (3.108) becomes

$$\rho_E A'(\phi)/A(\phi)(f(r) - q^2 B/M^4) + \partial_t \rho_E qB/M^4. \tag{3.114}$$

We now wish to substitute out the time derivative of the matter density in eq. (3.114). We can do this by using the fact that the Jordan frame energy momentum tensor is covariantly conserved, and then relating this equation to Einstein frame quantities to gain an expression for $\partial_t \rho_E$ in terms of the scalar and ρ_E. Specifically we have that

$$\tilde{\nabla}_\mu \tilde{T}^{\mu 0} = 0 \tag{3.115}$$

and the relation between the Einstein and Jordan frame energy momentum tensors [77] is

$$T_E^{\mu\nu} = A^6\sqrt{1-2BX/M^4}\tilde{T}^{\mu\nu}. \tag{3.116}$$

From now on we take $M = \mathscr{M}$, which is without loss of generality as the difference can be re-absorbed into the definition of B. Using eq. (3.115) and eq. (3.116) we have that

$$\partial_t(\rho_E/A^6) = -(\tilde{\Gamma}^{\mu}_{\mu 0} + \tilde{\Gamma}^{0}_{00})\rho_E/A^6. \tag{3.117}$$

$\tilde{\Gamma}^{0}_{00}$ can be calculated directly using

$$\tilde{\Gamma}^{\mu}_{\nu\tau} = \frac{1}{2}\tilde{g}^{\mu\sigma}(\partial_\nu\tilde{g}_{\tau\sigma} + \partial_\tau\tilde{g}_{\nu\sigma} - \partial_\sigma\tilde{g}_{\tau\nu}) \tag{3.118}$$

and

$$\tilde{g}^{\mu\nu} = A(\phi)^{-2}(g^{\mu\nu} - \frac{B/M^4}{1+B\partial^\sigma\phi\partial_\sigma\phi/M^4}\partial\phi^\mu\partial^\nu\phi) \tag{3.119}$$

where $\partial^\mu\phi = g^{\mu\nu}\partial_\nu\phi$.

This gives

$$\tilde{\Gamma}^{0}_{00} = qA'(\phi)/A(\phi) - \frac{qB\psi'(r)}{DM^4}(f'(r) - A'(\phi)\psi'(r)f(r)/A(\phi)) \tag{3.120}$$

where $D = -1+2B\chi$. Instead of calculating it directly, to find $\tilde{\Gamma}^{\mu}_{\mu 0}$ one can use the identity

$$\Gamma^{\mu}_{\mu\nu} = \partial_\nu Log(\sqrt{-g}). \tag{3.121}$$

Doing this gives

$$\tilde{\Gamma}^{\mu}_{\mu 0} = 4qA'(\phi)/A(\phi). \tag{3.122}$$

Using eqs. (3.117), (3.120) and (3.122) in eq. (3.114) gives us the final form of the scalar equation. The left-hand side is exactly the same as the conformal case, with the disformal modification taking the form of an alteration to the prefactor in the sourcing term:

$$\frac{1}{\sqrt{-g}}\frac{\delta\sqrt{-g}L_\phi}{\delta\phi} = \rho_E(A'(\phi)f(r)/A(\phi)+q^2B^2\psi'(r)(-f'(r)+A'(\phi)\psi'(r)f(r)/A(\phi))/M^8D). \tag{3.123}$$

When $B=0$ this coincides with the conformal coupling case. If we consider B to be small then we can estimate the effect of the additional term by evaluating the right-hand side of 3.123 with the conformal solution. As we established in chapter 2, this has $\psi'(r)>0$ which, because $D<0$, means that the effect of the disformal coupling has been to reduce the sourcing term. Upon increasing B further this perturbative treatment would break down and one would have to solve eq. (3.123) directly.

3.4 Concluding Remarks

In this chapter we have discussed disformal couplings to matter. These are best analysed in time-dependent situation and we have considered two such set-ups.

The first calculation that we did was to quantify the effect of a disformal coupling on the cosmological evolution of the universe. We discussed the behaviour of solutions for both the case of disformal only ($A=1$) and conformal plus disformal ($A=A(\phi)$). For the more tractable $A=1$ case we generated a number of plots, figs. 3.1 to 3.4, to quantify the effect of the coupling. We found that a large proportion of the parameter space provided universes close to that of ΛCDM. In particular we found that for models with large B, ρ_{eff} behaved like a cosmological constant throughout the history of the universe and so provided a viable model. This is perhaps unsurprising as taking B large amounts to taking the initial value of $\dot{\phi}/\mathscr{M}^2$ small. However for models with B small, in which case $\dot{\phi}$ was initially large and ρ_{eff} did not behave like a cosmological constant, a ΛCDM-like universe was still achieved.

This is because the large departures of ρ_{eff} from cosmological constant-like behaviour all came in the matter-dominated era, and so were suppressed. By the time the universe entered the dark energy dominated era, $\dot{\phi}$ was small enough that ρ_{eff} was cosmological constant-like and so deviations from ΛCDM were small. We also found that increasing ε, defined by eq. (3.61) led to the greatest departures from ΛCDM, as can be seen in fig. 3.2b.

The second time-dependent set up that we considered was to revisit the time-dependent black hole solutions that were looked at in chapter 2, this time with the addition of a disformal coupling. In this section we calculated the effect that the addition of the disformal coupling had on the sourcing term of the scalar equation of motion. This calculation showed that the addition of a disformal term reduced the magnitude of the sourcing term, thereby reducing the gradient of the scalar field. This is, in some sense, a new screening effect. In the absence of the disformal factor, the fifth force would be larger and potentially this could lead to predications that rendered the theory incompatible with observations. However, we have shown that with a disformal coupling, the fifth force is reduced and therefore theories that are incompatible with observations may now be viable again. In other words, we have shown that by considering time dependent effects in the presence of a disformal coupling, fifth force constraints may be more easily passed.

Chapter 4

Shape Dependence of K-mouflage

4.1 Introduction

In chapter 3 we considered a subset of K-mouflage theories that had not previously been considered in the literature - those with a disformal coupling - and in this chapter we will further analyse K-mouflage theories. We will return to considering the K-mouflage theories of chapter 2, those with only a conformal coupling, and will instead focus on analysing the effect of the shape of a source on the scalar profile that it generates.

The highly non-linear nature of the K-mouflage field equations make them difficult to solve for general source objects. Thus, when calculating the scalar profile generated by an object, it is generally assumed that the sources are spherically symmetric. This a reasonable assumption for stars and planets and it allows progress to be made in solving the field equation. However it is under this assumption of spherical symmetry that the screening mechanism of the K-mouflage model is demonstrated and in this chapter we will investigate the field profile generated by non-spherical objects. To make the field equations easily solvable we must assume symmetries and so we consider spherical, cylindrical and planar symmetry.

The shape dependence of Galileon and D-BIonic theories were investigated in Ref. [17]. It was shown that for Galileons screening is strongest in spherically symmetric setups, weaker in cylindrical cases and non-existent in situations with planar symmetry. D-BIonic theories are a specific form of K-mouflage theory with

$$K(\chi) = \sqrt{1+2\chi}. \tag{4.1}$$

These theories screen in regions of high Newtonian gravitational force but the precise behaviour differs somewhat from the polynomial forms of K-mouflage that we have considered here. This is because at large values of χ, $K'(\chi)$ cannot be taken to be dominated by its highest power.

One of the most striking findings of Ref. [17] was that the Galileon terms vanish identically for planar sources and consequently the ratio of scalar fifth force to gravitational force is constant,

$$F_\phi/F_N = 2\beta^2. \tag{4.2}$$

Thus there is no Vainshtein distance and, for order unity couplings, the fifth force is of gravitational strength. This is in contrast to the findings for the D-BIon in the planar case in which the exterior profile was also constant but, depending on the parameters of the theory could be either screened or unscreened. In the screened case, the force would be suppressed arbitrarily far from the object.

More familiarly, in the cylindrical and spherical cases the Galileon has an associated Vainshtein radius, beyond which the fifth force is of gravitational strength and inside of which the fifth force is suppressed. For the cubic Galileon, in the cylindrical case, deep inside the Vainshtein radius the ratio of scalar fifth force to gravitational force is

$$F_\phi/F_N \approx 4\beta^2 r/r_v \tag{4.3}$$

and for a sphere the force ratio is given by

$$F_\phi/F_N \approx 4\beta^2(r/r_v)^{3/2}. \tag{4.4}$$

In the cylindrical and spherical cases the behaviour of the D-BIon is similar to the Galileon. Deep inside the cylindrical screening radius the scalar force becomes constant, to give a force ratio of

$$F_\phi/F_N \approx 2\beta^2(r/r_v), \tag{4.5}$$

half that of the Galileon case, whereas in the spherical case the force ratio is

$$F_\phi/F_N \approx 2\beta^2(r/r_v)^2, \tag{4.6}$$

which is the same as the quartic Galileon, up to a factor of 3.

4.2 Set-up

We will consider three constant density objects: a sphere of radius r_0, an infinite cylinder of radius r_0 and an infinite plane of width $2z_0$. We will assume staticity and ignore the curvature induced by the scalar energy momentum and the matter. We will further impose the symmetries of the physical set-up upon the scalar, thus our calculation will amount to solving the field equation for a scalar that depends on one coordinate on a Minkowski background. As in previous chapters, we will assume a polynomial form for $K(\chi)$ of

$$K(\chi) = -1 + \chi + ... + c_n\chi^n. \tag{4.7}$$

The equation of motion for K-mouflage is

$$\frac{1}{\sqrt{-g}}\partial_\mu(\sqrt{-g}\partial^\mu\phi K'(\chi)) = \beta\rho/M_{Pl} \tag{4.8}$$

and we define the canonical scalar to be the solution to

$$\frac{1}{\sqrt{-g}}\partial_\mu(\sqrt{-g}\partial^\mu\phi_0) = \beta\rho/M_{Pl}. \tag{4.9}$$

Given that the Newtonian potential satisfies

$$\nabla^2\Phi_N = \rho/2M_{Pl}^2 \tag{4.10}$$

the canonical scalar is simply

$$\phi_0 = 2\beta M_{Pl}\Phi_N \tag{4.11}$$

and the ratio of scalar fifth force to Newtonian gravitational force is

$$F_\phi/F_N = 2\beta^2|\nabla\phi|/|\nabla\phi_0|. \tag{4.12}$$

If $|\nabla\phi|$ is not suppressed relative to $|\nabla\phi_0|$ then β needs to be tuned to a small value in order to avoid a gravitational strength fifth force.

In the one dimensional cases that we consider below one can simply equate the K-mouflage current to the canonical current, that is

$$\partial_\mu\phi K'(\chi) = \partial_\mu\phi_0. \tag{4.13}$$

Squaring this gives

$$\chi K'(\chi)^2 = \chi_0 \tag{4.14}$$

which, presuming we can invert this relation, gives us

$$\chi = \chi(\chi_0). \tag{4.15}$$

If $\chi_0 << 1$ then $K'(\chi) \approx 1$ and eqs. (4.14) and (4.15) become

$$\chi \approx \chi_0. \tag{4.16}$$

From eq. (4.12) we are then in an unscreened region. On the other hand, if $\chi_0 \gg 1$ then, eq. (4.14) becomes

$$c_n^2 n^2 \chi^{(2n-1)} \approx \chi_0. \tag{4.17}$$

Dropping the numerical factor from the front, this gives

$$\chi \sim \chi_0^{1/(2n-1)}. \tag{4.18}$$

We then have from eq. (4.12) that the force ratio is given by

$$F_\phi / F_N \sim 2\beta^2 \chi_0^{(1-n)/(2n-1)}. \tag{4.19}$$

As $\chi_0 \gg 1$ and $(1-n)/(2n-1) < 0$, the fifth force is indeed screened.

4.3 Spherical

In the spherically symmetric case we have

$$ds^2 = -dt^2 + dr^2 + r^2 d\theta^2 + r^2 sin^2\theta d\varphi \tag{4.20}$$

and

$$\phi = \phi(r). \tag{4.21}$$

We take our matter distribution to be

$$\rho(r) = \begin{cases} \rho_0 & r \leq r_0 \\ 0 & r > r_0 \end{cases} \tag{4.22}$$

and eq. (4.9) becomes

$$\phi_0'(r) = \begin{cases} \beta\rho_0 r/3M_{Pl} & r \leq r_0 \\ \beta\rho_0 r_0^3/M_{Pl}r^2 & r > r_0 \end{cases} \tag{4.23}$$

where we have imposed regularity at the origin. This gives

$$\chi_0(r) = \begin{cases} -(r/r_i)^2 & r \leq r_0 \\ -(r_e/r)^4 & r > r_0 \end{cases} \tag{4.24}$$

where we have and identified exterior (r_e) and interior (r_i) screening radii as

$$r_i = \frac{3\sqrt{2}M_{Pl}\mathscr{M}^2}{\beta\rho_0} \tag{4.25}$$

and

$$r_e = \sqrt{\frac{\beta r_0^3\rho_0}{3\sqrt{2}\mathscr{M}^2 M_{Pl}}}. \tag{4.26}$$

These are the r values for which $\chi_0 = -1$ and therefore represent the radius at which behaviour transitions between that of eq. (4.16) and that of eq. (4.18). The exterior field profile depends only on the mass of the object, thus for an object of a given mass the (exterior) screening radius will exist for a sufficiently small r_0 and will be independent of the size of the object if it does exist. Substituting into eq. (4.19) gives the ratio of K-mouflage force to

gravitational force

$$F^{\phi}/F_N \sim \begin{cases} 2\beta^2 & r \leq r_i \\ 2\beta^2 (r_i/r)^{2(n-1)/(2n-1)} & r_i < r \leq r_0 \\ 2\beta^2 (r/r_e)^{4(n-1)/(2n-1)} & r_0 < r \leq r_e \\ 2\beta^2 & r_e < r \end{cases} \tag{4.27}$$

where we have assumed that $r_i < r_0 < r_e$ else no screening would occur. For large n, $4(n-1)/(2n-1) \approx 2$ and therefore outside the object, but inside the exterior K-mouflage screening radius the ratio of force will be roughly

$$2\beta^2 (r/r_e)^2. \tag{4.28}$$

4.4 Cylindrical

We repeat the same procedure with an infinite cylinder of radius r. The metric, scalar and matter distribution are given by

$$ds^2 = -dt^2 + dr^2 + r^2 d\varphi^2 + dz^2, \tag{4.29}$$

$$\phi = \phi(r) \tag{4.30}$$

and

$$\rho(r) = \begin{cases} \rho_0 & r \leq r_0 \\ 0 & r > r_0. \end{cases} \tag{4.31}$$

In this case eq. (4.9) becomes

$$\frac{1}{r}\frac{d}{dr}(r\phi_0'(r)) = \begin{cases} \beta\rho_0/M_{Pl} & r \leq r_0 \\ 0 & r > r_0 \end{cases} \tag{4.32}$$

which we can solve to give

$$\phi_0'(r) = \begin{cases} \beta\rho_0 r/2M_{Pl} & r \leq r_0 \\ \beta\rho_0 r_0^2/2M_{Pl}r & r > r_0 \end{cases} \tag{4.33}$$

where we have imposed regularity at $r = 0$. This gives

$$\chi_0(r) = \begin{cases} -(r/r_i)^2 & r \leq r_0 \\ -(r_e/r)^2 & r > r_0 \end{cases} \tag{4.34}$$

where we have defined the interior and exterior screening radii as

$$r_i = \frac{2\sqrt{2}M_{Pl}\mathscr{M}^2}{\beta\rho_0} \tag{4.35}$$

and

$$r_e = \frac{\beta\rho_0 r_0^2}{2\sqrt{2}M_{Pl}\mathscr{M}^2}. \tag{4.36}$$

Thus the screening radius will exist if the object is sufficiently thin, and this radius will be independent of the thickness of the cylinder (for a fixed mass per unit length). Substituting into eq. (4.19), and again assuming that $r_i < r_0 < r_e$, gives the ratio of K-mouflage force to gravitational force to be

$$F^{\phi}/F_N \sim \begin{cases} 2\beta^2 & r \leq r_i \\ 2\beta^2 (r_i/r)^{2(n-1)/(2n-1)} & r_i < r \leq r_0 \\ 2\beta^2 (r/r_e)^{2(n-1)/(2n-1)} & r_0 < r \leq r_e \\ 2\beta^2 & r_e < r. \end{cases} \tag{4.37}$$

For large n we again consider the region outside the object but within the screening radius because this is the area of most interest. In this case we have

$$F^{\phi}/F_N \sim 2\beta^2 (r/r_e). \tag{4.38}$$

4.5 Planar

We now consider the planar case, an infinite plane of thickness $2z_0$ and proceed as we have in the previous two sections. The metric, scalar and matter distribution are

$$ds^2 = -dt^2 + dx^2 + dy^2 + dz^2, \tag{4.39}$$

$$\phi = \phi(z) \tag{4.40}$$

and

$$\rho(z) = \begin{cases} \rho_0 & |z| \leq z_0 \\ 0 & |z| > r_0. \end{cases} \tag{4.41}$$

In this case eq. (4.9) becomes

$$\frac{d^2}{dz^2}\phi_0(z) = \begin{cases} \beta\rho_0/M_{Pl} & |z| \leq z_0 \\ 0 & |z| > z_0. \end{cases} \tag{4.42}$$

Thus, imposing a $\phi(z) = \phi(-z)$ symmetry, gives

$$\phi_0'(z) = \begin{cases} \beta\rho_0 z_0/M_{Pl} & z > z_0 \\ \beta\rho_0 z/M_{Pl} & |z| \leq z_0 \\ -\beta\rho_0 z_0/M_{Pl} & z \leq -z_0 \end{cases} \tag{4.43}$$

and

$$\chi_0(z) = \begin{cases} -(z/z_i)^2 & |z| \leq z_0 \\ -(z_0/z_i)^2 & z > z_0. \end{cases} \tag{4.44}$$

Here we have defined the interior screening distance as

$$z_i = \frac{\sqrt{2}M_{Pl}\mathscr{M}^2}{\beta\rho_0}. \tag{4.45}$$

Whether screening occurs depends upon the mass per unit area of the matter. We note that in contrast to the spherical and cylindrical cases there is no exterior screening radius: screening persists infinitely far from the matter. The ratio of K-mouflage to gravitational force is

$$F^\phi/F_N \sim \begin{cases} 2\beta^2 & z \leq z_i \\ 2\beta^2(z_i/z)^{2(n-1)/(2n-1)} & z_i < z \leq z_0 \\ 2\beta^2(z_i/z_0)^{2(n-1)/(2n-1)} & z_0 < z \end{cases} \tag{4.46}$$

where we have assumed $z_i < z_0$. Outside the matter, the force is suppressed, but by a constant factor, not a power-law. If we consider n to be large, we have that outside the plane the ratio of fifth force to gravitational force is

$$F^\phi/F_N \sim 2\beta^2 z_i/z_0. \tag{4.47}$$

4.6 Comparison with D-BIon

The D-BIon's shape dependence was investigated in Ref. [17]. As it also exhibits screening when the first derivative of the field is large, we choose to compare the results for K-mouflage theories against it in fig. 4.1.

In all three cases the force ratios at the edge of the object are minimal. The ratio is around 0.1 for the plane and cylinder and smaller for the sphere and for all three objects it is largest for the $n = 2$ K-mouflage and lowest for D-BIon. This is because, up to numerical factors, integrating the equations of motion once simply amounts to multiplying though by z or r. The ratio is least for the sphere, but this is in part because we fixed the exterior screening radii to be equal. For the sphere this implies that the interior screening, which obeys $r_i/r_0 = (r_0/r_e)^2$ for the sphere and $r_i/r_0 = r_0/r_e$ for the cylinder, is $1/400$ whereas it is $1/20$ for the cylinder. The ratio increases towards the centre of the object because the gradient is zero here, and so screening is less.

The differences between the models are most pronounced on the exterior of the objects. Beyond the screening radius the ratio tends to $2\beta^2$, and the transition happens much more sharply for $n = 10$ K-mouflage than it does for $n = 2$ K-mouflage or for the D-BIon. For the sphere, close to the object all three theories are screened, with the higher order K-mouflage becoming more screened than quadratic K-mouflage and displaying the behaviour of eq. (4.28). The cylindrical profiles are similar to those of the spherical case but differences do exist. Must notably the power-law behaviour deep inside the outer screening radius differs - in particular the large n K-mouflage now obeys eq. (4.38) - and the value of the ratio at the edge of the cylinder is greater than at the edge of the sphere.

The behaviour in the planar case is qualitatively different from that of the sphere or cylinder with a fixed force ratio extending arbitrarily far from the object. In particular this means that the screening, which is maximised at the edge of the object, persists infinitely far from the plane. Thus it appears that planar objects behave very differently for theories

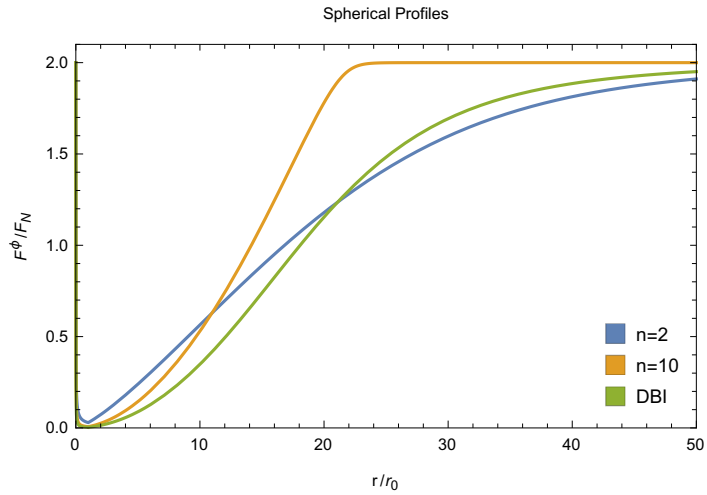

(a) Sphere with $r_e = 20r_0$

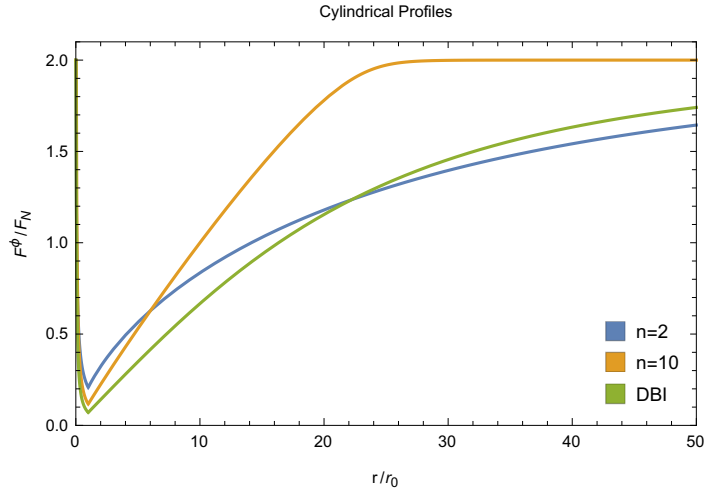

(b) Cylinder with $r_e = 20r_0$

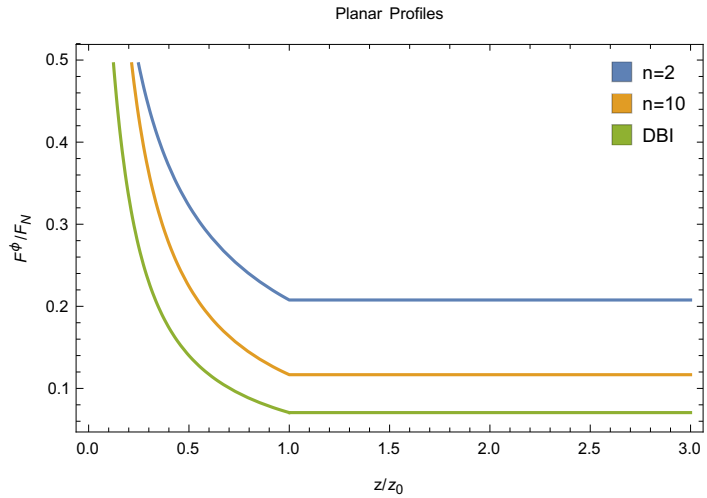

(c) Plane with $z_i = 1/20$

Fig. 4.1 Plots showing the ratio of fifth force to gravitational force for $K(\chi) = \chi - \frac{1}{2}\chi^2$, $K(\chi) = \chi - \frac{1}{10}\chi^{10}$ and the D-BIon. We have set $\beta = 1$.

that screen when the gravitational force is large as compared with Galileons, which screen when the curvature is sufficiently large. In the planar case screening was non-existent for Galileons whereas for K-mouflage models it is most effective.

4.7 Discussion

In this chapter we have compared the screening of K-mouflage models around a sphere, a cylinder and a plane. We showed that screening exists for all three shapes, but that the power-law behaviour around the object is shape dependent. In particular the planar object differs because there is no screening distance associated with the object. If the object is screened then screening will persist arbitrarily far from the plane. This is in contrast to the conventional screening, exhibited in both the spherical and cylindrical case, for which there is a screening radius beyond which the K-mouflage force is of gravitational strength.

We have already considered the ratio of fifth force to gravitational force for large n in eqs. (4.28), (4.38) and (4.47). If we evaluate these ratios just outside the object we attain

$$F^{\phi}/F_N \sim \frac{\beta \mathscr{M}^2 M_{Pl}}{r_0 \rho_0} \tag{4.48}$$

in all three cases. We have ignored numerical factors, and for the plane r_0 should be replaced by z_0. Thus it is clear that the screening is of similar strength for all three objects.

The results for K-mouflage are broadly similar to those of the D-BIonic scalar analysed in Ref. [17], which also screens for large values of the scalar gradient. In both theories the power-laws are similar for the cylindrical and spherical cases and, in the planar case, screening is either non-existent or persists arbitrarily far from the plane. This is very much in contrast to the results for the Galileon in Ref. [17] for which planar objects are entirely unscreened. For cylindrical or spherical objects the power-laws in Galileon theories are the same as eq. (4.38) (cubic) and eq. (4.28) (quartic).

The cosmological effects of the shape dependence of screening were considered in Ref. [27] for the cubic Galileon. As the screening in this theory uses non-linearities, shape dependent effects do not appear at first order in perturbation theory and so second order effects must be considered. Ref. [27] analysed the matter bispectrum and found small deviations of up to 2% for models whose linear growth rate deviated from that of ΛCDM by up to 5%.

Given the difference in the behaviour around planar objects one would expect some differences for the K-mouflage matter bispectrum. Additionally, although the power-law suppression for Galileons are the same as K-mouflage in eqs. (4.28) and (4.38), these were taken assuming n to be large. Therefore differences may be greater for quadratic or cubic K-mouflage.

In the following chapter we will move on from considering K-mouflage theories to consider another theory with a screening mechanism, Chameleon theories, which were introduced in chapter 1. These theories differ from K-mouflage theories as they are potential based, as opposed to screening based on the kinetic terms, and we will consider a form of potential that differs from the standard form considered in the literature.

Chapter 5

Chameleon Theories with a Log Potential

In previous chapters we have investigated Galileon and K-mouflage theories, both of which screen due to their unusual kinetic structure. In chapter 1 we categorised screening mechanisms and introduced Chameleon theories as an example of theories which have potential-based screening. We now move on to study these models, applying solar system constraints to a new form of potential.

5.1 Recap Chameleon Models of Gravity

In this chapter we consider Chameleon gravity with a form of potential that has not previously been considered [25, 61, 62]. The literature has so far focused on power-law potentials of the form

$$V(\phi) = \Lambda^{4+n}/\phi^n. \tag{5.1}$$

In this piece of work we have taken a different form of the potential, namely

$$V(\phi) = \Lambda^4/Log(\phi/\Lambda)^n. \tag{5.2}$$

This is still decreasing for positive ϕ, but does not have a power-law form, and the mass of fluctuations around a background value is still an increasing function of the density of the background, thus the potential is a viable candidate. We keep our coupling to matter as given by the function $A(\phi) = Exp(\beta\phi/M_{Pl}) \approx 1 + \beta\phi/M_{Pl}$, giving

$$V_{eff} = \Lambda^4/Log(\phi/\Lambda)^n + e^{\beta\phi/M_{Pl}}\rho \tag{5.3}$$

and consider the constraints that arise from two gravitational tests. These are the constraints of the Shapiro time delay, as measured by the Cassini spacecraft [16] and the relative acceleration of the Earth and Moon towards the Sun, as measured by lunar ranging experiments [69]. We will find that large portions of the parameter space can be excluded on the basis of these experiments.

5.1.1 Profile for an Isolated Object

For the tests we will need to calculate the profile for the Sun, Earth and Moon (denoted using the subscripts $\odot$, e and m respectively). We will now briefly review the solution for an isolated spherical object described in chapter 1. To do this we calculate the screening radius, r_*, which is defined implicitly [28] by the equation

$$\bar{\chi} \equiv \bar{\phi}/2\beta M_{Pl} = -\Phi_N(r_*) - r_*\Phi_N'(r_*) \tag{5.4}$$

where $\Phi_N(r)$ is the Newtonian potential. For simplicity we consider the bodies to be of uniform density. We then take the profile outside the bodies to be sourced only by the mass outside of the screening radius, where we take $r_* = 0$ if no solution to eq. (5.4) exists. In the case where we have screening r_* will be close to the radius of the object and therefore only

a thin shell of mass will source the external field. This gives the profile to be

$$\phi(r) = \beta(M - M(r_*))e^{-m_\infty r}/4\pi M_{Pl} r + \phi_\infty \tag{5.5}$$

where m_∞ is the mass of the field at densities far away from the source object and ϕ_∞ minimises the effective potential at this density. For solar system objects this will be the galactic density ($\rho = 10^{-24} g/cm^3$). Fields that are heavy at solar system scales ($m_\infty r \gtrsim 1$) will be suppressed and will not be cosmologically relevant. However this case does not apply to our calculation. For light fields we can neglect the exponential term and take the profile to be

$$\phi(r) = \beta(M - M(r_*))/4\pi M_{Pl} r + \phi_\infty. \tag{5.6}$$

5.2 Constraint from Cassini Probe

In Minkowski spacetime light travels in straight lines whereas in Newtonian gravity and General Relativity the presence of mass bends the path of light rays, but by differing amounts. This fact was famously used in the Eddington experiment of 1919 [43] as evidence in support of General Relativity. Eddington measured the position of a star in the sky during a solar eclipse. This allowed him to see starlight that had passed close to the Sun and measure that the star's position in the sky had been deflected.

Different theories of gravity predict different deflection angles and time delays to null geodesics, at first post-Newtonian order. Nowadays the most stringent constraints of this type come from the Cassini-Huyens spacecraft [16]. During its mission it sent and received radio waves to and from Earth which allowed constraints to be calculated on the deflection angle and the Shapiro time delay caused by the presence of the Sun.

In this section we will review the terms in the PPN expansion that are relevant to our calculation and then apply the Cassini constraints to our theory.

5.2.1 PPN Formalism

In the weak gravitational regime of the solar system one can expand the metric about flat space and the Parameterised Post-Newtonian (PPN) formalism systemises this process. The constraints from Cassini then translate into constraints on the value of the coefficients in this expansion. In fact, the defection angle and the Shapiro time delay depend on the same coefficient, and it is the time delay that provides the stronger constraint. In the PPN formalism, one takes an order of smallness and then expands in powers of it. This is taken to be the Newtonian potential which is indeed small in the solar system. Consider a non-relativistic body in a circular orbit. This has

$$v^2/r = GM/r^2 = \Phi_N/r \tag{5.7}$$

and so we take velocities of bodies in the solar system to obey

$$v^2 = O(\Phi_N). \tag{5.8}$$

The full treatment of all terms in a generic expansion can be found in Ref. [91] and, at first post-Newtonian order one finds ten parameters to be constrained by experiment. However, only two of these are relevant to conformally coupled scalar-tensor theories [28]. We begin the section by discussing the PPN expansion terms relevant to our calculation. We will show that we need the metric to first order in the Newtonian potential and then calculate the solution to this order. We will then compare the solution with the full PPN metric expansion and identify the γ parameter as the factor that is constrained.

To start we will recap the Newtonian limit for a non-relativistic body, and then move on to finding the relevant corrections for a relativistic body.

Newton's equations state that a test body will undergo acceleration

$$\mathbf{a} = \nabla\Phi_N \tag{5.9}$$

where

$$\nabla^2\Phi_N = \rho/2M_{Pl}^2. \tag{5.10}$$

We have also the action for a single particle

$$S = -m_0\int d\tau = -m_0\int(-\tilde{g}_{\mu\nu}\frac{dx^\mu}{dt}\frac{dx^\nu}{dt})^{1/2}dt \tag{5.11}$$

from which one can derive the geodesic equation

$$\frac{d^2x^\mu}{d\tau^2} + \tilde{\Gamma}^\mu_{\alpha\beta}\frac{dx^\alpha}{d\tau}\frac{dx^\beta}{d\tau} = 0. \tag{5.12}$$

By the definition of proper time ($\tilde{g}_{\mu\nu}\dot{x}^\mu\dot{x}^\nu = -1$), at lowest order $\frac{dt}{d\tau} = 1$ and $\frac{dx^i}{d\tau} = v = O(\sqrt{|\Phi_N|})$, and so eq. (5.12) amounts to

$$a^k = -\tilde{\Gamma}^k_{00} = \frac{1}{2}\tilde{g}^{kl}\tilde{g}_{00,l} + O((\sqrt{\Phi_N})). \tag{5.13}$$

Matching eq. (5.13) with eq. (5.9), together with the insistence that the metric tends toward the Minkowski metric far from the source of the gravitation field, gives that at Newtonian order

$$\tilde{g}^{jk} = \delta^{jk} \tag{5.14}$$

$$\tilde{g}_{00} = -1 + 16\pi M_{Pl}^2\Phi_N. \tag{5.15}$$

We now move on to considering the motion of photons as this is what is relevant because we are using the constraints from radio waves. Consider again our action eq. (5.11). We can

write this as

$$S = \int (-\tilde{g}_{00} - 2\tilde{g}_{0i}v^i - \tilde{g}_{ij}v^i v^j)^{1/2} dt. \tag{5.16}$$

Because the proper time of a photon is zero then the integrand of eq. (5.16) must vanish. At lowest order, that is $\tilde{g}_{\mu\nu} = \eta_{\mu\nu}$, this gives that integrand as

$$L = (1 - v^2)^{1/2}. \tag{5.17}$$

For this to vanish we require $v^2 = 1$. Thus in the Minkowski limit we recover that photons travel at the speed of light in straight lines. To recover the first order correction to the path of a photon we need to consider the next order corrections to eq. (5.16). This gives

$$1 - 16\pi M_{Pl}^2 \Phi_N - 2g_{0i}[2]v^i - g_{ij}[2]v^i v^j = 0 \tag{5.18}$$

where $g_{\alpha\beta}[2]$ denotes $g_{\alpha\beta}$ up to first order in the Newtonian potential.

Now that we have justified that we need to find the metric up to first order in the Newtonian potential, we will re-write the Einstein frame solution in the Jordan frame in the appropriate form so that it can be directly compared to the PPN expansion. This expansion [91] has

$$g_{00} = -1 + 2GM/r \tag{5.19}$$

$$g_{0i} = 0 \tag{5.20}$$

$$g_{ij} = -\delta_{ij} + 2\gamma GM/r\delta_{ij}. \tag{5.21}$$

The eq. (5.21) defines the parameter γ, which is one in General Relativity. We model the Sun as a static spherical object and ignore the scalar energy-momentum as that is subleading. Thus in the Einstein frame the metric is the Schwarzschild metric, which together

with eq. (5.5) gives our solution to be

$$\begin{aligned} g_{00} &= -(1 - M/4\pi M_{Pl}^2 r) \\ g_{0i} &= 0 \\ g_{ij} &= (1 - M/4\pi M_{Pl}^2 r)^{-1}\delta_{ij} \\ \phi(r) &= -\beta(M - M(r_*))/4M_{Pl}\pi r + \phi_\infty. \end{aligned} \tag{5.22}$$

We can see that $\phi - \phi_\infty = O(\Phi_N)$ and so we were justified in ignoring the scalar energy momentum. As $M/4\pi M_{Pl}^2 r = O(\Phi_N)$ we can take $g_{ij} = (1 + M/4\pi M_{Pl}^2 r)\delta_{ij}$.

We now convert this solution into the Jordan frame, in PPN form. We have that $\tilde{g}_{\mu\nu} = A^2(\phi)g_{\mu\nu}$ and, to first order, we have

$$\begin{aligned} A^2(\phi) &= A^2(\phi) + 2A(\phi_\infty)A'(\phi_\infty)(\phi - \phi_\infty) \\ &= A^2(\phi_\infty)(1 + 2\beta(\phi_\infty)(\phi - \phi_\infty)/M_{Pl}). \end{aligned} \tag{5.23}$$

We want $\tilde{g}_{\mu\nu} \to \eta_{\mu\nu}$ at large r and so we must rescale the coordinates according to $t \to t/A(\phi_\infty)$ and $r \to r/A(\phi_\infty)$. Furthermore the mass in eq. (5.22) is the Einstein frame mass defined by

$$M_E = 4\pi \int \rho_E(r')r'^2 dr'. \tag{5.24}$$

Rescaling the coordinates gives

$$M_E = 4\pi \int \rho_E(r'/A(\phi_\infty))r'^2 dr' = 4\pi A(\phi_\infty)^3 \int \rho_E(r')r'^2 dr' \tag{5.25}$$

and substituting in for the Jordan frame mass density, $\tilde{\rho} = A^4(\phi)\rho_E$, gives

$$M_E = 4\pi A(\phi_\infty)^3 \int \tilde{\rho}(r')r'^2/A^4(\phi(r'))dr'. \tag{5.26}$$

As we are only considering our solution up to first order it is sufficient to approximate $A^4(\phi) = A^4(\phi_\infty)$ within the integral. This gives

$$M_E = \int \tilde{\rho}(r')r'^2)dr'/A(\phi_\infty) = \tilde{M}/A(\phi_\infty). \tag{5.27}$$

Making this substitution and dropping the $\sim$ on M, gives eq. (5.22)

$$\begin{aligned}
\tilde{g}_{00} &= (1+2\beta(\phi_\infty/M_{Pl})(\phi-\phi_\infty))(-1+M/4\pi M_{Pl}^2 r) \\
&= -1+\frac{2\beta^2}{M_{Pl}}(M-M(r_*))/4\pi M_{Pl} r + M/4\pi M_{Pl}^2 r + o(\Phi_N) \\
&= -1+\frac{2M}{r}(\frac{2\beta^2(1-M(r_*)/M)+1}{8\pi M_{Pl}^2}) + o(\Phi_N).
\end{aligned} \tag{5.28}$$

By comparison of eq. (5.28) with eq. (5.19) we identify the effective Newton's constant to be

$$G = \frac{2\beta^2(1-M(r_*)/M)+1}{8\pi M_{Pl}^2}. \tag{5.29}$$

This gives us that

$$\begin{aligned}
\tilde{g}_{ij} &= (1+2\beta(\phi_\infty)(\phi-\phi_\infty))(1+M/4\pi M_{Pl}^2 r)\delta_{ij} \\
&= (1-\frac{2\beta^2}{M_{Pl}}(M-M(r_*))/4\pi M_{Pl} r + M/4\pi M_{Pl}^2 r)\delta_{ij} \\
&= \delta_{ij}+\frac{2GM}{r}(\frac{-2\beta^2(1-M(r_*)/M)+1}{8\pi M_{Pl}^2})(\frac{8\pi M_{Pl}^2}{2\beta^2(1-M(r_*)/M)+1})\delta_{ij} \\
&= \delta_{ij}+\frac{2GM}{r}(1-4\beta^2(1-M(r_*)/M))\delta_{ij}.
\end{aligned} \tag{5.30}$$

This is now in a form where we can compare it with eq. (5.21) and identify the γ parameter as given by

$$\gamma \approx 1-4\beta^2(1-M_\odot(r_*)/M_\odot) \tag{5.31}$$

which is constrained [34] to

$$|\gamma - 1| < (2.1 \pm 2.3) \times 10^{-5}. \tag{5.32}$$

Thus, taking the upper limit of eq. (5.32) and substituting in eq. (5.31), we can exclude the regions of parameter space that have

$$4\beta^2(1 - M_\odot(r_*)/M_\odot) > (4.4) \times 10^{-5}. \tag{5.33}$$

5.2.2 Applying the Constraint

The fig. 5.1 plots the region of the $\Lambda - M_c$ plane, where $M_c = M_{Pl}/\beta$, that eq. (5.33) excludes.

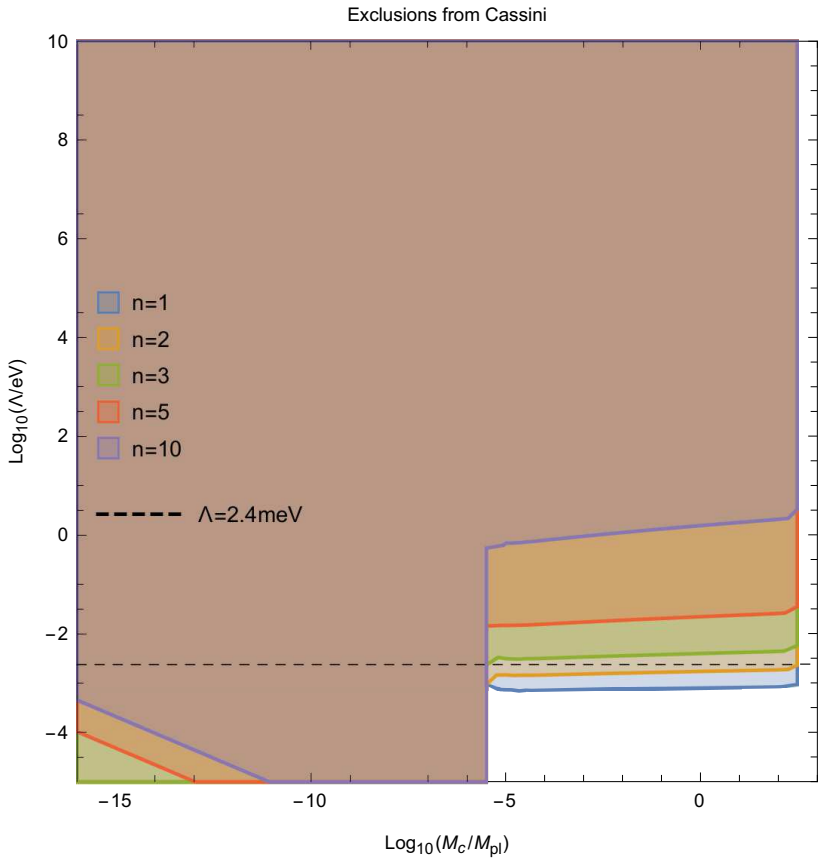

Fig. 5.1 Constraints from the Cassini probe

For large Λ we have that $Log_{10}(M_c/M_{Pl}) \lesssim 5/2$ is excluded. This is because, for unscreened objects $r_* = 0$ and so the constraint from the Cassini probe gives that $4\beta^2 < 4.4 \times 10^{-5}$, or in terms of the coupling scale used in fig. 5.1, $Log_{10}(M_c/M_{Pl}) \gtrsim 5/2$. Thus for large Λ the Sun is unscreened. For screened objects, $M_\odot(r_*) \approx M_\odot$ and so eq. (5.33) is less of a constraint. We can see that this is true for lower values of Λ, and that increasing n reduces the size of the exclusion region.

5.3 Constraint from Lunar Ranging

The distance between the Earth and Moon can be measured by firing lasers at retroreflectors that have been placed on the Moon [69]. Using these measurements the difference in free fall of Earth and Moon towards the Sun can be constrained [61] to

$$|\mathbf{a}_m - \mathbf{a}_e|/a_N < 10^{-13} \tag{5.34}$$

where a_N is the Newtonian acceleration.

Taking the Moon and Earth to be moving in the potential of the Sun we have

$$M_m \ddot{\mathbf{x}}_\mathbf{m} = -M_m(\nabla\Phi_N) - Q_m\beta\nabla\phi/M_{Pl} \tag{5.35}$$

$$M_e \ddot{\mathbf{x}}_\mathbf{e} = -M_e(\nabla\Phi_N) - Q_e\beta\nabla\phi/M_{Pl} \tag{5.36}$$

where Q_m and Q_e are the scalar charges of the Moon and Earth respectively. Assuming the Sun is spherical and of constant density, we can apply the analysis of section 5.1.1 to give the profile of the Sun to be

$$\phi \approx \phi_\infty - \beta(M_\odot - M(r_*))/4\pi M_{Pl} r. \tag{5.37}$$

Subtracting eq. (5.35) from eq. (5.36) then gives that

$$|\mathbf{a}_m - \mathbf{a}_e|/a_N = 2 \times \beta^2 |r_{*_m}^3/R_m^3 - r_{*_e}^3/R_e^3)|(1 - r_{*_\odot}^3/R_\odot). \tag{5.38}$$

The fig. 5.2 shows the region of the $\Lambda - M_c$ plane constrained by eq. (5.34).

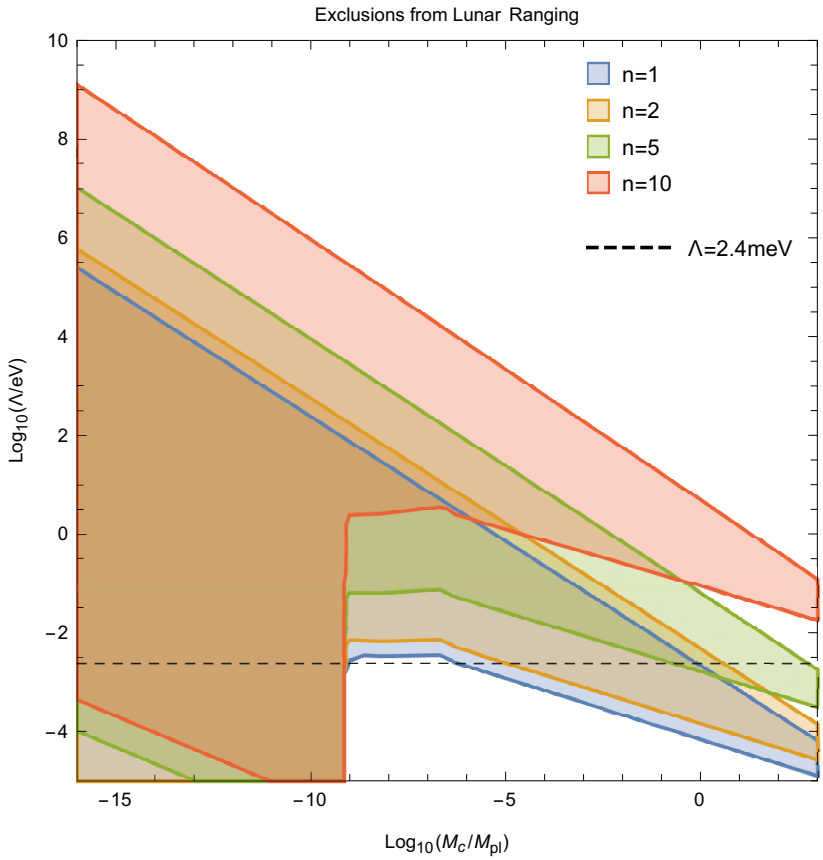

Fig. 5.2 Constraints from Lunar Ranging

In it we can see that lunar ranging constrains a large proportion of the $\Lambda - M_c$ plane, including some areas that were unconstrained by the Cassini probe. One may note that the top right region in fig. 5.2 is unconstrained. This is because eq. (5.34) constrains the relative acceleration of the Moon and Earth, and so if they are both unscreened then eq. (5.34) is satisfied. This is not a problem because this region has already been ruled out by the Cassini probe constraint. The eq. (5.34) will be most constraining when one of the Earth or Moon is screened and one is not; the Moon will always screen more easily than the Earth because

the Newtonian potential at the surface of the Moon is less than the potential at the Earth's surface.

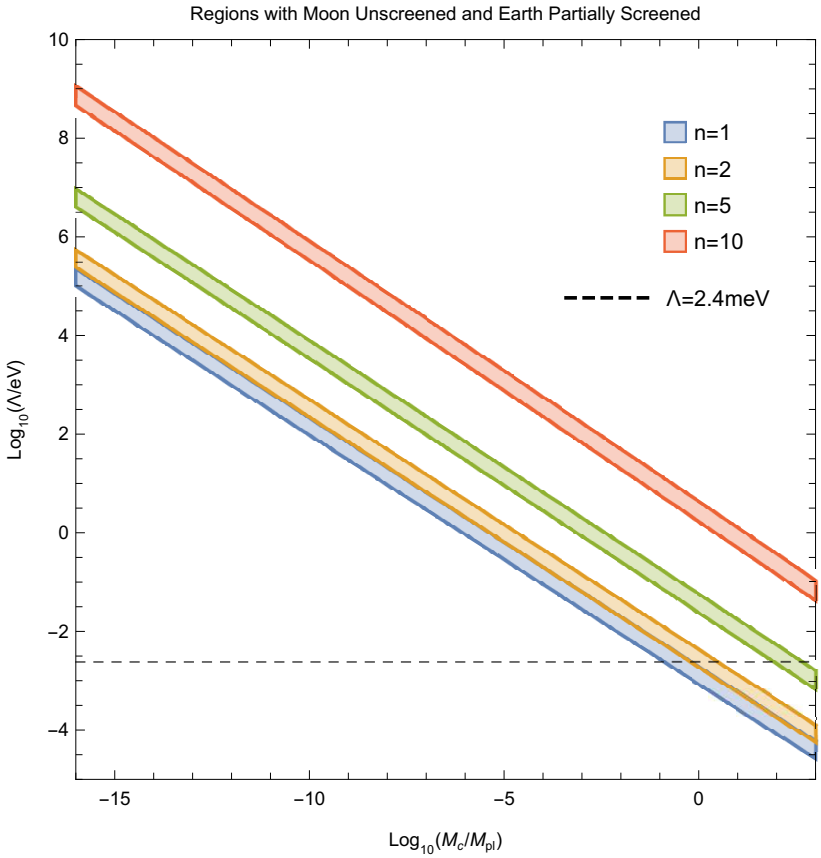

Fig. 5.3 Region for which the Moon is unscreened and the Earth is (at least) partially screened

Thus if the Moon is unscreened and the Earth is screened, eq. (5.34) will amount to

$$2\beta^2(1 - M_\odot(r_*)/M_\odot)) \lesssim 10^{-13} \tag{5.39}$$

which is more competitive than eq. (5.33), the constraint from Cassini. However as the Newtonian potential at the surfaces of the Moon ($\Phi_N \approx 4 \times 10^{-11}$) and Earth ($\Phi_N \approx 8 \times 10^{-10}$) are within an order of magnitude, there is only a small region of the $\Lambda - M_c$ plane for which this is true. The region for which the Moon is unscreened and the Earth is (at least partially) screened is depicted in fig. 5.3. One can indeed see that this corresponds to

part of the excluded area, including part of the area unconstrained by the Cassini probe. The majority of the area constrained occurs when both the Moon and Earth are screened.

5.4 Conclusion

In this chapter we have considered the Chameleon theories with a logarithmic potential, as opposed to the standard power-law potential. The theory has three free parameters; the energy scale associated with the bare potential, Λ, the strength of the coupling of matter to the scalar field, β and the power to which we raise the logarithm, N. We have used two solar system tests to constrain this parameter space. The combined constraints are displayed in fig. 5.4. One can see that large portions of the parameter space have been excluded: far more than the corresponding tests for power-law potentials.

One obvious avenue for future research would be to apply further tests to this potential. However it seems unlikely that the logarithmic potential would evade any of the other possible tests that one could envisage applying to it any better than the standard power-law potential. We also showed that increasing the power, N, could reduce the exclusion zone by a small amount, but we did not investigate how large N would need to be tuned in order to pass the tests well.

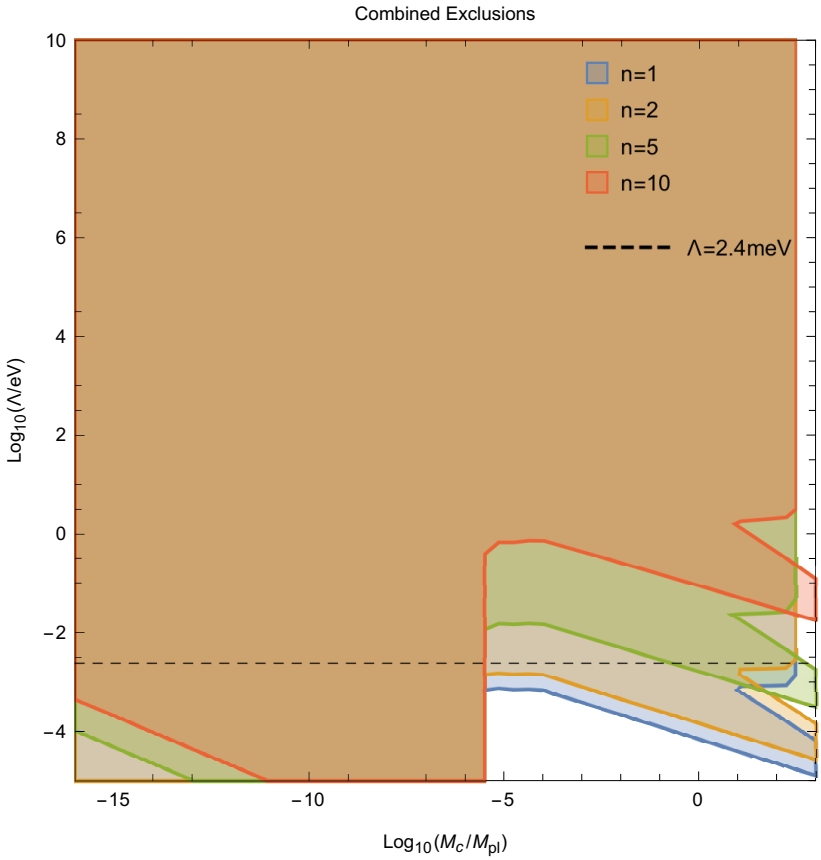

Fig. 5.4 Total exclusion zone using both tests

Chapter 6

Conclusion

Despite the overwhelming success of General Relativity as a theory of gravitational physics, modified gravity is an active area of research. In order to match observations these modifications to gravity must have mechanisms that screen the modification in regions where the deviations from General Relativity are tightly constrained. In this thesis we have considered three such theories - Galileon, K-mouflage and Chameleon - in various different physical scenarios.

In chapter 2 we considered the K-mouflage and Galileon fields that would be present around black holes. In the absence of matter no-hair theorems tell us that the scalar profile will be trivial, but astrophysical black holes have accretion disks and this chapter presents preliminary calculations of the effect that these have. We initially retain a static set-up and conclude that the deviation from General Relativity is small. This is for two reasons. Firstly the screening mechanisms suppress the fifth force relative to a canonical field, and secondly because even the fifth force of an unscreened field is not of gravitational strength. This is because the gravitational force is sourced by both the mass of the black hole and the mass of the accretion, whereas the scalar field is sourced by the accretion disk only. The no-hair theorems additionally assume time-independence. However time-dependent vacuum black hole cubic Galileon solutions have been found in Ref. [9], and in chapter 2

we demonstrate that de Sitter-Schwarzschild black hole solutions exist in K-mouflage with a scalar that depends linearly on time. We further use these vacuum solutions as a background on which to solve for a time-dependent scalar with an accretion disk. We find that the time-dependent solution for K-mouflage is similar to the static solution, whereas for the Galileon the addition of matter makes little difference to the vacuum solution. In chapter 2 we also consider the argument of Ref. [58] that supermassive black holes should be offset from the centre of their galaxy in Galileon theories. We argue that, when one considers the addition of the accretion disk, this effect is reduced slightly.

In chapter 3 we extended our analysis of K-mouflage models to include a disformal coupling to matter as well as the standard conformal coupling. These couplings are most effectively analysed in time-dependent situations, therefore we calculated the background cosmological evolution within these models. We also considered the effect of the coupling on the time-dependent black hole solutions found in chapter 2. For the cosmological evolution we found that the behaviour was qualitatively different to that of the conformal-only K-mouflage solution. The addition of the disformal term caused the time derivative of the scalar to tend towards a finite value at early times, as opposed to diverging as in the conformal-only case. We specified three necessary conditions for the theory to have an observationally viable cosmological evolution: matter domination at early times, a late time dark energy dominated universe and the correct energy of state for this dark energy. We showed that these conditions could be met by K-mouflage with a disformal factor. We explicitly calculated the background evolution for the case of constant conformal factor and the plots that we generated showed that large regions of the parameter space provided only small deviations from a ΛCDM universe.

The screening mechanism of K-mouflage is generally demonstrated under the assumption of spherical symmetry and so in chapter 4 we compared the screening around a spherical object against objects with cylindrical and planar symmetry. We then compared the results

to those of the D-BIon, another theory with screening in regions of high Newtonian gravitational force, for which the shape dependence of screening was analysed in Ref. [17]. For all three shapes the level of screening just outside the object is similar. For spherical objects and cylindrical objects the screening then persists up to a "K-mouflage radius". However for planar objects screening persists arbitrarily far from the object. This is in contrast to Galileon theories, for which there is no screening at all around planar objects.

We move on from derivative based screening mechanisms to consider Chameleon theories in chapter 5. Chameleon literature has so far focused on power-law potentials so in this work we considered logarithmic potentials. There are two free parameters within our model, the coupling strength to matter and the energy scale associated with the potential, and we constrain this parameter space with measurements from two solar system observations - lunar ranging and light bending from the Cassini-Huyens probe measurements. We exclude large regions of the parameter space and conclude that this particular potential does not warrant further investigation.

References

[1] Abbott, B. et al. (2016a). Observation of Gravitational Waves from a Binary Black Hole Merger. *Phys.Rev.Lett.*, 116(6):061102.

[2] Abbott, B. et al. (2016b). Tests of General Relativity with GW150914. *Phys.Rev.Lett.*, 116(22):221101. [Erratum: Phys.Rev.Lett. 121, 129902 (2018)].

[3] Abbott, B. et al. (2017a). GW170817: Observation of Gravitational Waves from a Binary Neutron Star Inspiral. *Phys.Rev.Lett.*, 119(16):161101.

[4] Abbott, B. et al. (2017b). Multi-Messenger Observations of a Binary Neutron Star Merger. *Astrophys.J.*, 848(2):L12.

[5] Abramowicz, M. A. and Fragile, P. (2013). Foundations of Black Hole Accretion Disk Theory. *Living Rev. Rel.*, 16:1.

[6] Adelberger, E., Gundlach, J., Heckel, B., Hoedl, S., and Schlamminger, S. (2009). Torsion Balance Experiments: a Low-Energy Frontier of Particle Physics. *Prog.Part.Nucl.Phys.*, 62:102–134.

[7] Andrews, M., Hinterbichler, K., Khoury, J., and Trodden, M. (2011). Instabilities of Spherical Solutions with Multiple Galileons and SO(N) Symmetry. *Phys. Rev.*, D83:044042.

[8] Anisimov, A., Babichev, E., and Vikman, A. (2005). B-inflation. *JCAP*, 06:006.

[9] Babichev, E., Charmousis, C., Lehébel, A., and Moskalets, T. (2016). Black Holes in a Cubic Galileon Universe. *JCAP*, 09:011.

[10] Babichev, E., Deffayet, C., and Ziour, R. (2009). K-mouflage Gravity. *Int. J. Mod. Phys.*, D18:2147–2154.

[11] Barreira, A., Brax, P., Clesse, S., Li, B., and Valageas, P. (2015). K-mouflage Gravity Models that Pass Solar System and Cosmological Constraints. *Phys. Rev.*, D91(12):123522.

[12] Baumann, D. (2018). Primordial Cosmology. *PoS*, TASI2017:009.

[13] Bekenstein (1993). Relation Between Physical and Gravitational Geometry. *Phys. Rev.*, D48(8):3641.

[14] Bekenstein, J. D. (1996). Black Hole Hair: 25 - Years After. In *2nd International Sakharov Conference on Physics*, pages 216–219.

[15] Benevento, G., Raveri, M., Lazanu, A., Bartolo, N., Liguori, M., Brax, P., and Valageas, P. (2019). K-mouflage Imprints on Cosmological Observables and Data Constraints. *JCAP*, 1905(05):027.

[16] Bertotti, B., Iess, L., and Tortora, P. (2003). A Test of General Relativity using Radio Links with the Cassini Spacecraft. *Nature*, 425:374–376.

[17] Bloomfield, J. K., Burrage, C., and Davis, A.-C. (2015). Shape Dependence of Vainshtein Screening. *Phys. Rev.*, D91(8):083510.

[18] Bondi, H. (1952). On Spherically Symmetrical Accretion. , 112:195.

[19] Brax, P. (2012). Screened Modified Gravity. *Acta Phys. Polon.*, B43:2307–2329.

[20] Brax, P. and Burrage, C. (2014). Constraining Disformally Coupled Scalar Fields. *Phys. Rev.*, D90(10):104009.

[21] Brax, P., Burrage, C., and Davis, A.-C. (2012). Shining Light on Modifications of Gravity. *JCAP*, 1210:016.

[22] Brax, P., Burrage, C., and Davis, A.-C. (2013). Screening Fifth Forces in K-essence and DBI Models. *JCAP*, 1301:020.

[23] Brax, P. and Valageas, P. (2014). K-mouflage Cosmology: the Background Evolution. *Phys.Rev.*, D90(2):023507.

[24] Brax, P. and Valageas, P. (2016). The Effective Field Theory of K-mouflage. *JCAP*, 01:020.

[25] Brax, P., van de Bruck, C., Davis, A.-C., Khoury, J., and Weltman, A. (2004). Detecting Dark Energy in Orbit: The Cosmological Chameleon. *Phys. Rev.*, D70:123518.

[26] Burrage, C., de Rham, C., Seery, D., and Tolley, A. J. (2011). Galileon Inflation. *JCAP*, 01:014.

[27] Burrage, C., Dombrowski, J., and Saadeh, D. (2019). The Shape Dependence of Vainshtein Screening in the Cosmic Matter Bispectrum. *JCAP*, 1910(10):023.

[28] Burrage, C. and Sakstein, J. (2018). Tests of Chameleon Gravity. *Living Rev.Rel.*, 21(1):1.

[29] Cardoso, V., Carucci, I. P., Pani, P., and Sotiriou, T. P. (2013). Black Holes with Surrounding Matter in Scalar-Tensor Theories. *Phys. Rev. Lett.*, 111:111101.

[30] Carroll, S. M. (2001). The Cosmological Constant. *Living Rev.Rel.*, 4:1.

[31] Charmousis, C., Copeland, E. J., Padilla, A., and Saffin, P. M. (2012a). General Second Order Scalar-Tensor Theory, Self Tuning, and the Fab Four. *Phys. Rev. Lett.*, 108:051101.

[32] Charmousis, C., Copeland, E. J., Padilla, A., and Saffin, P. M. (2012b). Self-Tuning and the Derivation of a Class of Scalar-Tensor Theories. *Phys. Rev.*, D85:104040.

[33] Chow, N. and Khoury, J. (2009). Galileon Cosmology. *Phys. Rev.*, D80:024037.

[34] Clifton, T., Ferreira, P. G., Padilla, A., and Skordis, C. (2012). Modified Gravity and Cosmology. *Phys.Rept.*, 513:1–189.

[35] Copeland, E. J., Padilla, A., and Saffin, P. M. (2012). The Cosmology of the Fab-Four. *JCAP*, 1212:026.

[36] Creminelli, P., D'Amico, G., Musso, M., Norena, J., and Trincherini, E. (2011). Galilean Symmetry in the Effective Theory of Inflation: New Shapes of Non-Gaussianity. *JCAP*, 02:006.

[37] Davis, A.-C., Gregory, R., and Jha, R. (2016). Black Hole Accretion Discs and Screened Scalar Hair. *JCAP*, 10:024.

[38] Davis, A.-C., Gregory, R., Jha, R., and Muir, J. (2014). Astrophysical Black Holes in Screened Modified Gravity. *JCAP*, 08:033.

[39] De Felice, A. and Tsujikawa, S. (2010). Cosmology of a Covariant Galileon Field. *Phys. Rev. Lett.*, 105:111301.

[40] de Rham, C. and Gabadadze, G. (2010). Generalization of the Fierz-Pauli Action. *Phys.Rev.*, D82:044020.

[41] de Rham, C. and Tolley, A. J. (2010). DBI and the Galileon Reunited. *JCAP*, 05:015.

[42] Dvali, G., Gabadadze, G., and Porrati, M. (2000). 4-d Gravity on a Brane in 5-d Minkowski Space. *Phys.Lett.*, B485:208–214.

[43] Dyson, F., Eddington, A., and Davidson, C. (1920). A Determination of the Deflection of Light by the Sun's Gravitational Field, from Observations Made at the Total Eclipse of May 29, 1919. *Phil.Trans.Roy.Soc.Lond.A*, 220:291–333.

[44] Einstein, A. (1905). On the Electrodynamics of Moving Bodies. *Annalen Phys.*, 17:891–921.

[45] Einstein, A. (1915). Explanation of the Perihelion Motion of Mercury from the General Theory of Relativity. *Sitzungsber Preuss Akad Wiss Berlin (Math.Phys.)*, 1915:831–839.

[46] Einstein, A. (1916). The Foundation of the General Theory of Relativity. *Annalen Phys.*, 49(7):769–822.

[47] Gannouji, R. and Sami, M. (2010). Galileon Gravity and its Relevance to Late Time Cosmic Acceleration. *Phys.Rev.*, D82:024011.

[48] Graham, A. A. H. and Jha, R. (2014). Non-existence of Black Holes with Non-canonical Scalar Fields. *Phys. Rev.*, D89(8):084056. [Erratum: Phys. Rev.D92,no.6,069901(2015)].

[49] Green, M. B., Schwarz, J., and Witten, E. (1988). *Superstring Theory. Volume 1: Introduction*. Cambridge Monographs on Mathematical Physics. Cambridge University Press.

[50] Gruzinov, A. (2005). On the Graviton Mass. *New Astron.*, 10:311–314.

[51] Hawking, S. (1972). Black Holes in General Relativity. *Commun.Math.Phys.*, 25:152–166.

[52] Hawking, S. and Ellis, G. (2011). *The Large Scale Structure of Space-Time*. Cambridge Monographs on Mathematical Physics. Cambridge University Press.

[53] Herdeiro, C. A. R. and Radu, E. (2014). Kerr Black Holes with Scalar Hair. *Phys. Rev. Lett.*, 112:221101.

[54] Heusler, M., Droz, S., and Straumann, N. (1992). Linear Stability of Einstein Skyrme Black Holes. *Phys. Lett. B*, 285:21–26.

[55] Horbatsch, M. and Burgess, C. (2012). Cosmic Black-Hole Hair Growth and Quasar OJ287. *JCAP*, 05:010.

[56] Horndeski, G. W. (1974). Second-Order Scalar-Tensor Field Equations in a Four-Dimensional Space. *Int. J. Theor. Phys.*, 10:363–384.

[57] Hubble, E. (1929). A Relation Between Distance and Radial Velocity Among Extra-Galactic Nebulae. *Proc.Nat.Acad.Sci.*, 15:168–173.

[58] Hui, L. and Nicolis, A. (2012). Proposal for an Observational Test of the Vainshtein Mechanism. *Phys. Rev. Lett.*, 109:051304.

[59] Hui, L. and Nicolis, A. (2013). No-Hair Theorem for the Galileon. *Phys. Rev. Lett.*, 110:241104.

[60] Joyce, A., Jain, B., Khoury, J., and Trodden, M. (2015). Beyond the Cosmological Standard Model. *Phys. Rept.*, 568:1–98.

[61] Khoury, J. and Weltman, A. (2004a). Chameleon Cosmology. *Phys.Rev.*, D69:044026.

[62] Khoury, J. and Weltman, A. (2004b). Chameleon Fields: Awaiting Surprises for Tests of Gravity in Space. *Phys.Rev.Lett.*, 93:171104.

[63] Kimura, R. and Yamamoto, K. (2011). Large Scale Structures in Kinetic Gravity Braiding Model that can be Unbraided. *JCAP*, 1104:025.

[64] Kobayashi, T., Yamaguchi, M., and Yokoyama, J. (2010). G-inflation: Inflation Driven by the Galileon Field. *Phys.Rev.Lett.*, 105:231302.

[65] Koivisto, T. S., Mota, D. F., and Zumalacarregui, M. (2012). Screening Modifications of Gravity through Disformally Coupled Fields. *Phys. Rev. Lett.*, 109:241102.

[66] Lovelock, D. (1971). The Einstein Tensor and its Generalizations. *J. Math. Phys.*, 12:498–501.

[67] Mizuno, S. and Koyama, K. (2010). Primordial Non-Gaussianity from the DBI Galileons. *Phys. Rev.*, D82:103518.

[68] Mota, D. F., Sandstad, M., and Zlosnik, T. (2010). Cosmology of the Self-Accelerating Third Order Galileon. *JHEP*, 12:051.

[69] Muller, J., Nordtvedt, K., and Vokrouhlicky, D. (1996). Improved Constraint on the Alpha-1 PPN Parameter from Lunar Motion. *Phys.Rev.*, D54:5927–5930.

[70] Newton, I. (1687). *Philosophiae Naturalis Principia Mathematica*. England.

[71] Nicolis, A., Rattazzi, R., and Trincherini, E. (2009). The Galileon as a Local Modification of Gravity. *Phys.Rev.*, D79:064036.

[72] Pena, I. and Sudarsky, D. (1997). Do Collapsed Boson Stars Result in New Types of Black Holes? *Class. Quant. Grav.*, 14:3131–3134.

[73] Reid, B. A. et al. (2010). Cosmological Constraints from the Clustering of the Sloan Digital Sky Survey DR7 Luminous Red Galaxies. *Mon. Not. Roy. Astron. Soc.*, 404:60–85.

[74] Renk, J., Zumalacarregui, M., Montanari, F., and Barreira, A. (2017). Galileon Gravity in Light of ISW, CMB, BAO and H_0 Data. *JCAP*, 10:020.

[75] Riess, A. G. et al. (1998). Observational Evidence from Supernovae for an Accelerating Universe and a Cosmological Constant. *Astron.J.*, 116:1009–1038.

[76] Rubin, V., Thonnard, N., and Ford, W.K., J. (1980). Rotational Properties of 21 SC Galaxies with a Large Range of Luminosities and Radii, from NGC 4605 /R = 4kpc/ to UGC 2885 /R = 122 kpc/. *Astrophys. J.*, 238:471.

[77] Sakstein, J. (2014). Disformal Theories of Gravity: From the Solar System to Cosmology. *JCAP*, 1412:012.

[78] Sakstein, J. (2015). Towards Viable Cosmological Models of Disformal Theories of Gravity. *Phys. Rev. D*, 91(2):024036.

[79] Sakstein, J. and Jain, B. (2017). Implications of the Neutron Star Merger GW170817 for Cosmological Scalar-Tensor Theories. *Phys. Rev. Lett.*, 119(25):251303.

[80] Sakstein, J., Jain, B., Heyl, J. S., and Hui, L. (2017). Tests of Gravity Theories Using Supermassive Black Holes. *Astrophys. J.*, 844(1):L14.

[81] Scolnic, D. et al. (2018). The Complete Light-Curve Sample of Spectroscopically Confirmed SNe Ia from Pan-STARRS1 and Cosmological Constraints from the Combined Pantheon Sample. *Astrophys. J.*, 859(2):101.

[82] Silva, F. P. and Koyama, K. (2009). Self-Accelerating Universe in Galileon Cosmology. *Phys. Rev.*, D80:121301.

[83] Sotiriou, T. P. (2015a). Black Holes and Scalar Fields. *Class. Quant. Grav.*, 32(21):214002.

[84] Sotiriou, T. P. (2015b). Gravity and Scalar Fields. *Lect. Notes Phys.*, 892:3–24.

[85] Sotiriou, T. P. and Zhou, S.-Y. (2014a). Black Hole Hair in Generalized Scalar-Tensor Gravity. *Phys. Rev. Lett.*, 112:251102.

[86] Sotiriou, T. P. and Zhou, S.-Y. (2014b). Black Hole Hair in Generalized Scalar-Tensor Gravity. *Phys. Rev. Lett.*, 112:251102.

[87] Stueckelberg, E. (1938). Interaction Energy in Electrodynamics and in the Field Theory of Nuclear Forces. *Helv. Phys. Acta*, 11:225–244.

[88] Susskind, L. (2003). The Anthropic Landscape of String Theory. pages 247–266.

[89] Vainshtein, A. (1972). To the Problem of Nonvanishing Gravitation Mass. *Phys.Lett.*, B39(3):393–394.

[90] Van Acoleyen, K. and Van Doorsselaere, J. (2011). Galileons from Lovelock Actions. *Phys.Rev.*, D83:084025.

[91] Will, C. M. (1993). *Theory and Experiment in Gravitational Physics*. Cambridge University Press, rev. ed. edition.

[92] Woodard, R. (2015). Ostrogradsky's Theorem on Hamiltonian Instability. *Scholarpedia*, 10(8):32243.

[93] York, D. G. et al. (2000). The Sloan Digital Sky Survey: Technical Summary. *Astron. J.*, 120:1579–1587.

[94] Zumalacarregui, M., Koivisto, T., Mota, D., and Ruiz-Lapuente, P. (2010). Disformal Scalar Fields and the Dark Sector of the Universe. *JCAP*, 05:038.

[95] Zumalacarregui, M., Koivisto, T. S., and Mota, D. F. (2013). DBI Galileons in the Einstein Frame: Local Gravity and Cosmology. *Phys. Rev.*, D87:083010.